Book of Abstract • 2026

Characterisation of Crack/Notch Tip Fields

Edited by Y. Hong, M. Vormwald, G. Meneghetti, T. Palin-Luc, L. Susmel

PADOVA UP

Prima edizione 2026, Padova University Press

Titolo originale: Characterisation of Crack/Notch Tip Fields. Book of Abstract 2026

ISBN 978-88-6938-530-8

Università degli Studi di Padova
Via 8 Febbraio 2, Padova
www.padovauniversitypress.it

https://www.padovauniversitypress.it/en/publications/9788869385308

EIGHTH IJFATIGUE & FFEMS
JOINT WORKSHOP

Characterisation of Crack/Notch Tip Fields

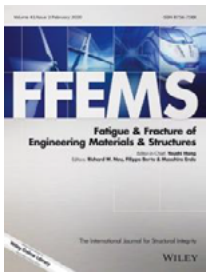

Book of abstracts

The Peace Gardens in the city centre

The Botanical Gardens

Sheffield Hallam University

Sheffield, UK, 2-4 June 2026

With the patronage of

Sheffield Hallam University

Sponsored by

ELSEVIER

WILEY

HBK
HOTTINGER BRÜEL & KJÆR

Foreword

It is our great pleasure to welcome the participants of the *8th IJFatigue & FFEMS Joint Workshop on Characterisation of Crack/Notch Tip Fields under Static, Dynamic or Cyclic Loading*, held at Sheffield Hallam University, Sheffield, United Kingdom, from 2 to 4 June 2026.

This workshop series originated from discussions held in 2009 between the Editors of International Journal of Fatigue and Fatigue & Fracture of Engineering Materials & Structures, who recognised the growing scientific importance of understanding crack and notch tip fields and the associated damage mechanisms across a wide range of loading conditions. Over the years, the workshop has evolved into a distinctive international forum bringing together leading researchers and engineers working at the forefront of fracture mechanics, fatigue, materials behaviour, and structural integrity.

The 2026 edition continues this tradition by providing an informal and highly interactive environment aimed at encouraging scientific discussion, exchange of ideas, and the development of new collaborations. The technical programme reflects both the breadth and the depth of current research activity in the field. Contributions cover topics ranging from fracture behaviour under static loading to fatigue crack propagation, experimental characterisation techniques, multiscale and microstructural approaches, notch mechanics, additive manufacturing, hydrogen-assisted damage, creep, multiaxial fatigue, advanced numerical modelling, and emerging artificial intelligence methodologies.

Particular attention has been devoted to multiparameter and cross-disciplinary approaches for characterising crack and notch tip fields, combining analytical and computational mechanics with full-field experimental techniques and microstructure-sensitive analyses. The programme also highlights the increasing integration of data-driven methods, neural-network-based frameworks, and uncertainty-aware modelling strategies into structural integrity assessment. Such developments demonstrate the continuing evolution of the discipline towards increasingly sophisticated and physically informed predictive methodologies.

We also wish to acknowledge the support provided by Elsevier, Wiley, HBK, and Sheffield Hallam University, whose contribution has been instrumental in making this workshop possible.

The extended abstracts collected in these Proceedings provide a snapshot of the current state of research in crack and notch tip field characterisation. At the same time, they highlight the many scientific challenges that remain open and the exciting opportunities for future advances in the understanding and assessment of structural integrity problems under static, dynamic, and cyclic loading conditions.

We sincerely hope that all participants will find this workshop scientifically stimulating, professionally rewarding, and personally enjoyable, while also taking the opportunity to experience the unique industrial heritage, cultural atmosphere, and natural surroundings of Sheffield and the nearby Peak District.

The Workshop Chairmen

Y. Hong - Chinese Academy of Sciences, China
M. Vormwald - Technical University Darmstadt, Germany
G. Meneghetti - University of Padova, Italy
T. Palin-Luc - Arts et Metiers Institute of Technology, France
L. Susmel – Sheffield Hallam University, UK

Authors' index

Authors' index

Workshop Programme

2 June (Day 1)

8.15-8.45 Registration
8.45-9.00 Workshop Opening

Session I: Fracture with an Industrial Focus – *Chairman:* **Luca Susmel**

9.00-9.20 **Modelling crack growth retardation through a multiaxial cyclic crack-tip plasticity model: a deep-dive into the 'Total-Life' method.** *C. Bagni, A. Halfpenny*
9.20-9.40 **Assessment on Fatigue Behaviour of Al7475 T7351 Subjected to Natural Corrosion, Accelerated Corrosion and Artificial Damages.** *D. Mezzanzanica, A. Baldi, G. Ratti, M. Giglio, A. Manes, M. Ormellese, A. Brenna*
9.40-10.00 **A Fracture-Mechanics-Based Thermo-Mechanical Fatigue Method for Automotive Exhaust Components.** *G. De Morais*
10.00-10.20 **A new fatigue damage evaluation for multiaxial variable amplitude fatigue lifetime assessment of steel welded joints according to the Peak Stress Method.** *A. Campagnolo, A. Visentin, G. Meneghetti*
10.20-10.40 **Crack initiation from pits.** *R. Akid*

10.40-11.00 Coffee break

Session II: Fracture Behaviour under Static Loading – *Chairman:* **Giovanni Meneghetti**

11.00-11.20 **Beyond the crack tip singularity.** *J. R. Yates*
11.20-11.40 **Displacement based determination of stress intensity factors for interacting cracks using crack opening profiles and digital image correlation.** *A. Allahdiniyan, L. Maggi, D. Hoey, D. Taylor, L. Vergani, F. Buccino*
11.40-12.00 **Contact Edge and Crack tip Eigensolutions are the same.** *D. Hills*
12.00-12.20 **Characterisation of the stress field around a flat elliptical crack: crack onset by the coupled criterion.** *P. Cornetti, A. Sapora, V. Mantič, Z. Yosibash*
12.20-12.40 **Fracture toughness of cast and additively manufactured aluminium–silicon–magnesium alloys with copper addition for automotive applications.** *N. D. Alexopoulos, I. Goulas, A. Kermanidis, L. Alberty, Ismail Ünsal, G. Schlick*

12.40-14.00 Lunch Break

Session III: <u>Fatigue Crack propagation & Modelling (I)</u> – *Chairman:* **Youshi Hong**

14.00-14.20 **Three-dimensional elasto-plastic simulation of fatigue crack growth using non-conforming finite element meshes.** *D. Neto, E. Sérgio, F. Antunes*

14.20-14.40 **The apparent success of ΔKeff-based codes revisited through crack tip stress–strain field analyses.** *J. T.Pinho de Castro, M. A. Meggiolaro, R. C. de Oliveira Góes, A. C. de Oliveira Miranda*

14.40-15.00 **Accurate modelling of elastic-plastic material behaviour for FCG analysis.** *F. Antunes, D. Neto, E. Sérgio*

15.00-15.20 **Discussion on the crack driving force along the 3D crack front of an internal short fatigue crack emanating from in internal defect.** *T. Palin-Luc, J.-Y. Buffiere, N. Ranc*

15.20-15.40 **Retardation Effects of Local Crack Branching in Fatigue Crack Growth at Different R-Ratios in AA2024-T3.** *F. Paysan, D. Melching, E. Breitbarth*

15.40-16.00 Coffee break

Session IV: <u>Microstructural Perspectives</u> – *Chairman:* **Harm Askes**

16.00-16.20 **Critical Resolved Shear Stress: Its Link to Fatigue.** *H. Sehitoglu*

16.20-16.40 **A framework of microstructure generation and fatigue life prediction of additively manufactured alloy.** *Q. Huang, T. Shi, J. Sun, G. Qian*

16.40-17.00 **In-situ Observation of the Dynamics of Grain Rotation and Slip Behavior**. *J.-B. Zhao, R. Chen, M.-L. Zhu, F.-Z. Xuan*

17.00-17.20 **A Creep Life Assessment Model for Defective Structures.** *R. Chen, C. Liu, M.-L. Zhu, F.-Z. Xuan*

17.20-17.40 **Crack initiation hotspot identification of LCPF alloys under fatigue loading based on CPFEM and graph neural networks.** *P. Wang, G. Qian*

17.40-18.00 **A recurrent neural operator UMAT for cyclic plasticity: uncertainty-aware training and conformal-prediction deployment.** *J. Abdolahi, S. Safari, D. Knowles, P. Wilcox, M. Mostafavi*

End of Day 1

3 June (Day 2)

8.30-9.00 Registration

Session V: Crack Propagation & Experimental Characterisation (I) – *Chairman:* **Thierry Palin-Luc**

9.00-9.20 **Experimental observations on CTOD measurements obtained by DIC.** *G. L. Gómez Gonzales, J. M. Vasco Olmo, L. F. Sesé, F. A. Díaz Garrido*

9.20-9.40 **Synchrotron-based 3D characterization of torsional fatigue crack propagation in cast Al–Si alloys: influence of defects and microstructure.** *V.-D. Le, F. Morel, N. Saintier, P. Osmond, D. Bellett, W. Ludwig, M. Majkute, J.-Y. Buffiere*

9.40-10.00 **Fatigue crack paths through additively manufactured AlSi10Mg.** *P. J. Withers, S. S. Ahmed, S. Rangaraj, A. Gholinia, J. Bao*

10.00-10.20 **3D characterisation of strain fields around propagating cracks in tailored fibre placement composites.** *G. Sun, R. L. Mitchell, F. Omrani, M Smith, C. Frias, J. P. A. Fairclough, C. Pinna*

10.20-10.40 **Non-destructive evaluation of crack propagation by infrared thermography and acoustic emission: A brief review.** *E. Kordatos*

10.40-11.00 Coffee break

Session VI: Defects and Notches – *Chairman:* **Philip Withers**

11.00-11.20 **The effect of notch on fatigue crack growth in a Charpy specimen.** *A. Sedmak, S. Sedmak, S. Kirin*

11.20-11.40 **Notch and Fracture Mechanics-Based Assessment of Multiaxial Fatigue Thresholds of Defects and Sharp Notches in Metallic Materials**. *F. Collini, D. Rigon, G. Meneghetti (27)*

11.40-12.00 **Theoretical and practical implications derived from the formulation of the Theory of Critical Distances.** *S. Cicero, D. Taylor, L. Susmel*

12.00-12.20 **Notch sensitivity of fatigue behaviour up to very-high-cycle fatigue regime for a structural steel.** *Y. Hong, Q. Jiang, C. Sun*

12.20-12.40 **Experimental fatigue behaviour and TCD-based life estimation of micro-defected X60 pipeline steel under unsoaked and hydrogen-soaked conditions in the medium-cycle regime.** *H. Wang, R. Best, D. Engelberg, I. Hajirasouliha, N. O. Larrosa, F. Scenini, L. Susmel*

12.40-14.00 Lunch Break

Session VII: Fracture Behaviour under Static Loading (II) – *Chairman:* **Aleksandar Sedmak**

14.00-14.20 **Damage tolerance assessment of hot-section components: Fracture toughness testing and fatigue life prediction.** *X. Song, S.-P. Zhu, Q. Wang*

14.20-14.40 **A novel double indentation method to evaluate mixed-mode stress intensity factors and cleavage toughness.** *Z. Zhang, J. Marrow*

14.40-15.00 **Size-dependent fracture in anisotropic beam lattice materials.** *I. Yagmuroglu, H. Askes*

15.00-15.20 **A review of the influence of manufacturing parameters on fracture toughness of additively manufactured polymers.** *L. Marsavina, S. Galatanu, E. Linul*

15.20-15.40 **Microstructure-Resolved Hydrogen Transport and Its Effect on Crack-Tip Fields in Polycrystalline Materials.** *A. Jivkov, A. Khajeian, K. Berbatov*

15.40-16.00 Coffee break

Session VIII: Crack Propagation & Experimental Characterisation (II) – *Chairman:* **John Yates**

16.00-16.20 **Influence of overloads on the propagation of 3D short fatigue cracks.** *L. Sanciet-Munier, N. Limodin, J.-Y. Buffiere, J.-F. Witz, J. R., M. C., G. B. Filali, A. King, J. Lachambre, A. Weck*

16.20-16.40 **Influence of Periodic Overloads and Underloads on Fatigue Crack Growth in ER70S-6 WAAM Carbon Steel.** *M. Mendez-Morales, R. Branco, J. Jesus, T. Tankova, C. Rebelo*

16.40-17.00 **Fast identification of the Paris law parameter during ultrasonic fatigue crack propagation test.** *N. Ranc, R. Delalande, L. Andenas, E. Monteiro, M. Ducousso*

17.00-17.20 **Multiscale analysis and prediction of crack-tip field for fatigue crack growth in anisotropic titanium alloys.** *H. Chen, Z. Liu, X. Chen*

17.20-17.40 **Bias reduction in Paris curve fitting to aggregate fatigue crack growth data.** *M. Stiven, C. Johnston, A. Mehmanparast*

19.00 – Workshop Dinner

End of Day 2

4 June (Day 3)

Session IX: Fatigue Crack propagation & Modelling (II) – *Chairman:* **Sergio Cicero Gonzalez**

8.30-8.50 **Energy release rate of a mixed-mode crack exposed to large deformation.** *A. Spagnoli, R. Macaluso, M. Terzano*

8.50-9.10 **A Fatigue Damage Parameter Incorporating the Micro-Porosity Distribution Field Effect on SLM Materials.** *P. Li, H. Yin*

9.10-9.30 **Effect of stochastic scatter Paris-Erdogan constants on in-plane mixed mode fatigue life predictions.** *O. Demir, M. F. Yaren*

9.30-9.50 **Local scale parameters in continuum damage mechanics and phase field fracture models for crack growth characterization.** *V. Shlyannikov, R. Khamidullin, D. Kosov*

9.50-10.10 **Fatigue Damage in Additively Manufactured Ti-6Al-4V Lattices: A New Parameter Based on Stiffness and Ratcheting.** *P. M. Cerezo, Y. Huang, A. S. Cruces, T. Guraya, P. Nieke, Z. W. Chen, P. Lopez-Crespo1*

10.10-10.30 **Numerical modelling of roughness-induced crack closure.** *E. Sérgio, F. Antunes, D. Neto*

10.30-11.00 Coffee break

11.00-13.00 **Discussion Session & Closure – *Chairman:* Youshi Hong**

End of Day 3

Modelling crack growth retardation through a multiaxial cyclic crack-tip plasticity model: a deep-dive into the 'Total-Life' method

Cristian BAGNI[1], Andrew HALFPENNY[1]

[1] Hottinger Bruel & Kjaer UK Ltd, Advanced Manufacturing Park Technology Centre, Brunel Way, Rotherham, S60 5WG, United Kingdom

cristian.bagni@hbkworld.com

Fatigue is the predominant mechanisms of structural failure in components subjected to cyclic loading. The fatigue process typically involves two phases: crack initiation, during which microstructural damage accumulates and one or more cracks form, and crack propagation, where these cracks grow under cyclic loading until final failure occurs. Conventional fatigue analysis methodologies generally address only one of these two phases, often leading to significant inaccuracies in fatigue life prediction when both initiation and propagation phases play a meaningful role in the total fatigue life of a component. This limitation is particularly important for key technologies in the journey towards weight reduction and improved environmental sustainability in modern engineering applications, such as welded assemblies, lightweight jointed systems, and cast structural components.

To address this challenge, Glinka and Mikheevskiy [1, 2] proposed a unified fatigue life method that bridges strain-life concepts with fracture mechanics principles, thereby enabling simultaneous consideration of crack initiation and crack growth within a single analytical framework. The present work examines one of the key features of this unified approach: an advanced multiaxial crack-tip plasticity formulation capable of capturing mean-stress effects and overload-induced crack growth retardation.

The unified model is based on Glinka's hypothesis that progressive fatigue crack growth can be interpreted as a series of successive initiation events occurring at the scale of individual grains. The opening and closing of the crack generate persistent slip bands ahead of the crack tip, resulting in local Stage I fatigue damage and progressive weakening of the affected grain. Each grain ultimately fails after accumulating sufficient damage, leading to the incremental propagation of the crack. The grain failure accelerates as the crack propagates, due to the rise in stress intensity and consequent strain energy increase, until rapid fracture occurs.

Although conceptually related to Linear Elastic Fracture Mechanics (LEFM), the Glinka model abandons the classical assumption of an infinitely sharp crack, in favour of the assumption of a blunt crack with a finite crack-tip radius, ρ^*, a material parameter typically comparable to the characteristic grain size. This assumption removes the singularity inherent in LEFM and allows the use of a nonlinear elastic–plastic stress field ahead of the crack.

The crack retardation framework originally introduced by Mikheevskiy and Glinka [2] is built upon the multiaxial cyclic crack-tip plasticity model developed by Moftakhar and Glinka [3]. This approach evaluates the evolution of the residual stress ahead of the crack and its influence as the crack advances through the plastic wake. The methodology incorporates the Neuber rule [4] in combination with the Ramberg–Osgood cyclic plasticity model [5], and it can be summarised in four stages:

1. Linear-elastic crack-tip stress profile. Classical fracture mechanics predicts a singular stress field at the tip of an idealised sharp crack, which is not physically realistic. A more

representative assumption involves modelling the crack tip as having a finite radius, ρ*. Under linear-elastic conditions, the stress distribution ahead of such a crack can be described using the Creager–Paris [6].

2. Effect of plastic redistribution at the crack-tip. The stresses predicted by the Creager–Paris law assume linear elasticity. However, localised plastic deformation inevitably develops ahead of the crack tip under cyclic loading. This plasticity causes redistribution of the stress and consequent increase in the apparent stress ahead of the crack. To represent this redistribution and to reflect the diminishing influence of plasticity with increasing distance from the crack tip, Glinka [7, 8] proposed an effective plasticity correction factor.
3. Uniaxial crack-tip cyclic plasticity model. During cyclic loading, the crack-opening portion of the load cycle drives the propagation of the crack, while the crack-closing portion induces residual compressive stresses ahead of the crack tip. These residual stresses must be overcome for the crack to propagate further. Using Neuber's rule together with the Ramberg–Osgood relationship, a cyclic residual stress field can be derived along the crack path for the uniaxial loading case.
4. Multiaxial crack-tip cyclic plasticity model. Extending the previous formulation, the combination of the multiaxial Neuber rule and the Ramberg–Osgood model enables evaluation of residual stress profiles under general multiaxial loading conditions. This extension is essential for practical engineering applications where components are rarely subjected to purely uniaxial loading.

The crack retardation model together with a series of cycle counting memory rules, to account for the retardation effect produced by tensile overloads in the case of variable amplitude loading, and a 'crack-tip driving force' crack growth model, constitute the so-called 'Total-Life' method. This unified approach has been implemented in commercial CAE software to facilitate its use in industrial fatigue assessment workflows. Validation conducted by the SAE Fatigue Design and Evaluation Committee [9] demonstrated strong agreement between numerical predictions and experimental observations, confirming the robustness of the model for engineering applications.

REFERENCES

1. Mikheevskiy, S. Elastic-plastic fatigue crack growth analysis under variable amplitude loading spectra, PhD thesis, University of Waterloo, (2009).
2. Mikheevskiy, S.; Glinka, G. Elastic–plastic fatigue crack growth analysis under variable amplitude loading spectra. Int. J. Fatigue, 31, 1828–1836 (2009).
3. Moftakhar, A.; Buczynski, A.; Glinka, G. Calculation of elasto-plastic strains and stresses in notches under multiaxial loading. Int. J. Fracture, 70, 357–373 (1995).
4. Neuber, H. Theory of stress concentration for shear-strained prismatical bodies with arbitrary nonlinear stress-strain law. J. Appl. Mech., 28, 544–550 (1961).
5. Landgraf, R.W.; Morrow, J.; Endo, T. Determination of the cyclic stress-strain curve. ASTM J. Mater., 4, 176–188 (1969).
6. Creager, M.; Paris, P.C. Elastic field equations for blunt cracks with reference to stress corrosion cracking. Int. J. Fract. Mech., 3, 247–252 (1967).
7. Glinka, G. Calculation of inelastic notch-tip strain-stress histories under cyclic loading. Eng. Fract. Mech., 22, 839–854 (1985).
8. Glinka, G. Personal correspondence on the effect of Cp at long distances from the crack tip, (2015).
9. SAE Fatigue Design and Evaluation Committee. Summary of fatigue life testing and analysis of the A36 T-joint specimens machined and welded completed to date. SAE FD&E Semi-Annual Meeting, (2018).

Assessment on fatigue behaviour of Al7475 T7351 subjected to natural corrosion, accelerated corrosion and artificial damages

Daniele MEZZANZANICA[1], Andrea BALDI[1], Giuseppe RATTI[1], Marco GIGLIO[2], Andrea MANES[2], Marco ORMELLESE[3], Andrea BRENNA[3]

[1] Leonardo Helicopters Division (LHD), via Giovanni Agusta 520, 21017 Samarate (VA), Italy
[2] Politecnico di Milano, Dipartimento di Meccanica, via La Masa 1, 20155 Milano, Italy
[3] Politecnico di Milano, Dipartimento di Chimica, Materiali e Ingegneria Chimica "G. Natta", via L. Mancinelli 7, 20131 Milano, Italy

daniele.mezzanzanica@leonardo.com

Corrosion is one of the most important threats which needs to be considered as source of accidental damage for the fatigue tolerance evaluation of susceptible metallic parts. Helicopter components can be subjected to possible in-service corrosion due to environmental operating conditions, controlled through the adoption of protective coatings and dedicated inspection plans. Into the mainstream of Leonardo Helicopters plan, for European Plan for Aviation Safety 2026 on "ageing of the fleet", this research activity is focused on experimental activities devoted to evaluating the fatigue material behaviour in presence of several kinds of corrosion pits, either from artificial and natural environmental attack, with the final aim of identifying a correlation with artificial defects made by Electrical Discharge Machining (EDM), when subjected to fatigue loads.

Corrosion pits act as a pre-existing flaw in the material, for the nucleation of fatigue cracks. While corrosion fatigue describes the material cracking under a combination of electrochemical and mechanical activity acting simultaneously; the present study is focused on cases where the two driving forces act separately, therefore cyclic loading is applied to a corrosion defect in an inert environment. Compared to pitting, cracking is predominantly a mechanical, fatigue cycle-dependent regime, although in the early stages of crack growth local crack tip chemistry is also a key condition to the development and propagation of small fatigue cracks [1]. In this framework, the Kitagawa-Takahashi diagram [2], which combine the fatigue crack growth threshold and the fatigue endurance limit into a single plot defining the area of non-propagating cracks, has been adopted; for cracks of given length and stress range the Kitagawa-Takahashi diagram allows to predict the allowable stress range for infinite life [3]. The fatigue strength of metallic materials in the presence of small defects are well predicted applying the $\sqrt{area}$ parameter model proposed by Murakami and Endo [4].

In this activity an experimental campaign has been performed on Aluminium Alloy 7475 T7351 specimens, applying an alternate bending fatigue with a constant stress ratio of R=0.1, on a RUMUL testing apparatus, in the presence of a defect with $\sqrt{area}$ = 0.445 mm (equivalent to a semi-circular flaw of 0.35 mm radius), with the final aim of determining the fatigue endurance limit. This limit has been obtained using the Hodge-Rosenblatt simplified stair-case statistical method [5]. Evaluated defects are EDM notch, artificial corrosion pits from galvanostatic and salt spray techniques, natural corrosion pits promoted by exposition in both urban and marine environments. Fatigue tests have been performed for each type of defects, selecting the specimens to have a nominal value of $\sqrt{area}$ as close as possible to the target value of 0.445 mm. Fatigue

tests urban environment specimens have not been performed because no significant localized corrosion attacks have been obtained. Fatigue tests on marine environment specimens have been performed for a smaller defect size, since none of them was able to reach the target value. Run-out was set at 10 million cycles. Ten specimens have been tested for each defect type.

The results of the Hodge Rosenblatt sequences for the four types of tested damage types are shown in Figure 1.(A), where artificial corrosions (Galvanostatic and Salt Spray) present the same fatigue strength of EDM defects; whereas natural corrosion is characterised by an higher fatigue strength. Indeed, natural corrosion pits are significantly smaller and thus not directly comparable with EDM flaws or artificial corrosion pits; for this reason, they are compared, in terms of El/Haddad model Figure 1.(B), with the Kitagawa plot obtained during a comprehensive material characterization carried out during a previous activity performed in the past on the same material, but with a different type of artificial defect (two micro-holes).

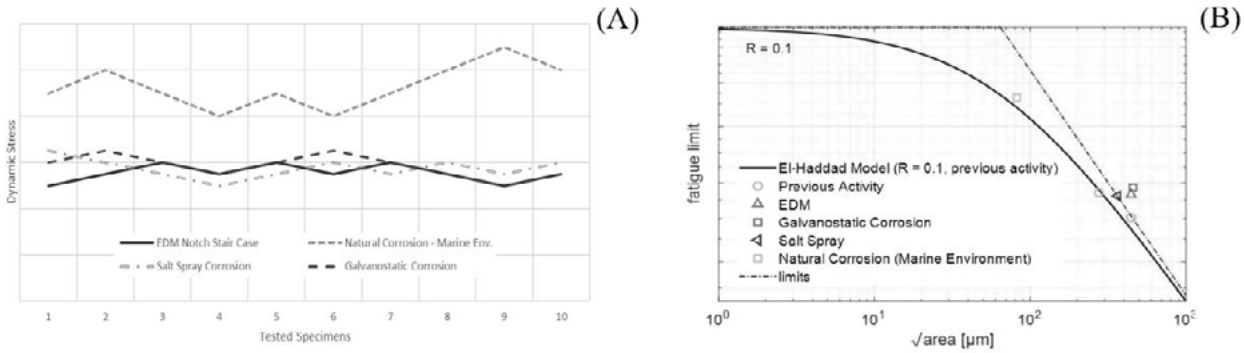

Figure 1. Comparison of Stair-Case Sequences (A); El-Haddad Model of Previous Activity (two micro-holes) and Current Activity results (B).

The results of the activity show a strong correlation among the threshold to propagation from accelerated corrosions, natural corrosion and the artificial flaws (EDM and two micro-holes), confirming the applicability of Kitagawa diagrams derived from artificial defects inflicted with the reported methodologies to describe the damage tolerance behaviour in presence of corrosion pits of equivalent √area. More in details, these results demonstrate that fatigue material behaviour in presence of a corrosion pit, either from natural and accelerated process, when subjected to fatigue loads is equivalent to results obtained with artificial defects inflicted by EDM with the same √area; fatigue behaviour of natural corrosion specimens, that resulted in a smaller value of √area, are well in accordance with the El-Haddad model defined for the Al7475 T7351.

REFERENCES

1. Larrosa, N.; Akid, R.; Ainsworth, R. Corrosion-Fatigue: a Review of Damage Tolerance Models, International Materials Reviews, Vol. 63, n. 5, 283-308 (2018).
2. Kitagawa, H.; Takahashi, S. Applicability of Fracture Mechanics to Very Small Cracks or Cracks in the Early Stage, in Proceeding of the 2nd International Conference on Mechanical Behavior of Materials, ASM (1976).
3. Maierhofer, J.; Ganser, H. -P.; Pippan, R. Modified Kitagawa-Takahashi Diagram Accounting for Finite Notch Depths, Int. Journal of Fatigue, n. 70, 503-509 (2017).
4. Murakami, Y. E. M. Effect of Hardness and Crack Geometries on ΔKth of Small Cracks Emanating from Small Defect, in Mechanical Engineering Publications, Miller KJ, de Los Rios ER, editors, pp. 275-293 (1986).
5. Brand, A.; Grégoire, R. Donnéès Technologiques sur la Fatigue, CETIM (1991).

A fracture-mechanics-based thermo-mechanical fatigue method for automotive exhaust components

Giovanni DE MORAIS[1]

[1] Research and Development, Dassault Systemes, Sheffield, UK

Giovanni.demorais@3ds.com

Thermo-mechanical fatigue (TMF) is one of the main durability challenges in high-temperature automotive components such as exhaust manifolds, cylinder heads and pistons. These components experience severe thermal gradients, cyclic plasticity, creep, and oxidation, all interacting in a way that is difficult to capture using conventional high temperature fatigue approaches.

This work presents a mechanism-based TMF methodology (DTMF) that links material behaviour to component-level life prediction. The approach is rooted in fracture mechanics and relates fatigue damage to the cyclic crack tip opening displacement, while accounting for crack closure, creep, and oxidation effects. Fatigue life is defined as the propagation of an existing microcrack from an initial to a critical size, which is consistent with the behaviour of cast alloys typically used in exhaust systems.

The material response is described using a temperature-dependent Chaboche viscoplastic model. A practical calibration strategy is shown, combining stabilized hysteresis data with Ramberg–Osgood fitting and nonlinear regression. This allows the model to capture cyclic hardening/softening, mean stress effects, and rate dependency over a wide temperature range.

The DTMF damage parameter is derived from a cyclic J-integral formulation, including both elastic and viscoplastic contributions. Crack closure is explicitly considered through an effective stress range, which reduces conservatism under compressive loading. Creep is introduced via a multiplicative factor (Fcr) dependent on stress, temperature, and time, while oxidation is accounted for through a diffusion-based contribution (as proposed by the Fraunhofer Institute).

In the paper the methodology is applied to an automotive exhaust manifold subjected to thermal shock loading. The results show that the predicted fatigue hot spots are located in regions known to be prone to cracking, indicating that the approach captures the dominant damage mechanisms. A key advantage of the method is that it provides a consistent framework from material calibration to component analysis, making it suitable for early-stage design assessments where experimental data is limited.

Although the calibration effort remains significant and oxidation effects are difficult to isolate experimentally, the proposed approach offers a practical compromise between physical accuracy and industrial applicability for TMF life prediction.

Table 1. Main ingredients of the proposed DTMF methodology.

Step	Description
Material model	Temperature-dependent Chaboche viscoplasticity
Fatigue parameter	Crack-tip-opening-displacement-based DTMF parameter
Closure correction	Effective stress range including crack closure
Creep effect	Multiplicative creep factor, Fcr
Oxidation effect	Diffusion-based oxidation damage contribution, Dox
Structural application	Exhaust manifold under thermal shock loading

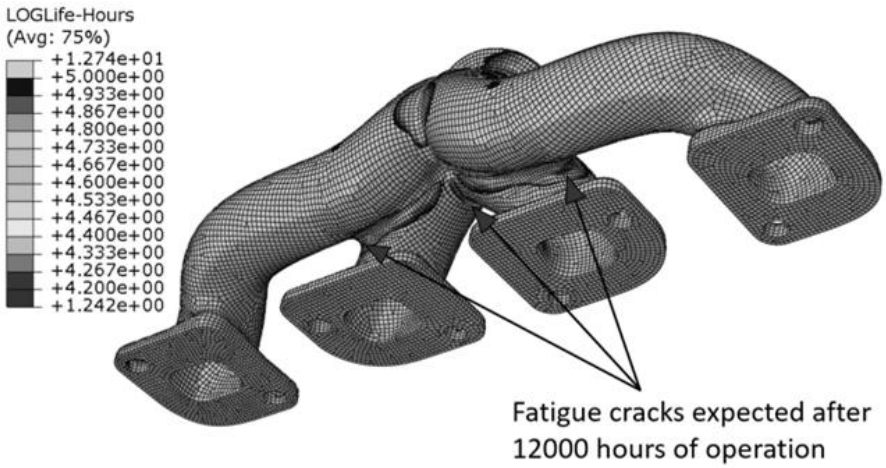

Figure 1. Exhaust manifold fatigue life in Log(hours)

REFERENCES

1. Taira, S. Relationship between thermal fatigue and low-cycle fatigue at elevated temperature. Fatigue at Elevated Temperature, ASTM STP 520, 80–101 (1973).
2. Neu, R.W.; Sehitoglu, H. Thermomechanical fatigue, oxidation, and creep: Part I. Damage mechanisms. Metall. Trans. A, 20, 1755–1767 (1989).
3. Zhuang, W.Z.; Swansson, N.S. Thermo-mechanical fatigue life prediction: a critical review, (1998).
4. Kang, H.T.; et al. Fatigue life prediction of Al319-T7 subjected to thermo-mechanical loading conditions. Procedia Eng., 213, 730–742 (2018).
5. Liu, S.; Liang, G.; Yang, Y. A strategy to fast determine Chaboche elasto-plastic model parameters by considering ratcheting. Int. J. Pressure Vessels Piping, 172, 251–260 (2019).
6. Srnec Novak, J.; De Bona, F.; Benasciutti, D. An isotropic model for cyclic plasticity calibrated on the whole shape of hardening/softening evolution curve. Metals, 9, 950 (2019).
7. Freed, A.D.; Walker, K.P. Viscoplasticity with creep and plasticity bounds. Int. J. Plast., 9, 213–242 (1993).
8. Novak, J.; et al. Estimation of material parameters in nonlinear hardening plasticity models and strain life curves for CuAg alloy. IOP Conf. Ser. Mater. Sci. Eng., 119, 12-20 (2016).

A new fatigue damage evaluation for multiaxial variable amplitude fatigue lifetime assessment of steel welded joints according to the Peak Stress Method

Alberto CAMPAGNOLO[1], Alberto VISENTIN[1], Giovanni MENEGHETTI[1]

[1] Department of Industrial Engineering, University of Padova, Via Venezia 1, 35131 Padova, Italy

giovanni.meneghetti@unipd.it

The fatigue life assessment of welded structures is a critical task of structural engineering, particularly under complex multiaxial variable amplitude (VA) loading. Among local approaches, the Peak Stress Method (PSM) [1] is an FE-oriented tool for estimating Notch Stress Intensity Factors (NSIFs). By modeling weld toes and roots as sharp V-notches ($\rho = 0$), the PSM enables the use of coarse FE meshes to calculate singular peak stresses, which are converted into NSIF-based parameters through calibrated coefficients.

In a previous study [2], the PSM was extended from constant amplitude (CA) to variable amplitude (VA) uniaxial and multiaxial loadings. For each local stress mode, I, II and III, the procedure consists of applying the Rainflow cycle counting algorithm to the peak stress time histories, defining the corresponding peak stress spectra, and determining an equivalent CA peak stress range that produces the same damage as the VA spectrum over a reference number of cycles N_0. Then, a multiaxial equivalent peak stress range referred to N_0 cycles, i.e. $\Delta\sigma_{eq,peak}$, is defined and compared with a fatigue design curve selected according to the local biaxiality ratio λ. Although validated against approximately 900 experimental data points with good agreement for the majority of test series, the calculated fatigue damage depended on the choice of N_0, and defining a limiting value of the local biaxiality ratio to select the proper design curve proved critical.

In the present work, a new formulation of the fatigue damage estimation is proposed to address these limitations. While still utilizing the Palmgren-Miner LDR to analyze individual loading modes, the new approach estimates the fatigue damage contributions from mode I (D_I), mode II (D_{II}), and mode III (D_{III}) local stresses independently (Fig. 1) and addressing the respective mode-specific design curves. The total damage is then evaluated as the sum of these components: $D_{tot} = D_I + D_{II} + D_{III}$, the critical damage being $D_{tot,critical} = 1$ for 50% survival probability. By adopting this mode-based damage summation approach, previous limitations could be fixed. The new fatigue evaluation has been validated against experimental fatigue data from the literature (Fig. 1), demonstrating good accuracy and ease of implementation for complex industrial applications.

REFERENCES

1. Meneghetti, G.; Campagnolo, A. State-of-the-art review of peak stress method for fatigue strength assessment of welded joints. Int. J. Fatigue, 139, 105705 (2020).
2. Campagnolo, A.; Vecchiato, L.; Meneghetti, G. Multiaxial variable amplitude fatigue strength assessment of steel welded joints using the peak stress method. Int. J. Fatigue, 163, 107089 (2022).

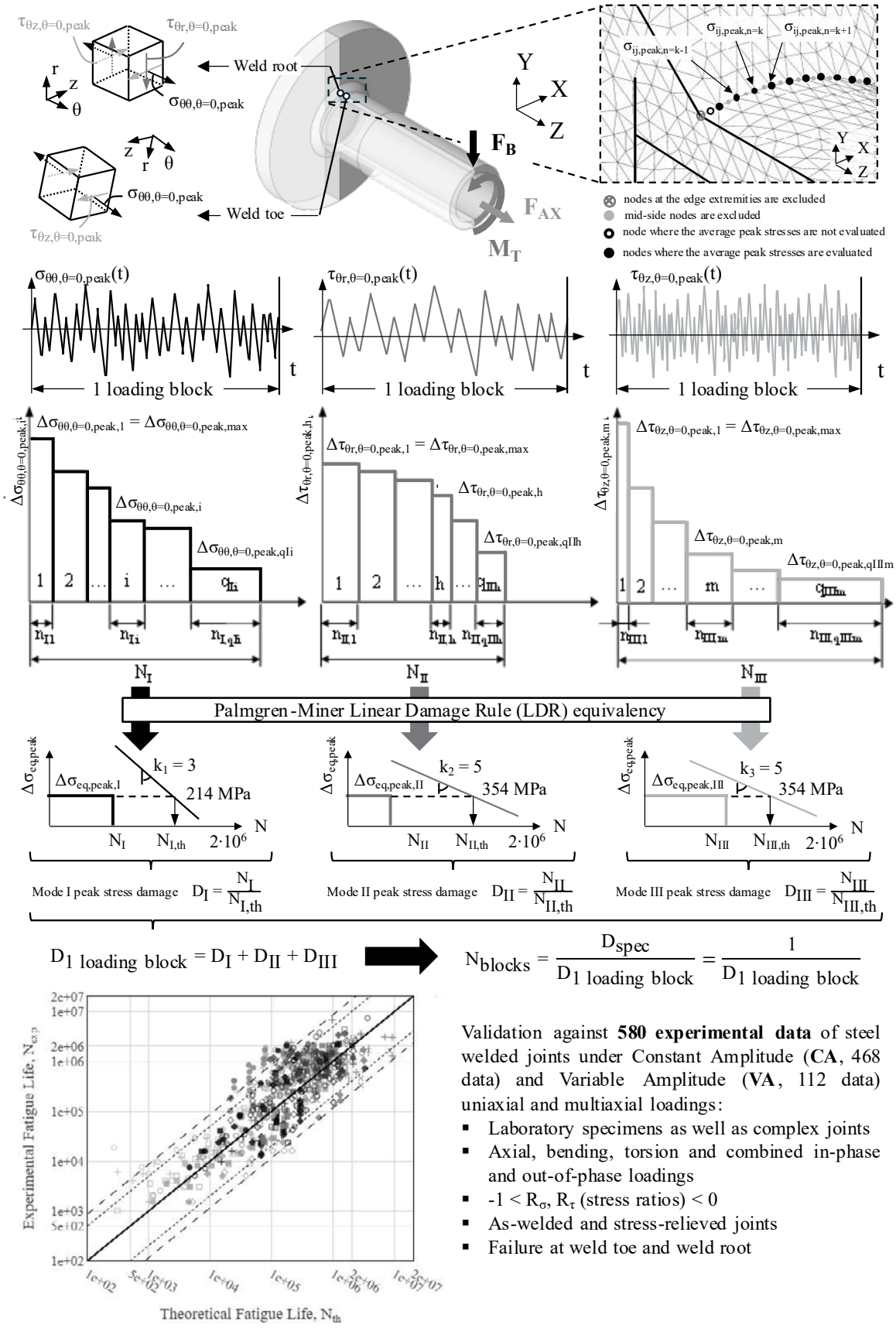

Validation against **580 experimental data** of steel welded joints under Constant Amplitude (**CA**, 468 data) and Variable Amplitude (**VA**, 112 data) uniaxial and multiaxial loadings:

- Laboratory specimens as well as complex joints
- Axial, bending, torsion and combined in-phase and out-of-phase loadings
- $-1 < R_\sigma, R_\tau$ (stress ratios) < 0
- As-welded and stress-relieved joints
- Failure at weld toe and weld root

Figure 1. Procedure to apply the PSM under multiaxial variable amplitude local stresses.

Crack initiation from pits

Robert AKID[1]

[1] Department of Materials, University of Manchester, UK.

robert.akid@manchester.ac.uk

Corrosion pits are geometrical features that, from a mechanical standpoint, act as notches and as a consequence, locally concentrate and amplify any stresses imposed upon a component or structure. This increase in stress concentration provides local sites that are favoured for crack initiation. However, it should be recognised that corrosion pits are unlike mechanical notches that are mechanically formed by, for example, drilling, in that their geometry is constantly evolving, as is the stress state around the surface of the pit. In addition, a major difference between pits and mechanical notches is that the sub-surface stresses induced by machining can be either tensile or compressive, and the microstructure of the sub-layers can be changed during the mechanical forming of the notch.

The negative impact of pitting is clearly seen on the fatigue strength of a material. Pitting decreases the fatigue strength of a material, the extent of the decrease being primarily a function of pit size, aspect ratio and any multiple pit-pit interactions, see Figure 1[1].

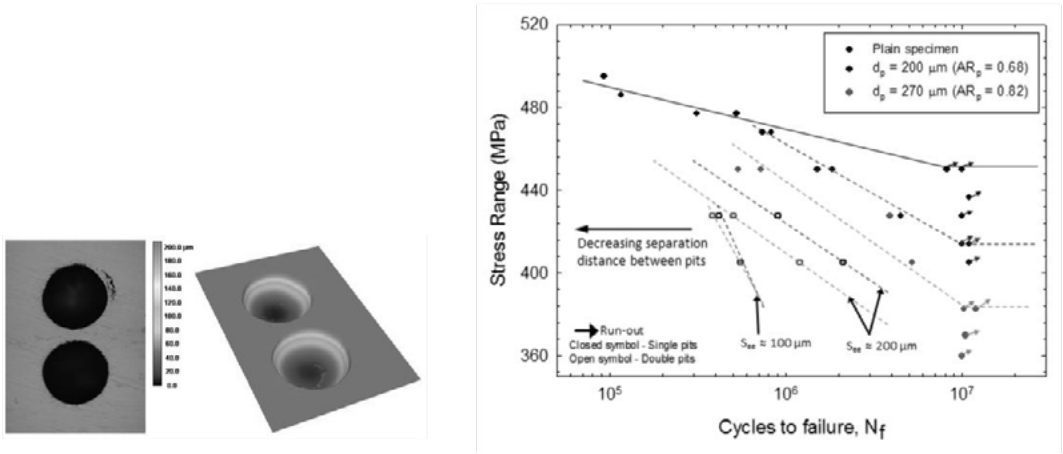

Figure 1. S-N Plots showing the dependence of fatigue endurance on pitting. Single pit depths of 270 µm (two different aspect ratios) and separation distances (S_{ee}) between double pits separated at 100 and 200µm. Images to the left include a micrograph of two adjacent pits and depth contour plots of the pits.

A major engineering challenge is that of the lifetime prediction of components subject to corrosion fatigue, wherein the damage mechanism is that of pit-induced cracking. Here models should represent both the synergistic effect of stress on corrosion and corrosion on crack growth. Furthermore, a key parameter in such a model is the pit to crack criterion. Traditionally this has been based upon the threshold stress intensity factor K_{TH}[2]. However, it has been shown that pit-crack transitions occur below this threshold. An alternative approach that has been

proposed is to adopt the threshold strain for the pit-crack transition[3]. Details of this will be presented.

REFERENCES

1. Fatoba, O.; Akid, R. The influence of corrosion pit–pit spacing on the pit-to-crack transition and fatigue lifetime. Fatigue Fract. Eng. Mater. Struct., 45, 2676–2692 (2022).
2. Larrosa, N.O.; Akid, R.; Ainsworth, R.A. Corrosion-fatigue: a review of damage tolerance models. Int. Mater. Rev., 63, 283–308 (2018).
3. Ramesh Babu, J.; Gopalakrishnan, S.; Fatoba, O.O.; Leiva-Garcia, R.; Akid, R. Modeling fatigue-assisted pitting in pipeline steel with PCA-XFEM. Corros. Sci., 228, 111772 (2024).

Beyond the crack tip singularity

John Robert YATES[1]

[1] Sheffield Fracture Mechanics Ltd

docjry@gmail.com

Failure of structural materials occurs by the propagation of defects through the microstructure. The physical processes arise from the complex interaction between the externally applied displacements with the many features of the microstructure. These interactions occur over many length scales and are responsible for the complex displacement field that we try and describe at the tip of defects with, for example, the stress intensity factor.

As pragmatic engineers, we rely on empirical correlations between an observable phenomenon, like crack extension or specimen failure, and a measurable macroscopic parameter that is usually just displacement dressed up as something else. We find it convenient to use these empirical correlations as a framework and usually invoke some mathematical formulism to provide that framework.

However, we always come up against the issue problem of assigning a length scale to our analyses. Ultimately, this will limit our ability to truly master fracture mechanics, structural integrity, fatigue and suchlike, unless we can break free from this limitation.

The reason why we are shackled by these empirical correlations is the 'Scale Gap'. A crack tip is a regarded as a singularity where the assumptions of continuum mechanics break down. So, unless we stop using continuum mechanics and discard the notion of a crack tip singularity, we will always be constrained by a length scale at which the singularity is no longer valid.

If we were to start from the idea that the crack tip is a mathematical artifact, we might be able to take a fresh look at the problem. We could, for example, regard the region immediately ahead of the crack as a cloud of micro-damage and displacements. The displacements arising from dislocations, microvoids, grain boundary sliding, fracture and decohesion of second phase particles and so on. We could then separate the 'state' of the material at the scale of each physical process from the mechanics of the deformation [1-3].

A potential mathematical approach would be to use multilayered graphs, or multiplex networks, to build a digital surrogate of the microstructure. Such a model would overcome the singularity length scale problem as the displacement field is governed by the topology of connectivity and the state of the bonds; the imposed $1/\sqrt{r}$ singularity ceases to be needed.

In a multilayered graph, the edges and vertices describe the state and interactions and each layer is associated with a particular microstructural feature. In Figure 1, as an example, the lowest layer might describe the size and spatial distribution of second phase particles, which act as the sites from which the ultimate failure orginates. The second layer could describe the topology of the grains with crystallographic orientation and Taylor factors. The third layer might capture the global displacements imposed on the boundaries of the component and define the local conditions for the lower layers.

In such a model, the crack displacement field becomes a global emergent property of the graph's internal reorganization. This architecture would allow for a true multiscale physics approach without the information loss inherent in homogenization processes.

Whilst this is, at the current stage, simply a thought experiment, the presentation will explore these ideas further and hopefully provide some inspiration for future research.

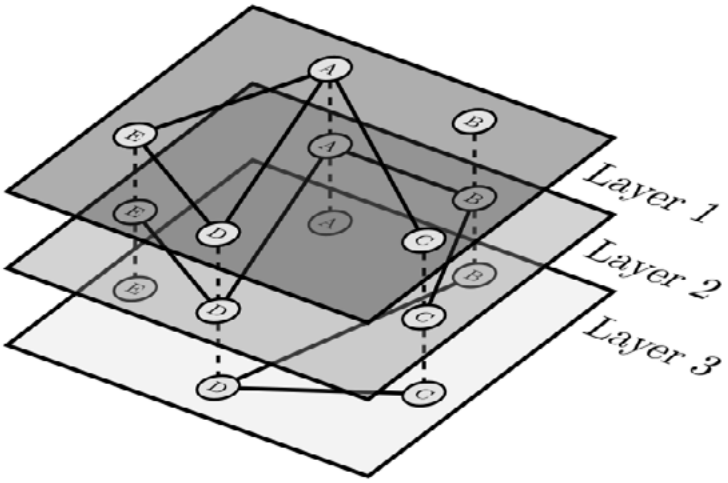

Figure 1. Schematic of an example of a multiplex network [4].

REFERENCES

1. Das, S.; Shterenlikht, A.; Howard, I.C.; Palmiere, E.J. A general method for coupling microstructural response with structural performance. Proc. R. Soc. A, 462, 2085–2096 (2006).
2. Ayvar-Soberanis, S.; Tai, Y.H.; Yates, J.R. 3D CAFE modelling and CTOA measurements of X100 pipeline steels in DCB specimen geometry. Proceedings of the 12th International Conference on Fracture (ICF12), Ottawa, ON, Canada, (2009).
3. Jivkov, A.P.; Yates, J.R. Elastic behaviour of a regular lattice for meso-scale modelling of solids. Int. J. Solids Struct., 49, 3089–3099 (2012).
4. Koll, C.; Lindell, M.; Chen, C.; Wang, H. Emergency warning dissemination in a multiplex social network. JASSS-J. Artif. Soc. S., 26, 10.18564/jasss.4946 (2023).

Displacement-based determination of stress intensity factors for interacting cracks using crack opening profiles and digital image correlation

Anis ALLAHDINIYAN[1], Linda MAGGI[2,3], David A. HOEY[2,3], David TAYLOR[2,3], Laura Maria VERGANI[1], Federica BUCCINO[1]

[1] Department of Mechanical Engineering, Politecnico di Milano, Milano, Italy
[2] Department of Mechanical, Manufacturing and Biomedical Engineering, Trinity College Dublin, Ireland
[3] Trinity Centre for Biomedical Engineering, Trinity College Dublin, Ireland

anis.allahdiniyan@polimi.it

Cracks and other stress-raising features are a frequent cause of failure in engineering components, so reliable evaluation of the stress intensity factor K_I remains central to design, life prediction and structural health monitoring. In complex geometries involving free edges, multiple cracks or material interfaces, conventional approaches based on detailed finite element (FE) stress analysis can be highly sensitive to uncertain loading and boundary conditions. With modern digital image correlation (DIC), it is now possible to measure crack opening displacements directly with high spatial resolution, suggesting a displacement-based route to K_I that can be applied directly to laboratory specimens and real components [1].

Previously we developed solutions that allowed K_I to be determined from measured crack opening profiles (COPs) for a variety of centre and edge crack configurations [2]. Here we extended this approach to cases where crack interaction and material mismatch produce non-symmetric opening fields. Starting from Westergaard's classical centre-crack solution [3], we introduced a two-parameter COP expression that incorporates independent K_A and K_B for the two crack tips, allowing for asymmetric loading while preserving the correct square-root behaviour near each tip.

$$\delta T(x) = \left[K_B \cdot \frac{a-x}{2a} + K_A \cdot \frac{a+x}{2a}\right]\frac{2}{E}\sqrt{\frac{a^2-x^2}{\pi a}} \tag{1}$$

Here a is the crack half-length and x is distance from the crack centre. The method was first calibrated and validated by FEA on three classes of problems of structural interest, crack–edge interaction, crack–crack interaction and a crack approaching a bi-material interface with different Young's moduli (Figure 1a,b as examples). Two-dimensional plane-stress FE models in ABAQUS with refined quarter-point elements were used to compute crack opening profiles over a wide range of non-dimensional parameters (a/b, a/c, h/a, E_1/E_2), and the proposed COP form was fitted to these profiles to obtain $K_A$and K_B, which agree with J-integral and handbook values within a few percent ($R^2 > 0.99$), showing that the method can represent strongly asymmetric opening fields.

To demonstrate experimental feasibility with standard laboratory equipment, the approach was applied to polymethylmethacrylate (PMMA) plates containing centre cracks, single edge cracks, crack–edge and crack–crack interaction geometries. Specimens were loaded in uniaxial tension while a commercial 3D DIC system (ARAMIS 12M) recorded full-field displacements on a

speckled surface, and crack opening profiles were extracted along the crack line after rigid-body and far-field strain correction. For simple centre and edge cracks, COP-based KI values obtained by fitting symmetric expressions showed good agreement with standard handbook solutions, with errors of about 3–6% for the centre crack and 3–17% for the edge crack over the examined load range. For the interacting crack geometries, the non-symmetric COP form (Eqn.1) was used to identify K_A and K_B from the experimental profiles within a central fitting window, and the resulting stress intensity factors scaled linearly with nominal stress, as expected from LEFM, while generally remaining within about 10–20% of theoretical reference values depending on configuration and load level.

From an engineering perspective, the proposed COP methodology offers a practical displacement-based route to obtain local stress intensity factors in situations where direct stress analysis is difficult or where loading is not precisely known, such as in components with multiple cracks, repairs, stiffeners or bonded interfaces. Overall, the results indicate that crack opening profiles measured by DIC can be used to estimate tip-wise stress intensity factors directly, reducing dependence on complex full-field simulations and providing a robust experimental tool for fracture mechanics in non-ideal engineering geometries.

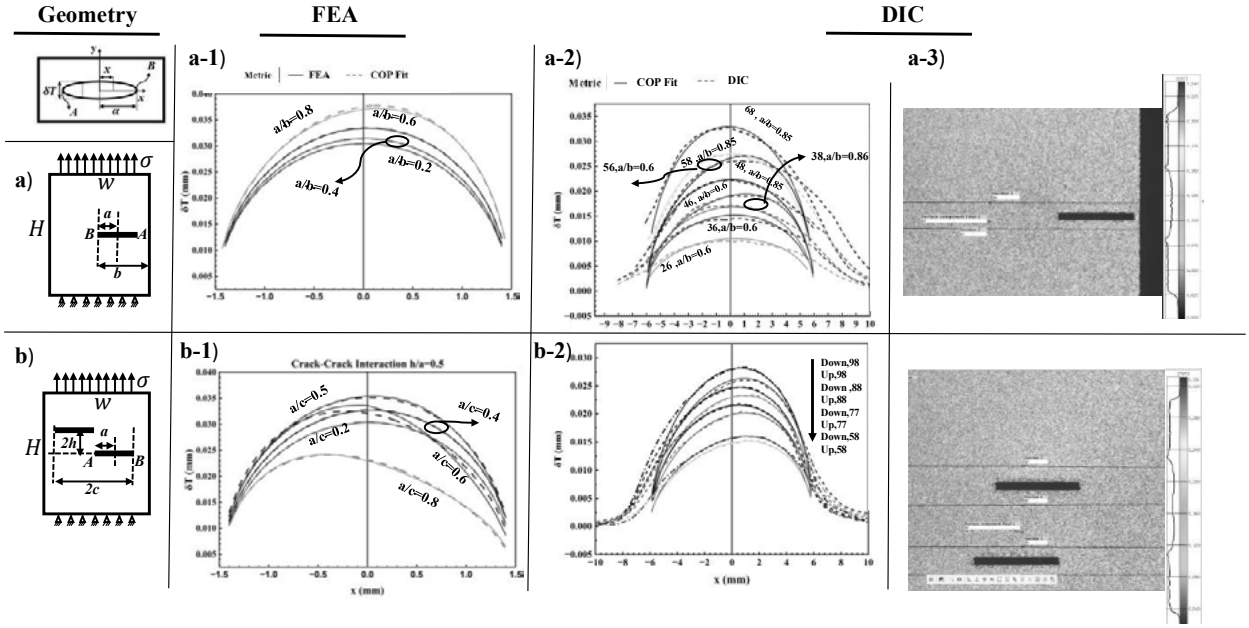

Figure 1. Numerical and experimental crack opening profiles for interacting cracks. (a) Crack–edge configuration: (a-1) FEA crack opening profiles and COP fits for different a/b ratios; (a-2) corresponding DIC-measured profiles at different load steps; (b) Crack–crack configuration: (b-1) FEA crack opening profiles and COP fits for different a/c ratios; (b-2) DIC-measured profiles for $a/c = 0.8$ at different load levels; (a-3), (b-3) DIC speckle images before crack propagation.

REFERENCES

1. Vasco-Olmo, J.M.; Díaz, F.A.; Antunes, F.V.; James, M.N. Experimental characterisation of fatigue crack growth based on the CTOD measured from crack tip displacement fields using DIC. Frattura ed Integrità Strutturale, 49, 658–666 (2019).
2. Allahdiniyan, A.; Taylor, D. Using crack face displacement to measure stress intensity. Theor. Appl. Fract. Mech., 134, 104184 (2025).
3. Westergaard, H.M. Bearing pressures and cracks. J. Appl. Mech., 6, A49–A53 (1939).

Contact edge and crack tip eigensolutions are the same

David HILLS[1]

[1] Department of Engineering Science, University of Oxford, Parks Road, Oxford OX1 3PJ

david.hills@eng.ox.ac.uk

Cracks nucleate not infrequently from the edges of contact, which act as stress concentrators and which often display fretting damage arising from slip which stems from small fluctuations in load, usually arising from vibration. Because the location of nucleation is known it is feasible to describe the nucleation environment using a set of eigensolutions which may be used to match the edge of a prototype to a laboratory experiment. Here, we restrict ourselves to non conforming contacts (where the contact edge position depends on the load); this encompasses a wide range of practical problems include gas turbine blade dovetail roots, firtree roots and locking segments for risers. A recent observation is that all contact edges of this class display behaviour which is the same as that at a crack tip, which has far-reaching consequences.

Some contact problems may be modelled using a half-plane representation of each body, but even when this is not possible -such as when we have a pin journalled in a slightly larger hole - points may always be found in the region of the contact edge which are distant from other features so that *locally* the bodies behave like half planes. A powerful result by Andersson and colleagues [1] shows that under cyclic loading any transient frictional slip region will shake down to a stuck state, so that under any small oscillatory load cyclic slip is restricted to a very small region at the contact edge. Thus, most of the contact interface is stuck (and hence tractions, displacements are continuous across it), like continuous material, and hence the domain is one of two half-planes 'bonded' up to the contact edge – exactly like a crack tip. In the case of a crack tip the implied elastic singularity is relieved by plastic slip; in the case of a contact edge it is usually relieved by frictional slip, although possibly, in some very heavily loaded cases, also by plasticity.

The basic description of the steady state contact edge problem is therefore straightforward: the contact is subject to whatever mean loads are present, giving rise to modes *I* and *II* loading. The mode I element gives rise to a square root bounded contact pressure at the contact edge so that, if the contact edge is located at point a, the local pressure will be of the form $p(x) = L_I\sqrt{a-x}$, where L_I depends on the contact geometry and the attendant stress field is that of the third (square root bounded) term in a Williams expansion for a wedge of total included angle 2π radians[2].

As discussed, subsequent small fluctuations in load are now experienced by what is effectively a crack tip, and, if the two bodies are glued together at this mean contact length, they will generate square root singular terms K_I, K_{II}. The latter is relieved by plastic slip and the former by a small movement of the contact edge. Note, too, that what we normally think of as the T-stress in fracture mechanics notation (the second term in a series expansion) is simply the stress parallel with the free surface of the contact, and this, too, will play an influence.

The process of relaxation of the singular terms will be derived in full [3], but, in summary, if the contact edge is now permitted to change it will move with an amplitude Δa. This is related to the quantities defined by $\Delta a = 2K_I/L_I$. Similarly, the mode II singularity is relaxed by permitting slip, and if the length of the cyclic slip length is d, $d = 2K_{II}/fL_I$, where f is the coefficient of fiction.

The expenditure of frictional energy per cycle, in a pointwise sense, has also been found as have other internal properties of the solution, but the more important practical result is that we can see that by matching up L_I, K_I, K_{II} in a laboratory test we may expect the test and prototype to have precisely the same crack nucleation behaviour. Thus, just as we can establish crack propagation life by establishing (say) the coefficients in a Paris-type equation, we should also be able to establish nucleation lives in laboratory tests of wide ranging applicability in terms of, at most, these three quantities. In the case of finite lives complications will arise because of the transition from the nucleation field to the propagation field, but the conditions for a nucleation threshold should be straightforward to sort out and free of complications. Re-working of existing experimental data obtained under constant load conditions (so $K_I = 0$) shows a well defined threshold condition dependent mainly on K_{II} [4], so the next steps in a development of the process are to look more carefully at the effects of the mean (L_I) and fluctuating (K_{II}) normal load.

REFERENCES

1. Andersson, L.-E.; Barber, J.R.; Ponter, A.R.S. Existence and uniqueness of attractors in frictional systems with uncoupled tangential displacements and normal tractions. Int. J. Solids Struct., 51, 3710–3714 (2014).
2. Barber, J.R. Elasticity, 4th ed., Springer, 154–163 (2022).
3. Barber, J.R.; Hills, D.A. Periodic loading of a frictional contact. J. Mech. Phys. Solids, under review.
4. Barber, J.R.; Hills, D.A. Fretting fatigue starting from the edges of incomplete contacts under general periodic loading. Theor. Appl. Fract. Mech., 139, 105054 (2025).

Characterisation of the stress field around a flat elliptical crack: crack onset by the coupled criterion

Pietro CORNETTI[1], Alberto SAPORA[1], Vladislav MANTIČ[2], Zohar YOSIBASH[3]

[1] Department of Structural, Geotechnical and Building Engineering, Politecnico di Torino, Corso Duca degli Abruzzi 24, 10129 Torino, Italy
[2] Grupo de Elasticidad y Resistencia de Materiales, Escuela Técnica Superior de Ingeniería, Universidad de Sevilla, Camino de los Descubrimientos s/n, Sevilla, 41092, Spain
[3] Computational Mechanics and Experimental Biomechanics Lab, School of Mechanical Engineering, Iby and Aladar Fleischman Faculty of Engineering, Tel Aviv University, Ramat Aviv 69978, Israel

pietro.cornetti@polito.it

In recent years, the coupled criterion of Finite Fracture Mechanics (FFM), first introduced by Leguillon [1], has been effectively applied to a variety of material and geometric configurations. However, most studies so far have focused on two-dimensional cases. In this paper, we examine a simple yet demanding three-dimensional problem, namely the flat elliptical crack, and present the results in analytical form.

FFM is based on the idea that cracks, particularly at their initiation, propagate in a finite and discontinuous manner, advancing through discrete increments known as crack steps [1]. This approach has demonstrated strong effectiveness as a fracture criterion for estimating the applied stress responsible for crack initiation in two-dimensional geometries. Efforts have been made to generalize the method to three-dimensional cases [2], but this extension introduces additional challenges. In particular, differently from 2D configuration, the failure stress is influenced not only by the magnitude of the crack increment but also by its shape.

In this study, we concentrate on the analysis of flat elliptical cracks subjected to uniform remote stresses acting perpendicular to the crack plane (Fig.1). This problem can be interpreted as a direct extension of the penny-shaped crack configuration previously investigated using FFM in [3]; however, in this case, the radial symmetry is no longer present.

On the crack plane (x, y), only the normal stress component σ_z is present. Its distribution over the entire crack surface can be obtained from the full solution provided by Green and Sneddon [4], and is given by:

$$\frac{\sigma_z}{\sigma_\infty}=1+\frac{1}{E(k^2)}\left[\frac{a}{\sqrt{\xi}}\sqrt{\frac{b^2+\xi}{a^2+\xi}}-E\left(\arcsin\frac{a}{\sqrt{a^2+\xi}}\,\middle|\,k^2\right)\right] \tag{1}$$

where a and b are respectively the major and minor semi-axes of the ellipse describing the crack, k is the eccentricity, σ_∞ is the remote applied stress, $E(\cdot|\cdot)$ is the incomplete elliptical integral of the second kind and $E(\cdot)$ is its complete counterpart; ξ is an ellipsoidal coordinate whose relationship with the cartesian coordinates (x,y) on the $z = 0$ plane is:

$$\frac{x^2}{a^2+\xi}+\frac{y^2}{b^2+\xi}=1 \tag{2}$$

Because of the applied remote stress, the elliptical crack opens, taking the shape of an ellipsoid whose semi-axes are a,b and $w_{\max}$. The third one, representing half of the crack opening at the crack centre, is:

$$w_{\max} = \frac{2\sigma b}{E(k^2)E'} \tag{3}$$

E' being the material Young's modulus in plane strain conditions. Based on Eqs. (1-3), Linear Elastic Fracture Mechanics (LEFM) can be applied by considering an infinitesimal crack extension of arbitrary elliptical shape. A natural assumption is to adopt an iso-stress crack increment. This hypothesis is equivalent to assuming that the crack advance occurs normal to the crack front and is proportional to the square of the Stress Intensity Factor (SIF) at each point, or, alternatively, that the equivalent Strain Energy Release Rate (SERR) - the value to be compared with the material's fracture energy for crack propagation - is given by the contraharmonic mean of the SERR distribution along the crack front.

Nevertheless, if the crack grows infinitesimally by extension of the minor axis only, this configuration always yields the maximum energy release rate and is therefore the most favourable within the LEFM framework. A similar investigation can be carried out using the FFM approach. In this case, however, the conclusions differ: there exists a threshold crack size below which a finite iso-stress crack extension becomes more favourable, as it satisfies the onset condition at a lower remote stress level. This threshold depends on both the eccentricity of the ellipse and Irwin's characteristic length. As a result, minor-axis crack growth is expected for highly eccentric cracks, large crack sizes, and very brittle materials, whereas iso-stress crack growth dominates for nearly circular cracks, small defects, and materials with lower brittleness, as illustrated in Fig. 1.

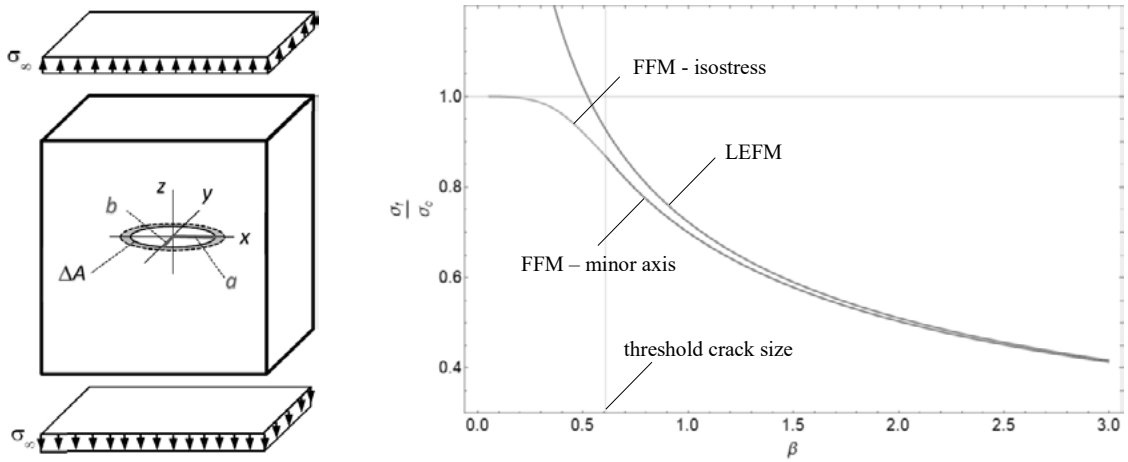

Figure 1. Failure remote stress σ_f vs. crack size for $b/a = 0.5$; σ_c is the tensile strength, $\beta = b / l_{ch}$ the dimensionless crack size, l_{ch} is Irwin's material length, ΔA is the finite crack extension.

REFERENCES

1. Leguillon, D. Strength or toughness? A criterion for crack onset at a notch. Eur. J. Mech. A Solids, 21, 61–72 (2002).
2. Yosibash, Z.; Mittelman, B. A 3-D failure initiation criterion from a sharp V-notch edge in elastic brittle structures. Eur. J. Mech. A Solids, 60, 70–94 (2016).
3. Cornetti, P.; Sapora, A. Penny-shaped cracks by finite fracture mechanics. Int. J. Fract., 219, 153–159 (2019).
4. Green, A.E.; Sneddon, I.N. The distribution of stress in the neighborhood of a flat elliptical crack in an elastic solid. Proc. Cambridge Philos. Soc., 46, 159–164 (1950).

Fracture toughness of cast and additively manufactured aluminium – silicon – magnesium alloys with copper addition for automotive applications

Nikolaos D. ALEXOPOULOS[1], Ioannis GOULAS[1,2], Alexis KERMANIDIS[2], Leonard ALBERTY[3], Ismail ÜNSAL[3], Georg SCHLICK[3]

[1] University of the Aegean, Department of Financial and Management Engineering, Research Unit of Advanced Materials, 82100, Chios, Greece
[2] University of Thessaly, Department of Mechanical Engineering, Laboratory of Mechanics and Strength of Materials, Volos, 38334, Greece
[3] Fraunhofer Institute for Casting, Composite and Processing Technology IGCV, Am Technologiezentrum 10, 86159 Augsburg, Germany

nalexop@aegean.gr

Cast Aluminium – Silicon – Magnesium (Al-Si-Mg) alloys are widely employed to produce complex-shape aeronautical and automotive components owing to their excellent castability and favourable strength-to-weight ratio. Key factors governing the mechanical properties of the alloy are classified into two principal categories: (a) those predominantly determined by the casting process, and (b) those governed by the alloy's physical metallurgy, e.g. [1]. Enhanced controls and advancements in modern casting processes have significantly minimized structural defects—such as porosity (pores) and oxide bifilms—in cast components. These defects act as stress concentrators and crack initiation sites, severely compromising key mechanical properties like tensile mechanical strength, tensile ductility, as well as fatigue resistance, as previously documented e.g. [1]-[3].

Additive Manufacturing (AM), also known as layered manufacturing, encompasses fabrication techniques that progressively deposit material—typically in a layer-by-layer fashion—guided by a three-dimensional (3D) Computer Aided Design (CAD) model. AM constructs components by sequentially adding material rather than removing it, thereby substantially enhancing design freedom and facilitating the fabrication of intricate geometries that are challenging or infeasible with traditional manufacturing techniques. In recent years, AM technologies have attracted significant interest for their capacity to minimize material waste, accelerate development timelines, and enable the creation of bespoke, lightweight components. These benefits render AM especially appealing for high-performance sectors like aerospace, and automotive, which demand intricate geometries and customized material characteristics.

The common ground for cast and additively manufactured Al-Si-Mg alloys is the presence of copper (Cu) element. For such aluminium castings, in order to increase the quasi-static yield stress (R_p) it was recommended to add Cu [4], aiming to increase the mechanical properties by solid solution strengthening as well as by precipitation hardening. Cu addition therefore not only increases the rate at which β'' (Mg_2Si) precipitates [5] but also results in the precipitation of the quartenary Q' ($Al_5Cu_2Mg_8Si_6$) phase when Cu additions are less than 1.0 wt.% [4, 6]. In the present work, microstructure and fracture surfaces of the tensile specimens of cast Al-7Si-Mg alloys having different minor additions of Cu, Ag, and Sm will be quantitatively analysed. Fracture toughness experiments will be analysed and fracture toughness K_{cr} will be evaluated. Tensile ductility and fracture toughness will be post-correlated to microstructural characteristics

in order to seek the critical microstructure features that govern each macroscopical mechanical property.

For additively manufactured specimens, there is a current trend for bi-metallic printing of Al-Cu components for electric car vehicles that needs to be printed with copper wiring included for electrical circuits. In this regard, additive manufacturing of bi-metals, e.g. AlSiMg/CuCrZr products is feasible, nevertheless there is high probability of cross-contamination with Cu powder and for different concentrations. The effectiveness of laser powder bed fusion in such combinations, however, can be constrained by particle contamination, which often affects the integrity of the printed structure [7]. Previous studies have shown that the introduction of foreign particles in the metal powder feedstock not only alters microstructural characteristics but also has adverse effects on tensile mechanical properties as well as fatigue life [8, 9]. Several powder contamination grades ranging from 0.5 to 5.0 volumetric percent (vol. %) are processed and compared with uncontaminated powder feedstock for both cases. In the present contribution, a preliminary study was performed to investigate the resistance to fracture of additively manufactured AlSi10Mg material with varying thicknesses. To this end, fracture toughness specimens of compact tension geometry with varying thicknesses from 3 to 15 mm were additively manufactured using PBF-LB/M, machined and tested. The results showed that with increasing the specimen thickness, critical stress intensity factor K_{cr} decreases gradually from 38 MPa√m up till 31 MPa√m for the lower and higher investigated thicknesses, respectively. As a second step, the effect of Cu cross-contamination level was related to the fracture toughness values of additively manufactured specimens and valuable comments on the fracture mechanisms were pointed out.

REFERENCES

1. Campbell, J. The new metallurgy of cast metal castings, 2nd ed., Butterworth-Heinemann, (2003).
2. Tiryakioğlu, M.; Campbell, J.; Staley, J.T. The influence of structural integrity on the tensile deformation of cast Al-7Si-0.6Mg alloys. Scr. Mater., 49, 873–878 (2003).
3. Nyahumwa, C.; Green, N.R.; Campbell, J. Influence of casting technique and hot isostatic pressing on the fatigue of an Al-7Si-Mg alloy. Metall. Mater. Trans. A, 32A, 349–358 (2001).
4. Chakrabarti, D.J.; Laughlin, D.E. Phase relations and precipitation in Al-Mg-Si alloys with Cu additions. Prog. Mater. Sci., 49, 389–410 (2004).
5. Murayama, M.; Hono, K.; Miao, W.F.; Laughlin, D.E. The effect of Cu additions on the precipitation kinetics in an Al-Mg-Si alloy with excess Si. Metall. Mater. Trans. A, 32A, 239–246 (2001).
6. Li, Y.J.; Brusethaug, S.; Olsen, A. Influence of Cu on the mechanical properties and precipitation behavior of AlSi7Mg0.5 alloy during aging treatment. Scr. Mater., 54, 99–103 (2006).
7. Herzog, D.; Seyda, V.; Wycisk, E.; Emmelmann, C. Additive manufacturing of metals. Acta Mater., 117, 371–392 (2016).
8. Horn, M.; Schlick, G.; Lutter-Guenther, M.; Anstaett, C.; Seidel, C.; Reinhart, G. Metal powder cross-contaminations in multi-material laser powder bed fusion: influence of CuCr1Zr particles in AlSi10Mg feedstock on part properties. Proceedings of the Lasers in Manufacturing Conference, 1–11 (2019).
9. Mumtaz, K.A.; Hopkinson, N. Selective laser melting of aluminum and copper materials for multi-material production. Addit. Manuf., 31, 100970 (2020).

Three-dimensional elasto-plastic simulation of fatigue crack growth using non-conforming finite element meshes

Diogo NETO[1], Edmundo SÉRGIO[1], Fernando ANTUNES[1]

[1] Centre for Mechanical Engineering, Materials and Processes, University of Coimbra, Portugal

diogo.neto@dem.uc.pt

Fatigue crack growth (FCG) is governed by complex interactions between plastic deformation, crack closure, and three-dimensional stress states along the crack front. Conventional two-dimensional numerical models, which assume either plane stress or plane strain simplifications, fail to capture these coupled effects, particularly in thin specimens where the stress state varies continuously across the thickness. In this study, a fully three-dimensional elasto-plastic model is developed to simulate FCG under constant-amplitude loading in a pure titanium CT specimen. The numerical framework explicitly accounts for crack closure and employs non-conforming finite element meshes with a minimum element size of 8 μm, enabling accurate crack-front evolution without remeshing. Simulations were performed on a 1 mm-thick specimen, allowing direct observation of the stress-state transition and its influence on local fatigue mechanisms.

Considering the crack propagation from the left to the right, the plastic strain fields in the crack plane, obtained after 5, 100 and 300 load cycles, are presented in Figures 1a-c, respectively, showing a smooth plastic strain distribution. Initially there is steep gradient of plastic strain from the surface to the middle section, indicating that the model is changing the initial straight crack shape. Similar results were obtained by Camas *et al.* [1]. After 100 load cycles, the crack already shows the typical curvature, with a higher crack length in the middle section [2]. Additionally, the plastic zone size is maximum close to the free surface, but not on the free surface.

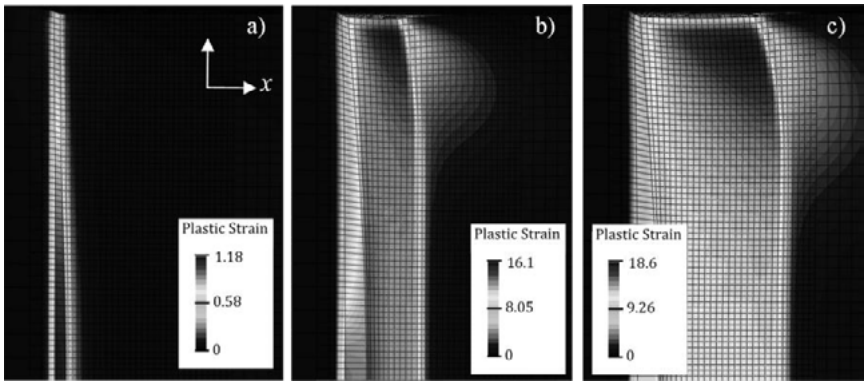

Figure 1. Plastic strain fields in the crack plane, considering the non-conforming mesh, after: (a) 5 load cycles, (b) 100 load cycles and (c) 300 load cycles.

The considered 3D FCG framework allows to predict non-straight crack front geometries, that occurs due to several mechanisms/conditions. Figure 2 presents the evolution of the crack front curvature during the initial propagations. The results show that the initial straight crack tends to accumulate a certain degree of curvature with the successive crack extensions. This transient behaviour is caused by the evolution of the plastic fields. The stationary curvature in the final extensions indicates that a stable FCG regime has been achieved.

The stress state along the crack front was analysed to evaluate the plane strain/stress dominance. The stress state metric considers the magnitude of the out of plane stress in relation to the von Mises equivalent stress, as plane stress is characterized by a null Cauchy stress component in this direction. This crack front stress state is presented in Figure 3, at maximum and minimum load instants for various crack lengths. The results show that the out of plane stress component is higher than the equivalent stress in almost all the material bulk, with the ratio decreasing the unity only for a thickness of ≈ 0.41 mm. This means that, despite the very small thickness of the specimen, the plane stress condition is not verified in the majority of the material bulk, indicating that plane stress is not the dominant state at the crack front.

The work demonstrates strong three-dimensional variations in plastic strain, crack opening displacement, and crack-tip shielding, which cannot be reproduced by conventional 2D approaches.

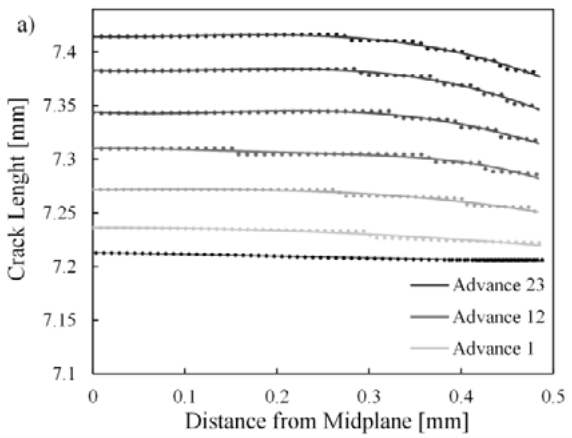

Figure 2. Crack front curvature at several crack lengths, presenting an evolution of the crack concavity with the successive crack extension.

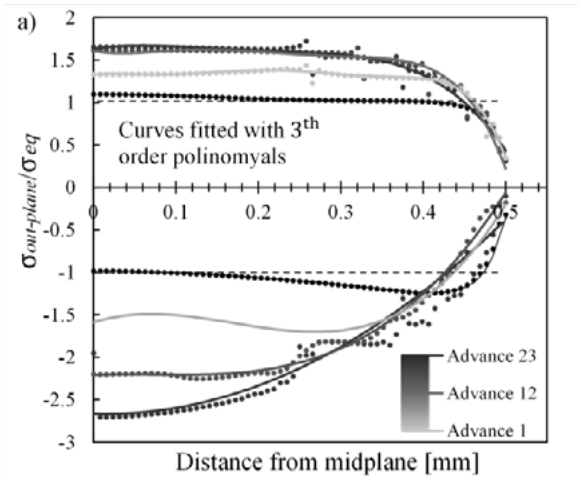

Figure 3. Stress state characterized by the magnitude of the out of plane stress in relation to the von Mises equivalent stress for several crack lengths.

REFERENCES

1. Camas, D.; Garcia-Manrique, J.; Gonzalez-Herrera, A. Crack front curvature: influence and effects on the crack tip fields in bi-dimensional specimens. Int. J. Fatigue, 44, 41–50 (2012).
2. Besel, M.; Breitbarth, E. Advanced analysis of crack tip plastic zone under cyclic loading. Int. J. Fatigue, 93, 92–108 (2016)

The apparent success of ΔK_{eff}-based codes revisited through crack tip stress–strain field analyses

Jaime Tupiassú Pinho de CASTRO[1], Marco Antonio MEGGIOLARO[1], Rafael César de Oliveira GÓES[1], Antonio Carlos de Oliveira MIRANDA[2]

[1] Pontifical Catholic University of Rio de Janeiro, PUC-Rio, Brazil
[2] University of Brasilia, UnB, Brazil

jtcastro@puc-rio.br, meggi@puc-rio.br, rafael.goes@petrobras.com.br, acmiranda@unb.br

González et al. [1] made a comprehensive series of fatigue crack growth (FCG) tests to check if they were controlled by the effective stress intensity factor (SIF) range $\Delta K_{eff} = K_{max} - K_{op}$. In those tests the FCG rates da/dN remained essentially constant under fixed $\{\Delta K, R = K_{min}/K_{max}\}$ loads, but the *measured* K_{op}/K_{max} ratio between the opening K_{op} and peak SIFs K_{max} changed significantly while the cracks grew. This indicates that their FCG driving force was ***not*** ΔK_{eff}. However, ΔK_{eff}-based codes have been used successfully to estimate FCG lives in many engineering applications. This apparent contradiction naturally raises the question of why such methods can work in practice, if their ΔK_{eff} hypothesis is not generally valid. The reliability of González's results has sometimes been questioned for this reason, even though the corresponding experiments are straightforward and readily reproducible in any well-equipped fatigue laboratory.

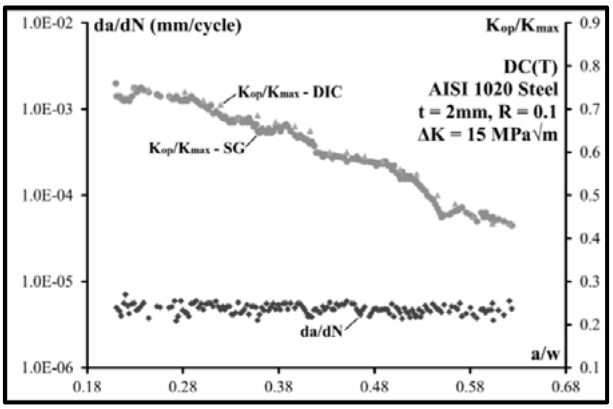

Figure 1. da/dN and K_{op}/K_{max} rates continuously and redundantly measured by near and far-field DIC and compliance techniques under $\{\Delta K = 15MPa\sqrt{m},\ R = 0.1\}$ fixed loading conditions in a thin 1020 steel DC(T) specimen, with *2mm* thickness.

Ferreira et al. [2] addressed this issue by revisiting Newman's strip-yield mechanics [3]. Although Newman's original elastoplastic (EP) bar elements ahead of and behind crack tips were devised to estimate K_{op} loads from the plastic wake and the associated crack-face interference, the same framework can also be used to estimate the strain distribution *ahead* of the crack tips, as schematically indicated in Fig. 2. Using this idea, Ferreira showed that da/dN versus ΔK curves, for various stress ratios $R = K_{min}/K_{max}$, can be predicted from the crack-tip strain field using εN fatigue crack *initiation* properties and proper damage accumulation concepts, indicating that the key physical quantity is the local cyclic elastoplastic field ahead of the crack tip rather than ΔK_{eff} itself. A central concept behind this approach is that an open crack tip is not singular in a physical

sense, but instead operates under very high yet finite strains related to the crack-tip opening displacement. This feature is already implicit in Newman's bar-element description and in the subsequent damage-based interpretations built upon it. Ferreira's analyses also showed that crack closure may affect fatigue damage, but much less strongly than assumed by the classical ΔK_{eff} hypothesis, because closure mainly modifies the local loading cycle instead of completely suppressing crack-tip deformation below K_{op}.

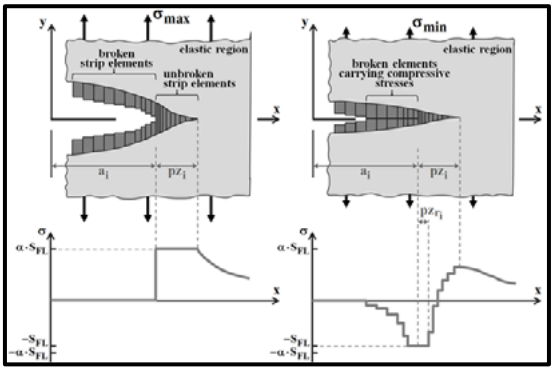

Figure 2. Crack surface displacements and stress distribution along the crack line.

These arguments are consistent with the experimental evidence that Elber's original idea cannot be universally correct. Even so, ΔK_{eff}-based procedures may still provide reasonable life estimates because in many cases the width of the EP $\Delta\sigma\Delta\varepsilon$ stress/strain loops ahead of crack tips, which depends on ΔK and K_{max}, is only weakly affected by K_{op}. This is especially true when K_{op} is associated with the elastic part of the loops rather than with their plastic part, the one directly related to fatigue damage. In this sense, the practical success of closure-based life-prediction codes does not necessarily validate ΔK_{eff} as the physical driving force for FCG; instead, it suggests that such codes may work because they correlate indirectly with the cyclic stress/strain fields that actually govern the FCG behavior around crack tips.

Motivated by this interpretation, the objective of the present work is to extend the ideas behind Newman's simplified mechanics using more advanced EP finite-element analyses to directly evaluate the cyclic stress/strain fields generated by the growing fatigue crack. The focus here is to quantify how K_{op}, ΔK, and K_{max} affect the local stress/strain fields ahead of fatigue crack tips, especially within the reverse plastic zones that always follow them, providing a sound physical explanation for the experimental trends reported by González et al., and justifying the mechanistic interpretation presented above. In addition, this approach may enable future analyses of multiaxial FCG effects, particularly those associated with T-stress influences on plastic-zone sizes and on the distribution of cyclic stresses and strains ahead of crack tips.

REFERENCES

1. González, J.A.O.; Castro, J.T.P.; Gonzáles, G.L.G.; Meggiolaro, M.A.; Freire, J.L.F. Challenging the "ΔKeff is the driving force for fatigue crack growth" hypothesis. Int. J. Fatigue, 136, 105577 (2020).
2. Ferreira, S.E.; Castro, J.T.P.; Meggiolaro, M.A.; Miranda, A.C.O. Crack closure effects on fatigue damage ahead of crack tips. Int. J. Fatigue, 125, 187–198 (2019).
3. Newman, J.C. Jr. Prediction of fatigue crack growth under variable-amplitude and spectrum loading using a closure model. Design of Fatigue and Fracture Resistant Structures, ASTM STP 761, 255–277 (1982).

Accurate modelling of elastic-plastic material behaviour for FCG analysis

Fernando ANTUNES[1], Diogo NETO[1], Edmundo SÉRGIO[1]

[1] CEMMPRE, Department of Mechanical Engineering, University of Coimbra

fernando.ventura@dem.uc.pt

Numerical simulation of fatigue crack growth (FCG) presents different complexities, namely, simulation of 3D crack propagation, simulation of realist load patterns and modelling of material behaviour. This study addresses this last complexity, which usually is not properly handled.

In ductile materials, cyclic plastic strain at the crack tip is widely accepted as the primary driving mechanism for FCG. The proper simulation of FCG assuming this damage mechanism requires the accurate modelling of material elastoplastic behaviour, and particularly of isotropic and kinematic hardening. Conventional approaches typically focus on the cyclic response of the material, using data obtained from low-cycle fatigue (LCF) tests to fit the material constants. However, the strain ranges usually applied in the LCF tests are relatively small, when compared to the crack tip ranges and cumulative strains observed at the crack tip. Also, tensile-compressive asymmetry is often overlooked. Finally, the monotonic behaviour may play a role, particularly in the presence of overloads.

This study aims to analyse different issues in this context, namely: (i) how the material's monotonic behaviour affects the predictions FCG under constant and variable amplitude loading conditions; (ii) what is the impact of different constitutive models, all well fitted to the cyclic behaviour; on FCG predictions; (iii) define a strategy to choose the best model among different proposals that can be defined from the same LCF and monotonic experimental results.

Results showed that, under constant amplitude loading, including monotonic tensile data in the material calibration procedure provides minimal benefit. However, under variable amplitude loading, incorporating monotonic behaviour increases the overload-affected zone (Figure 1a), leading to results that more closely match the experimental observations (Figure 1b).

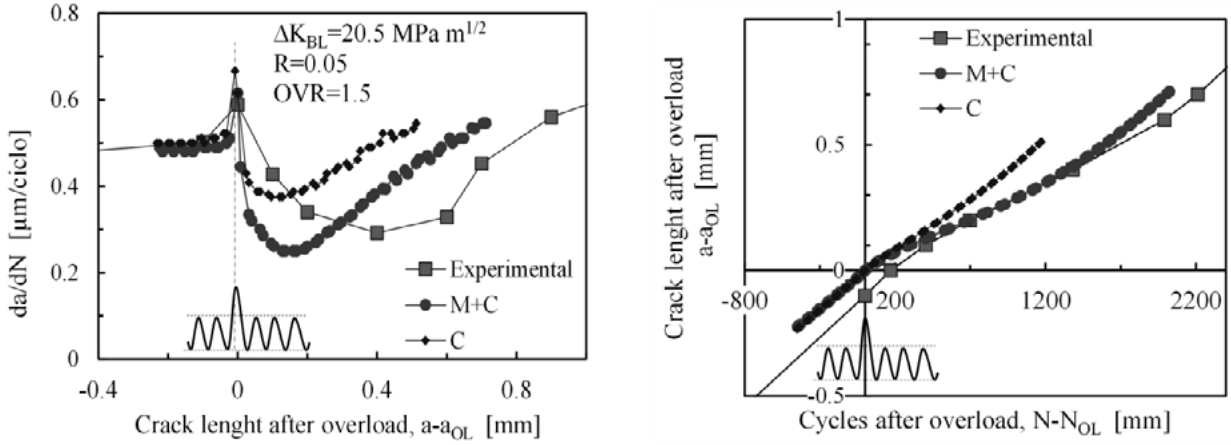

Figure 1. Comparisons of models fitted with LCF results (C) and with monotonic and LCF results (C+M) of titanium. (a) da/dN-ΔK results. (b) crack length versus number of load cycles.

A strategy to check the quality of the numerical model was proposed in a previous work [2]. A comparison was made between DIC experimental results and numerical predictions obtained with FEM in CT specimens with a thickness of 1 mm made of 2024-T3 aluminium alloy. Three material models were considered. The first one was obtained assuming Swift and Lemaître-Chaboche hardening laws for isotropic and kinematic hardening, and using only LCF experimental results. In the second approach the LCF fatigue results were complemented with monotonic results (C+M). In the third proposal, the Swift law was replaced by Voce's law in the characterization of isotropic hardening, and both cyclic and monotonic curves were fitted. Figure 2 shows that a good fitting is obtained with the third model, although the other two also had a good fitting to the LCF results. The change of isotropic hardening to Voce significantly increased COD_p, putting it in the scatter band of the experimental results.

Accordingly, a suggestion for a proper identification of material constants, and therefore for a better modelling of elastic-plastic behaviour, was: (i) consider one LCF stress-strain curve with a relatively large strain range; (ii) consider the monotonic curve; (iii) Define alternative models for the characterization of elastic-plastic behaviour; (iv) test the models in a thin CT specimen performing a DIC-FEM validation.

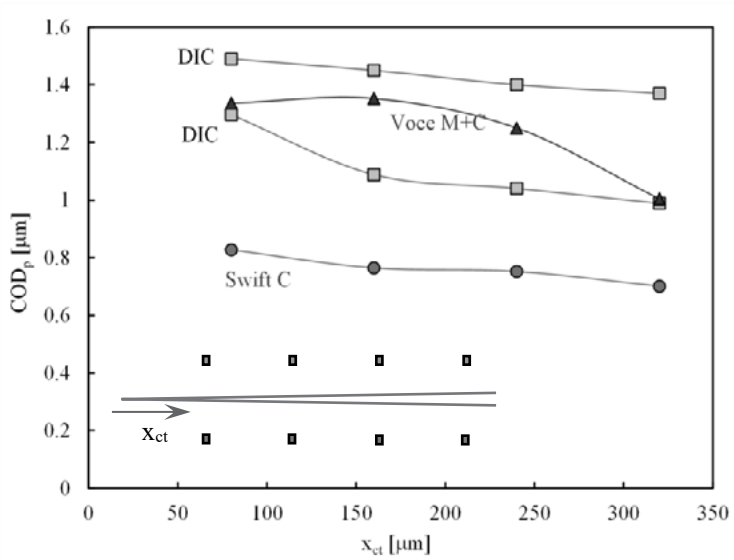

Figure 2. Plastic CTOD versus horizontal distance to crack tip (x_{ct}) evaluated in a CT specimen with 1 mm of thickness made of 2024-T3 aluminium alloy.

REFERENCES

1. Sérgio, E.R.; Antunes, F.V.; Neto, D.M. Improving the fatigue crack growth prediction by accurate calibration of the constitutive material parameters. Theor. Appl. Fract. Mech., 138, 104957 (2025).
2. Sérgio, E.R.; Gómez Gonzáles, G.L.; Vasco-Olmo, J.M.; Antunes, F.V.; Prates, P.; Díaz, F.A.; Neto, D.M. A comparison between FEM predictions and DIC results of crack tip displacement field in AA2024-T3 CT specimens. Eng. Fract. Mech., 318, 110964 (2025).

Discussion on the crack driving force along the 3D crack front of an internal short fatigue crack emanating from an internal defect

Thierry PALIN-LUC[1,2], Jean-Yves BUFFIERE[3], Nicolas RANC[4]

[1] Univ. Bordeaux, CNRS, Bordeaux INP, I2M, UMR 5295, F-33400, Talence, France
[2] Arts et Metiers Institute of Technology, CNRS, Bordeaux INP, I2M, UMR 5295, F-33400 Talence, France
[3] INSA Lyon, MATEIS, CNRS UMR 5510, F-69621 Villeurbanne, France
[4] PIMM Laboratory, Arts et Metiers Institute of Technology, CNRS, Cnam, HESAM University, Paris, France

thierry.palin-luc@ensam.eu

In metallic alloys, it is well known that very low stress amplitudes leading to very long life promote internal fatigue cracks whereas under higher load levels, leading to high cycle fatigue regime, surface crack initiations are most frequently observed. Even if these typical scenari are known for more than 25 years, in literature there are only a few direct observations of this mechanism for internal cracks [1-3]. Internal crack initiation is usually explained by the presence of material defects (non metallic inclusions, pores, shrinkages...) even if non-defect induced subsurface crack initiations are also reported. Many authors claim that in VHCF regime crack initiation dominates the total fatigue life compared to the crack growth duration. However, in-situ synchrotron ultrasonic fatigue tests under fully reversed tension on a cast Al-Si alloy by Messager et al. [2] demonstrated that a fatigue crack initiated from an internal defect can first propagate, then stops and another crack can initiate elsewhere from the same defect and finally leads to final fracture of the specimen in VHCF regime for σ_{max}~60% of σ_y.

Such observations were carried out on smooth specimens (diameter 3 mm) in cast aluminum alloy (mean grain size 600 µm) containing an artificial internal defect. X-ray synchrotron tomography allowed us to observe and quantify internal crack growth rates all along the crack front after different number of loading cycles (Figure 1). Furthermore, before fatigue loading the grain orientations around the defect were characterized by DCT [4]. The artificial defect and the 3D real cracks were reconstructed from tomography and meshed.

Finite element analysis were carried out to compute, along the 3D crack front, the stress intensity factor ranges ΔK_I, ΔK_{II}, ΔK_{III}, and its equivalent value under mode I, ΔK_{eq} , with regard to the strain energy release rate, G. Two hypothesis were considered for the material: (i) homogeneous isotropic linear elastic, (ii) polycristal with anisotropic elasticity. The analysis of the stress intensity factor ranges shows high mode mixity along the 3D crack front (based on the real crack shape geometry). But the differences between the simulations for a polycrystalline material and an homogeneous one are small. This lead us to focus on the isotropic linear elastic simulations with an homogenous material. In that case, surprisingly ΔK_i (i=I, II, III) along the crack fronts (Figure 2) exhibit high values at some tortuous locations (high crack front curvatures) where the observed crack growth rates remain very small (less than 10^{-12} m/cycle, i.e. quasi-stopped crack). Since in such cases, it is tempting to regularize the values of ΔK along the crack front, these a priori non-consistent values (high ΔK and very low observed local crack growth rates) are discussed.

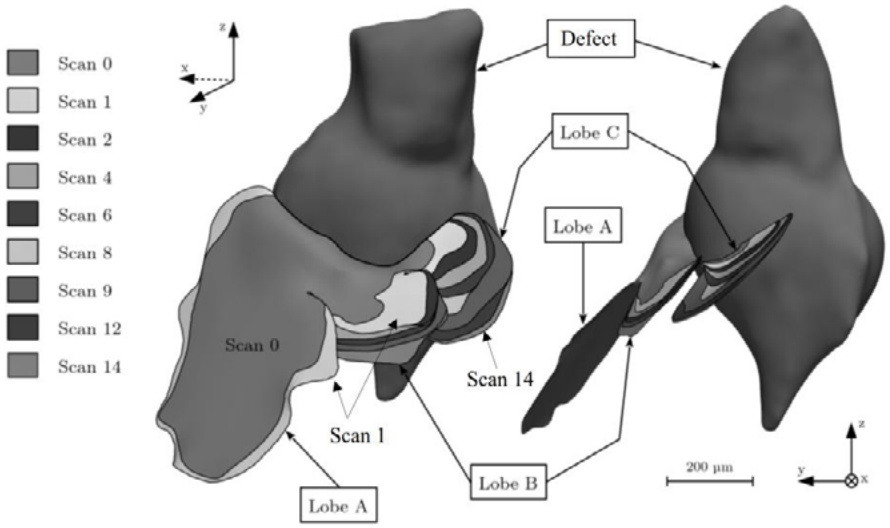

Figure 1. 3D rendering of an internal fatigue crack initiated from the internal defect under Ds/2=75 MPa and its evolution versus several number of cycles: scan 0 (N=1.85×10^7 cycles) and scan 14 (N= 1.99×10^7 cycles); 3 lobes (A, B and C) can be distinguished.

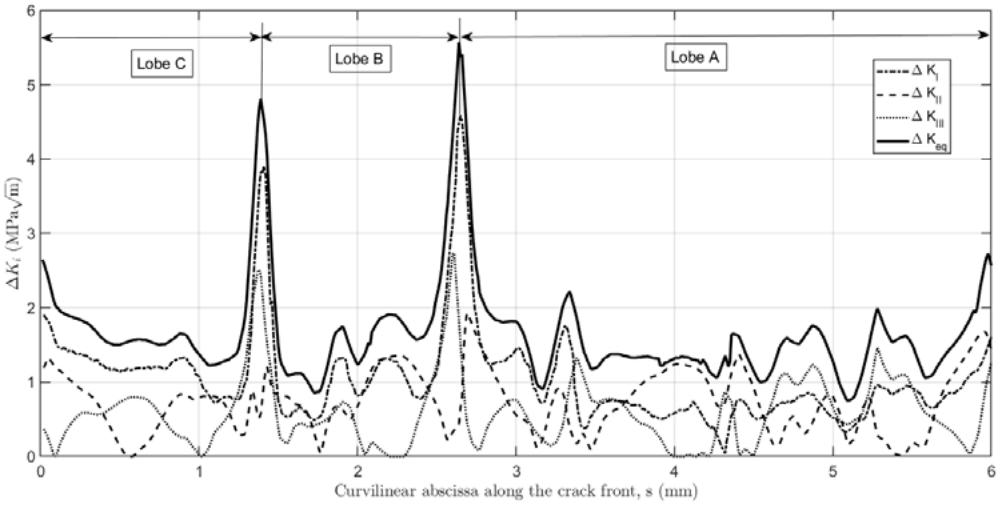

Figure 2. Evolution of the stress intensity factor ranges DK_I, DK_{II}, DK_{III}, DK_{eq}, along the front of the internal crack illustrated in Figure 1 at 1.85×10^7 cycles.

REFERENCES

1. Yoshinaka, F.; Nakamura, T.; Nakayama, S.; Shiozawa, D.; Nakai, Y.; Uesugi, K. Non-destructive observation of internal fatigue crack growth in Ti-6Al-4V by using synchrotron radiation μCT imaging. Int. J. Fatigue, 93, 397–405 (2016).
2. Messager, A.; Junet, A.; Palin-Luc, T.; Buffiere, J.-Y.; Saintier, N.; Ranc, N.; El May, M.; Gaillard, Y.; King, A.; Bonnin, A.; Nadot, Y. In-situ synchrotron tomography characterization of internal crack propagation in cast aluminum alloy in very high cycle fatigue regime. Fatigue Fract. Eng. Mater. Struct., 43, 558–567 (2020).
3. Hebrard, L.; Buffiere, J.-Y.; Palin-Luc, T.; Ranc, N.; Majkut, M.; King, A.; Weck, A. Environment effect on internal fatigue crack propagation studied with in-situ X-ray microtomography. Mater. Sci. Eng. A, 882, 145462 (2023).
4. Ludwig, W.; King, A.; Herbig, M.; Reischig, P.; Marrow, J.; Babout, L.; Lauridsen, E.M.; Proudhon, H.; Buffiere, J.-Y. Characterization of polycrystalline materials using synchrotron X-ray imaging and diffraction techniques. JOM, 62, 22–28 (2010).

Retardation effects of local crack branching in fatigue crack growth at different R-ratios in AA2024-T3

Florian PAYSAN[1], David MELCHING[1], Eric BREITBARTH[1]

[1] German Aerospace Center, Institute for Frontier Materials on Earth and in Space, Linder Höhe, 51147 Köln, Germany

eric.breitbarth@dlr.de

Fatigue crack propagation in ductile materials is governed by the interaction of damaging intrinsic and shielding extrinsic mechanisms. According to Ritchie [1], crack deflection and crack branching are classified as extrinsic mechanisms and can lead to crack growth retardation. At the microscopic scale, however, both the identification of crack branching and the quantification of its retardation effect remain challenging.

This talk addresses these challenges using six fatigue crack propagation experiments on MT160 specimens with a thickness of 2 mm made of the aluminum alloy AA2024-T3. Tests were conducted at R ratios of 0.1, 0.3, and 0.5 in L-T orientations. Crack branching is identified using a robot assisted DIC microscopy system [2], while crack tip loading is quantified via path independent J integral [3]. As an exact separation of the primary and secondary crack contributions to the crack driving force is difficult even with this approach, the influence of branching angle and branch length is additionally investigated using finite element simulations.

The experimentally obtained crack tip loadings from DIC displacement fields are correlated with the individual crack tip loadings of the primary and secondary cracks obtained from the simulations [4]. Therefore, we defined a linear elastic 2D finite element (E = 73 GPa, v = 0.33) model with linear plane elements under plane stress conditions and parameterized the crack path (see Figure 1). We are also able to model a branched crack path which is approximated by the lengths a and b as well as the angle between the branches. Using deep symbolic regression [5], we derived a retardation factor λ_{ret} to compute the reduced J integral of a primary crack with regard to the geometry of the secondary crack (see Equation 1).

$$\lambda_{\mathrm{ret}} = \tanh\left(\left(\frac{a}{b}\right)^{\alpha-\pi} + \alpha\right)^{\gamma} = \frac{J}{J_0} \tag{1}$$

Here, a and b represent the lengths of the crack branches, α is the angle between them, γ is a retardation exponent, J is the actual present driving force, and J_0 is the driving force of a crack without branching.

The numerical results are finally validated against the experimental observations. The results show that local crack branching primarily leads to a reduction in K_{max}, resulting in a temporary decrease in the fatigue crack growth rate which is mainly related to the angle between the primary and secondary cracks. Furthermore, the frequency of crack branching decreases with increasing R ratio, providing a mechanistic explanation for the observed R dependence of fatigue crack propagation curves.

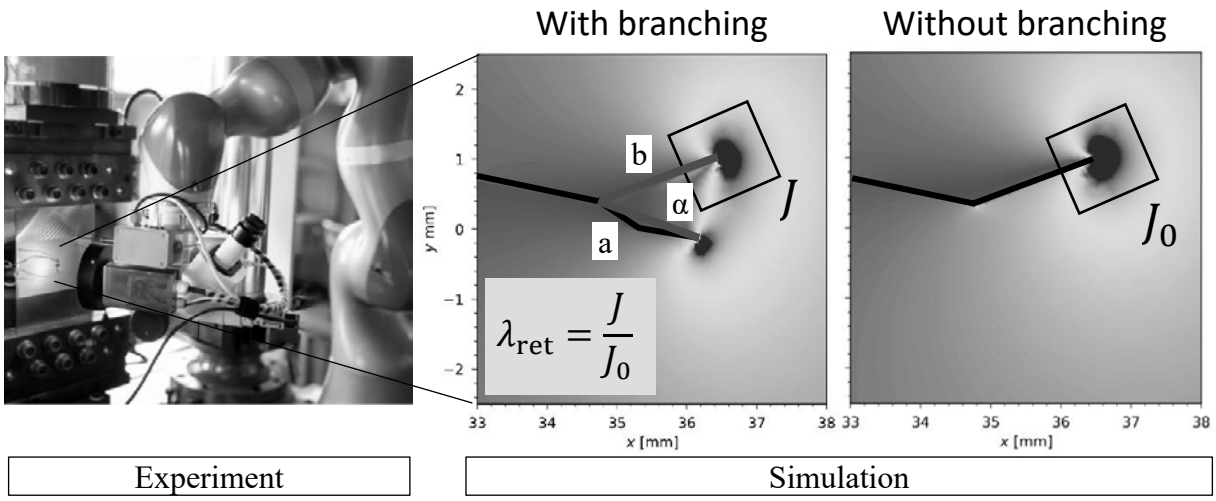

Figure 1. Simulation approach to investigate the crack driving force with regard to crack branching and secondary cracks

Finally, the simulations provide an explanation for the *R* ratio dependent characteristics identified in the experiments. Here, two interacting effects can be identified. First, the branching angle decreases, which leads to an acceleration of crack growth at *R* ratios greater than 0.1 and also contributes to the shift in the crack propagation curves. These results indicate that the *R* ratio behavior of the crack propagation curves is not exclusively attributable to crack closure effects. Second, the small branching angles at *R* ratios greater than 0.1 lead to a more uniform distribution of the crack tip loading compared to an *R* ratio of 0.1, causing the crack pairs to grow longer than at $R = 0.1$, thus increasing the secondary crack length.

REFERENCES

1. Ritchie, R.O. Mechanisms of fatigue-crack propagation in ductile and brittle solids. Int. J. Fract., 100, 55–83 (1999).
2. Paysan, F.; Dietrich, E.; Breitbarth, E. A robot-assisted microscopy system for digital image correlation in fatigue crack growth testing. Exp. Mech., 63, 975–986 (2023).
3. Strohmann, T.; Melching, D.; Paysan, F.; et al. Next generation fatigue crack growth experiments of aerospace materials. Sci. Rep., 14, 14075 (2024).
4. Melching, D.; Paysan, F.; Strohmann, T.; Breitbarth, E. An iterative crack tip correction algorithm discovered by physical deep symbolic regression. Int. J. Fatigue, 187, 108432 (2024).
5. Cranmer, M. Interpretable machine learning for science with PySR and SymbolicRegression.jl. arXiv, 2305.01582 (2023).

Critical resolved shear stress: its link to fatigue

Huseyin SEHITOGLU[1]

[1] Mechanical Science and Engineering, University of Illinois at Urbana-Champaign, Urbana, Illinois 61801, USA

huseyin@illinois.edu

The critical resolved shear stress (CRSS) is an essential parameter that links atomic-scale resistance to dislocation motion to macroscopic fatigue deformation. Fatigue involves cyclic activation of slip systems, which occurs when the resolved shear stress reaches the CRSS [1, 2]. As detailed below, CRSS represents the lattice's inherent resistance, which depends on dislocation core structure, elastic interactions, and the generalized stacking fault energy (GSFE) landscape. When cyclic stresses are close to this threshold, dislocations are repeatedly mobilized along specific crystallographic planes, gradually accumulating plastic strain. This process results in localized deformation features, such as residual displacements [3] (due to the buildup of the residual Burgers vectors), which are known as primary sites for fatigue crack initiation. Thus, CRSS influences the ease of slip and the distribution of local plasticity. Although CRSS can be measured experimentally, obtaining accurate values is challenging for many alloys with various compositions. It has also been estimated using continuum simulations, such as crystal plasticity, but these methods may not always provide precise CRSS values. Determining CRSS from atomistic/continuum theory has considerable advantages, which we elaborate below.

A crucial element of CRSS in fatigue is its dependence on the energy landscape and dislocation core characteristics [3-8]. It is important to note that CRSS depends primarily on parameters such as core width, dislocation character, and the full GSFE profile, rather than on a single scalar barrier. During fatigue, dislocations interact and reorganize, leading to spatial and temporal variations in the effective resistance to their motion. Mechanisms such as the intermittent movement of partial dislocations and fluctuations in stacking fault width demonstrate that slip occurs via non-uniform pathways, even under constant cyclic loading. These processes cause heterogeneous deformation at the microscale: some regions exhibit more slip activity than others. Therefore, CRSS's role goes beyond merely setting a threshold stress; it also affects how deformation localizes and evolves across microstructural features during fatigue [9, 10].

The importance of CRSS becomes even clearer in materials where its value depends on crystallography and the overall stress condition. In systems exhibiting non-Schmid behavior, particularly BCC and ordered alloys, the effective CRSS is influenced by non-glide stress components that modify the dislocation core prior to movement. During cyclic loading, this leads to deformation behavior that varies with orientation and loading path, making a single resolved shear-stress criterion insufficient to fully describe the response. Moreover, in complex alloys with variable local composition, local chemical fluctuations cause variations in CRSS, creating a heterogeneous landscape of slip resistance. This heterogeneity affects where and how fatigue damage initiates and develops, influencing crack formation and early crack growth. Consequently, CRSS should be viewed as a microstructure-sensitive, evolving parameter essential for assessing fatigue performance across different materials systems.

REFERENCES

1. Chowdhury, P.; Sehitoglu, H. Mechanisms of fatigue crack growth–a critical digest of theoretical developments. Fatigue Fract. Eng. Mater. Struct., 39, 652–674 (2016).
2. Sangid, M.D.; Maier, H.J.; Sehitoglu, H. An energy-based microstructure model to account for fatigue scatter in polycrystals. J. Mech. Phys. Solids, 59, 595–609 (2011).
3. Celebi, O.K.; Mohammed, A.S.K.; Krogstad, J.A.; Sehitoglu, H. Evolving dislocation cores at twin boundaries: theory of CRSS elevation. Int. J. Plast., 148, 103141 (2022).
4. Celebi, O.K.; Mohammed, A.S.K.; Sehitoglu, H. Effect of dislocation character on the CRSS. Acta Mater., 254, 118982 (2023).
5. Mohammed, A.S.K.; Celebi, O.K.; Sehitoglu, H. Critical stress prediction upon accurate dislocation core description. Acta Mater., 233, 117989 (2022).
6. You, D.; Celebi, O.K.; Gengor, G.; Mohammed, A.S.K.; Abuzaid, W.; Sehitoglu, H. Short-range ordering mechanics in FCC materials. Int. J. Plast., 174, 103919 (2024).
7. Celebi, T.B.; Celebi, O.K.; You, D.; Mohammed, A.S.K.; Bucsek, A.; Sehitoglu, H. Cross-slip and easy-glide CRSS in titanium: theoretical predictions and in-situ TEM measurements. Int. J. Plast., 104605 (2026).
8. You, D.; Celebi, O.K.; Mohammed, A.S.K.; Abueidda, D.W.; Koric, S.; Sehitoglu, H. CRSS determination combining ab-initio framework and surrogate neural networks. Int. J. Plast., 162, 103524 (2023).
9. Anjaria, D.; Heczko, M.; You, D.; Calvat, M.; Sanandiya, S.; Rajkowski, M.; Tirunilai, A.S.; Sehitoglu, H.; Laplanche, G.; Stinville, J.C. Dynamic plastic deformation delocalization in FCC solid solution metals. Nat. Commun., 17, 2262 (2026).
10. Stinville, J.C.; Charpagne, M.A.; Cervellon, A.; Hemery, S.; Wang, F.; Callahan, P.G.; Valle, V.; Pollock, T.M. On the origins of fatigue strength in crystalline metallic materials. Science, 377, 1065–1071 (2022).

A framework of microstructure generation and fatigue life prediction of additively manufactured alloy

Qinghui HUANG[1,2], Tao SHI[1,2], Jingyu SUN[1], Guian QIAN[1]

[1] State Key Laboratory of Nonlinear Mechanics (LNM), Institute of Mechanics, Chinese Academy of Sciences, Beijing 100190, China
[2] School of Engineering Science, University of Chinese Academy of Sciences, Beijing 100049, China

qianguian@imech.ac.cn

Laser powder bed fusion (LPBF) enables the fabrication of geometrically complex metallic components [1,2]; however, the resulting alloys typically exhibit pronounced microstructural heterogeneity and significant scatter in fatigue life [3,4]. For LPBF GH4169 (equivalent to the American brand Inconel 718), realistic grain morphology and its statistical variability are essential for representative volume element (RVE) modelling. Conventional Voronoi-based constructions remain overly idealized [5], and direct EBSD-based modelling is constrained by limited measurements. To address this gap, a novel Grain Boundary-Denoising Diffusion Probabilistic Model (GB-DDPM) was developed to generate statistically equivalent digital microstructures (as shown in Figure 1), which were subsequently integrated with crystal plasticity finite element (CPFE) simulations and machine learning (ML) for fatigue-life prediction.

Electron Backscatter Diffraction (EBSD) data from heat-treated LPBF GH4169 was used, a U-Net backbone with spatial self-attention was trained within a DDPM framework using only 200 diffusion steps, substantially reducing memory demand and inference time. The trained model generated a physically realistic grain boundary images in approximately 2 seconds, with quantitative comparisons showing great agreement in grain size, aspect ratio, and circularity distributions after grain orientation assigned processing.

These digital microstructures were employed as RVEs in crystal plasticity simulations under various loading conditions. The expected decrease in fatigue life with increasing strain amplitude was captured, while greater life dispersion was observed at lower strain amplitudes where microstructural heterogeneity dominates crack initiation, as shown in Table 1. To accelerate evaluation, regression models were trained using loading parameters and microstructural descriptors. XGBoost delivered the best prediction accuracy, with an R^2 of 0.9356, outperforming other algorithms. Feature-importance analysis revealed that strain amplitude and load ratio were the dominant predictors, with grain morphology also contributing measurably to fatigue response.

Overall, this framework offers a practical pathway from EBSD-informed generative modelling to high-throughput fatigue assessment, establishing a new basis for microstructure-sensitive design of additively manufactured alloys.

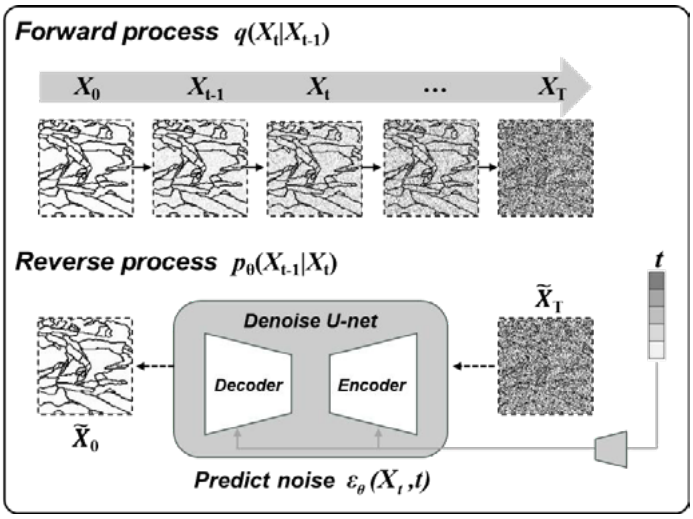

Figure 1. A workflow of microstructure generation.

Table 1. Fatigue life under different loading conditions.

Load ratio	Strain amplitude (%)	Mean fatigue life values	Standard deviation values
-1	0.15	6763640	1190943
	0.195	605465	54674
	0.25	158897	7616
0	0.15	16099524	4739028
	0.195	749722	92240
	0.25	174249	5736
0.1	0.15	20384123	2509919
	0.195	733436	39489
	0.25	162236	21171

REFERENCES

1. Enrique, P.D.; Minasyan, T.; Toyserkani, E. Laser powder bed fusion of difficult-to-print γ′ Ni-based superalloys: a review of processing approaches, properties, and remaining challenges. Addit. Manuf., 106, 104811 (2025).
2. Ghosh, S.; Zollinger, J.; Založnik, M.; Banerjee, D.; Newman, C.K.; Arroyave, R. Modeling of hierarchical solidification microstructures in metal additive manufacturing: challenges and opportunities. Addit. Manuf., 78, 103845 (2023).
3. Motaman, S.A.H.; Roters, F.; Haase, C. Anisotropic polycrystal plasticity due to microstructural heterogeneity: a multi-scale experimental and numerical study on additively manufactured metallic materials. Acta Mater., 185, 340–369 (2020).
4. Narayana Samy, V.P.; Brasche, F.; Šulák, I.; Verma, B.; Nowak, B.; Chlup, Z.; Záležák, T.; Schleifenbaum, J.H.; Krupp, U.; Haase, C. The influence of microstructural heterogeneities on high-temperature mechanical properties of additively manufactured γ′-forming Ni-based alloys. Addit. Manuf., 88, 104267 (2024).
5. Fritzen, F.; Böhlke, T.; Schnack, E. Periodic three-dimensional mesh generation for crystalline aggregates based on Voronoi tessellations. Comput. Mech., 43, 701–713 (2008).

In-situ observation of the dynamics of grain rotation and slip behavior

Jing-Bo ZHAO[1], Rong CHEN[1], Ming-Liang ZHU[1], Fu-Zhen XUAN[1]

[1] Key Laboratory of Pressure Systems and Safety, Ministry of Education; School of Mechanical and Power Engineering, East China University of Science and Technology, Shanghai 200237, China

mlzhu@ecust.edu.cn

Cr-Mo-V steels with a BCC crystal structure are widely used in engineering [1,2]. Their plastic deformation behavior is governed by the interaction between grain-scale deformation and local microstructural constraints [3,4]. In this work, the deformation mechanisms of the 12Cr2Mo1VR welded joint were systematically investigated using *in-situ* tensile testing combined with electron backscatter diffraction (EBSD) and digital image correlation (DIC) techniques.

During the tensile test, EBSD maps were captured at strain levels of 0%, 1%, 6%, and 10%. Grain-scale strain fields were obtained by DIC and correlated with crystallographic information extracted from the EBSD data. The crystallographic orientation of each grain was represented by its mean orientation, and grain rotations were quantified across different deformation stages [5]. The activation of slip systems and the evolution of grain rotation were quantitatively analyzed to reveal the underlying deformation mechanisms.

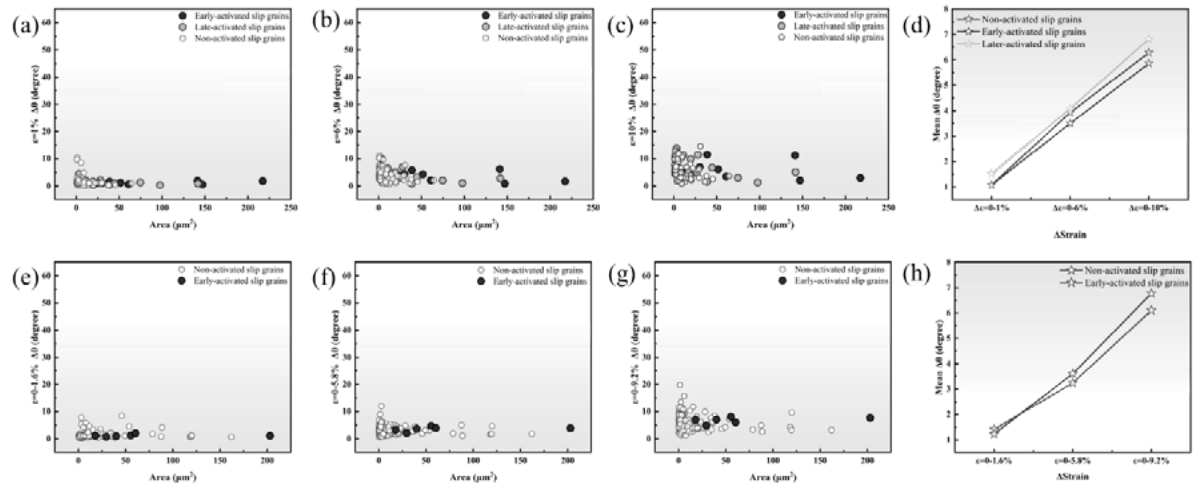

Figure 1. Grain rotation evolution during deformation for base metal (a-d) and weld metal (e-h) of the welded joint.

Figure 1 shows the relationship between grain size and grain rotation in base metal and weld metal at different deformation stages. Grains were categorized according to their slip activation behavior into early-activated slip grains, late-activated slip grains, and non-activated slip grains. The results indicated that grain rotation was strongly dependent on both the slip activation mode and the deformation level. In the base metal, late-activated slip grains generally exhibited higher average grain rotation than the other grains. In contrast, early-activated slip grains of weld metal

appeared significantly larger grain rotations at high strain levels, even exceeding those of non-activated grains. Generally, the average grain rotation increased progressively with increasing macroscopic strain, indicating a continuous accumulation of plastic deformation at the grain scale.

The relationship between slip activation and the number of neighboring grains was analyzed to clarify the role of local microstructural arrangement, as shown in Figure 2. The results demonstrated that the probability of slip activation was determined by the local grain neighborhood. In particular, grains with more than six neighboring grains exhibited the highest slip probability, indicating that local microstructural constraints significantly affected the activation of slip systems.

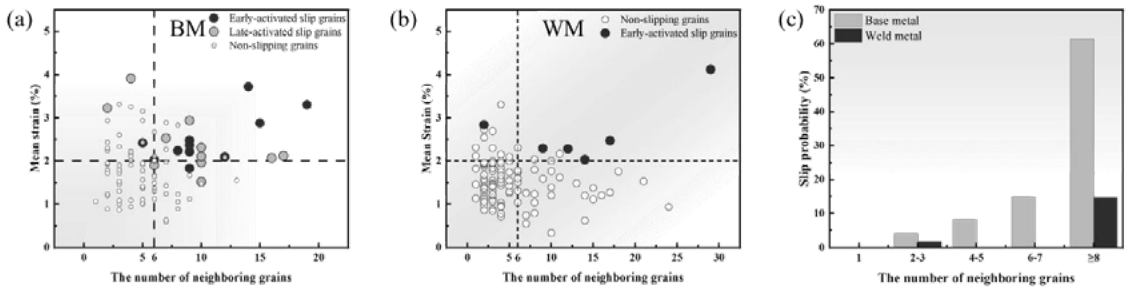

Figure 2. Relationship between slip activation and the number of neighboring grains in base metal and weld metal.

In addition, two parameters were introduced to evaluate deformation heterogeneity, namely the plastic deformation sensitivity parameter (PDSP) and the *R* parameter. PDSP describes the sensitivity of individual grains to plastic deformation, whereas *R* characterizes the dispersion of misorientation angles along grain boundaries. These findings demonstrate that grain-scale deformation in polycrystalline BCC steel is strongly influenced by grain size, the number of neighboring grains, and the grain boundary misorientation. The proposed PDSP–R framework provides a quantitative approach for classifying grain deformation modes and analyzing the relationship between microstructural arrangement and plastic deformation.

REFERENCES

1. Xie, X.; Yi, H.; Xu, J.; Gen, L.M.; Chen, L.Y. Effect of load ratio and saltwater corrosive environment on the initiation life of fatigue of 10Ni5CrMoV steel. 2017 2nd International Seminar on Advances in Materials Science and Engineering, 231 (2017).
2. Wang, W.; Zhao, Z.; Guo, Y.; Chen, Y.; Ai, Z.; Guo, W.; Zhang, J. Low-cycle fatigue and fracture behaviors of NiCrMoV multi-layer and multi-pass welded metal at different sampling locations. Mater. Sci. Eng. A, 942, 148698 (2025).
3. Gautier, R.; et al. Quantifying grain boundary deformation mechanisms in small-grained metals. Nature, 648, 327–332 (2025).
4. Abdolvand, H.; Wright, J.; Wilkinson, A.J. Strong grain neighbor effects in polycrystals. Nat. Commun., 9, 171 (2018).
5. Hémery, S.; Villechaise, P. In situ EBSD investigation of deformation processes and strain partitioning in bimodal Ti-6Al-4V using lattice rotations. Acta Mater., 171, 261–274 (2019).

A creep life assessment model for defective structures

Rong CHEN[1], Chao LIU[1], Ming-Liang ZHU[1], Fu-Zhen XUAN[1]

[1] Key Laboratory of Pressure Systems and Safety, Ministry of Education; School of Mechanical and Power Engineering, East China University of Science and Technology, Shanghai 200237, China

mlzhu@ecust.edu.cn; rongchen@ecust.edu.cn

High-temperature pressurized structures serve as key components in critical industrial systems, including nuclear power, advanced thermal power generation, and petrochemical processing, where long-term integrity governs operational safety and durability [1]. Welding is a typical fabrication method for these large and geometrically complex structures. Under prolonged exposure to elevated temperatures and mechanical loading, defects in welded structures can disturb the local strain field, leading to stress concentration and localized strain accumulation, thereby increasing the risk of time-dependent creep damage [2,3]. In contrast to crack-like defects, the effect of volumetric defects on structural life is determined by the combined influence of their size, shape, and spatial distribution. However, there is still a lack of a unified parameter that can simultaneously quantify geometric features and correlate them with life reduction.

In this work, the Liu-Murakami model was modified to improve the accuracy of creep damage description. Based on the finite element method, a parametric creep life dataset for 316H weld metal containing defects was constructed using the modified Liu-Murakami model. Using symbolic regression, a unified C parameter was proposed to bridge the correlation between defect features and creep life, as shown in Eq. (1).

$$C = A \cdot D^{1.312} \cdot Y^{0.174} \tag{1}$$

Where relative area A is defined as the ratio of the area of the ellipse enclosing the defect on the loading projection plane to the cross-sectional area of the specimen, D describes the relative depth of the micro defect, and Y represents the aspect ratio of the major axis to the minor axis of the defect.

It was found that C parameter and creep life exhibited a linear relationship, as expressed in Eq. (2):

$$t / t_r = -10.46C + 1.03 \tag{2}$$

Where t and t_r are the creep life of specimens with and without defects, respectively. Figure 1 shows that the C parameter can effectively capture the combined influence of defect geometric characteristic on creep life. Furthermore, the effectiveness of the linear relationship between t/t_r and C was verified by a physics-informed neural network. The C parameter exhibits a sound physical basis, as shown in Figure 2.

The main conclusions are listed as follows.

(1) The classical Liu-Murakami damage model was modified by introducing a hyperbolic sine function, which enabled more accurate description of the creep strain rate.

(2) The influence of defect geometric characteristics on structural performance was clarified, and the relative area was found to dominate creep life.

(3) The C parameter was proposed as a life controlling factor for defects induced creep failure, by taking defect size, depth and shape into account.

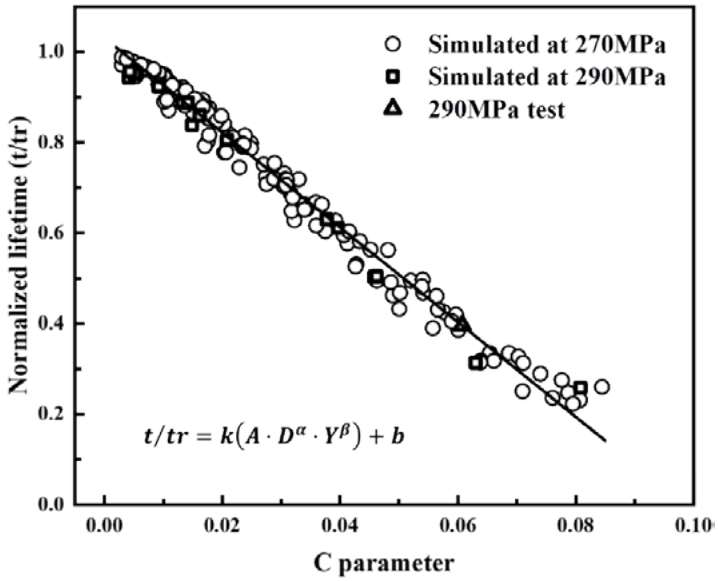

Figure 1. Relationship between *C* parameter and creep life t/t_r.

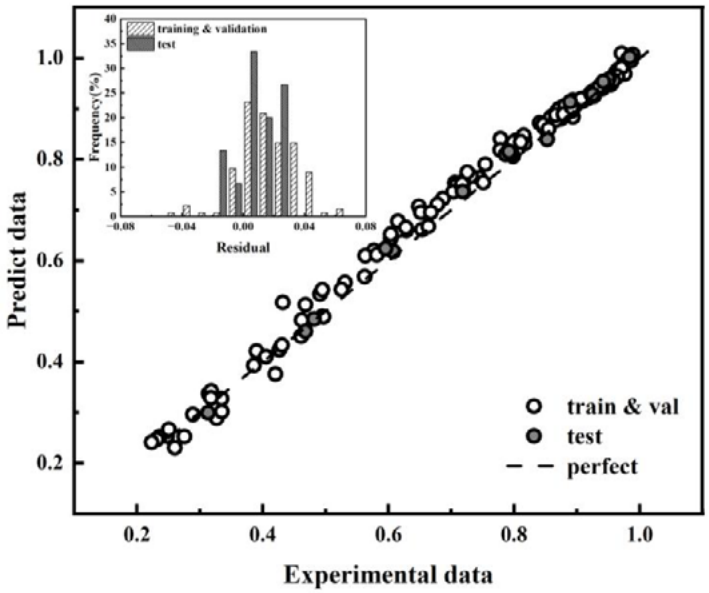

Figure 2. Comparative analysis of model architectures and physics integration.

REFERENCES

1. Lee, H.-Y.; Eoh, J. Securing integrity of high-temperature pressure boundary components in supercritical thermal plants with application of alternative design rules. Int. J. Pressure Vessels Piping, 195, 104598 (2022).
2. Liu, Y.; Murakami, S. Damage localization of conventional creep damage models and proposition of a new model for creep damage analysis. JSME Int. J. Ser. A Solid Mech. Mater. Eng., 41, 57–65 (1998).
3. Yang, X.; Meng, T.; Su, Y.; He, X.; Guo, Z.; Wu, D.; Ma, T.; Li, W. The effect of inclusions and pores on creep crack propagation of linear friction welded joints of GH4169 superalloy. J. Mater. Res. Technol., 29, 4636–4649 (2024).

Crack initiation hotspot identification of LCPF alloys under fatigue loading based on CPFEM and graph neural networks

Pengbo WANG[1,2], Guian QIAN[1]

[1] State Key Laboratory of Nonlinear Mechanics (LNM), Institute of Mechanics, Chinese Academy of Sciences, Beijing, China
[2] School of Engineering Science, University of Chinese Academy of Sciences, Beijing, China

qianguian@imech.ac.cn

Fatigue crack initiation in polycrystalline alloys is strongly governed by microstructure-sensitive heterogeneity [1]. However, the reliable identification of crack initiation hotspots remains challenging [2] because local cyclic deformation is affected by both intragranular responses and grain boundary interactions. The experimental material of this study is the laser cladding with coaxial powder feeding (LCPF) K477 alloy. This study aims to develop a physically informed and interpretable framework for identifying hotspot grains in LCPF alloys under fatigue loading through the integration of the crystal plasticity finite element method (CPFEM) [3] and graph neural networks (GNNs). The core lies in converting cyclic micromechanical information obtained from representative volume elements into grain level graph data and predicting the probability of each grain acting as a crack initiation hotspot [4,5]. In this study, hotspot labels are defined on the basis of a dissipated energy-based fatigue indicator parameters (FIPs), which are the cyclic plastic work density, thereby ensuring that the framework remains physically consistent and directly connected to fatigue damage accumulation.

The proposed framework begins with representative volume element (RVE) that explicitly incorporates grain morphology and grain boundary topology under fatigue loading and boundary conditions. CPFEM simulations are subsequently performed under cyclic loading to obtain microstructure resolved mechanical fields, including stress, strain, slip activity and most importantly, the dissipated energy per cycle [6]. Previous studies [7,8] have quantified grain-level fatigue damage using fatigue indicator parameters (FIPs) such as accumulated plastic slip and plastic strain amplitude, while this work uses a dissipated energy-based FIP. The local field variables are then aggregated from integration points to individual grains, and a grain-level FIP is calculated for each grain. Grains with the highest FIP values (top 5 %) are labeled as crack initiation hotspots. Based on the same representative volume element, a grain-interaction graph is constructed in which nodes denote grains and edges denote grain boundary adjacency. Node features include morphological descriptors, crystallographic characteristics, and CPFEM-derived response variables, and edge features describe neighbouring relationships and grain-boundary attributes. On this basis, graph attention networks (GAT) are trained to predict hotspot probabilities and to identify the neighbouring grains and grain boundary features that contribute most strongly to hotspot formation. The framework of GAT is shown as Figure 1.

The proposed framework is expected to provide an efficient approach for hotspot identification while preserving the physical significance of CPFEM-based fatigue damage assessment. By adopting dissipated energy as the fatigue indicator, the model output remains directly interpretable in terms of local cyclic plastic dissipation rather than a combination of empirical or weakly related features. The graph-based representation further enables the model to capture neighbourhood effects naturally, which are difficult to represent using grain-wise

independent predictors, thereby improving the identification of hotspot grains governed by collective microstructural interactions. Compared with conventional machine learning models that neglect topological information, the proposed GNN-based approach is expected to deliver superior performance in the imbalanced classification of hotspot grains, particularly in terms of Precision-Recall AUC (PR-AUC) and recall for the most critical grains. In addition, the framework can provide interpretable outputs, including grain-level hotspot maps and the relative importance of key neighboring regions and grain-boundary characteristics. These findings indicate that the CPFEM–GNN coupling strategy constitutes a promising route for microstructure-sensitive fatigue assessment and for data-driven screening of crack initiation susceptibility in polycrystalline alloys.

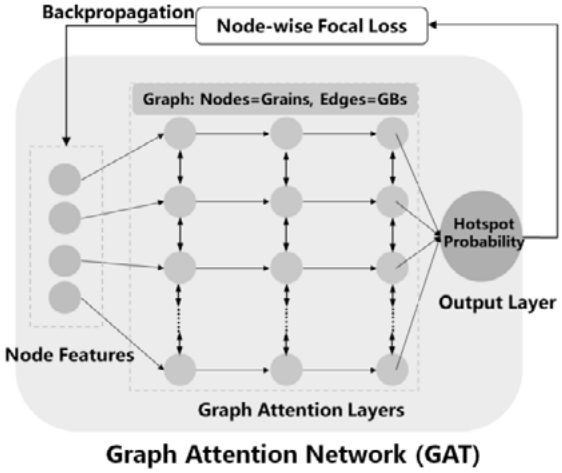

Figure 1. Schematic of the GAT model for fatigue crack initiation hotspot prediction.

REFERENCES

1. Zhou, S.; Huang, M.; Häffner, C.; Stebner, S.; Cai, M.; Wei, Z.; Yang, B.; Münstermann, S. Microstructure-sensitive crystal plasticity and fatigue indicator modeling for LZ50 steel. Int. J. Fatigue, 203, 109302 (2026).
2. Zhai, H.; Jiang, J.; Zhang, W.; Zhang, Q.; Ma, X.; Wang, S.; Li, Z.; Qiu, W.; Xiao, C.; Lin, H. Microstructure sensitivity of the low cycle fatigue crack initiation mechanisms for the Al0.3CoCrFeNi high entropy alloy: in-situ SEM study and crystal plasticity simulation. Int. J. Fatigue, 176, 107871 (2023).
3. Thomas, A.; Durmaz, A.R.; Alam, M.; Gumbsch, P.; Sack, H.; Eberl, C. Materials fatigue prediction using graph neural networks on microstructure representations. Sci. Rep., 13, 12562 (2023).
4. Trivedi, A.; Tiwari, K.; Kumar, J.; Salem, M.; Alankar, A. A crystal plasticity and data-driven approach for analyzing the effect of porosity and surface roughness on fatigue behavior. Int. J. Fatigue, 206, 109440 (2026).
5. Hansen, C.K.; Whelan, G.F.; Hochhalter, J.D. Interpretable machine learning for microstructure-dependent models of fatigue indicator parameters. Int. J. Fatigue, 178, 108019 (2024).
6. Dindarlou, S.; Castelluccio, G.M. Assessment of fatigue crack initiation after overloads with substructure-sensitive crystal plasticity. Int. J. Fatigue, 198, 108937 (2025).
7. Sim, G.J.; Lee, M.G.; Latypov, M.I. FIP-GNN: graph neural networks for scalable prediction of grain-level fatigue indicator parameters. Scr. Mater., 255, 116407 (2025).
8. Muth, A.; Venkatraman, A.; John, R.; Pilchak, A.; Kalidindi, S.R.; McDowell, D.L. Neighborhood spatial correlations and machine learning classification of fatigue hot-spots in Ti-6Al-4V. Mech. Mater., 182, 104679 (2023).

A recurrent neural operator UMAT for cyclic plasticity: uncertainty-aware training and conformal-prediction deployment

Jalal ABDOLAHI[1], Sina SAFARI[2], David KNOWLES[2,3], Paul WILCOX[2], Mahmoud MOSTAFAVI[1,2]

[1] Department of Mechanical and Aerospace Engineering, Monash University, Australia
[2] School Electrical, Electronics, and Mechanical Engineering, University of Bristol, UK
[3] Henry Royce Institute, Manchester, UK

jalal.abdolahi@monash.edu

Microstructure-resolved crystal-plasticity finite-element (CPFE) analysis is a perfect vehicle for including the effects of the microstructure of metals in structural integrity assessment. However, CPFE computational cost is prohibitive at component scale. This motivates developing history-aware machine-learning surrogate models to be deployed at the component scale [1]. In the present work we use Lemaitre–Chaboche (LC) [2] as an inexpensive benchmark to produce cyclic results that can also be obtained from CPFE models. We use the results of LC to construct a surrogate model and validate the surrogate against the ground truth (i.e. LC). We argue that the same procedure can be applied on the results of CPFE. We show that the low cycle fatigue stress-strain response of a 3D LC model for stainless steel type 316H at 550 °C can be replaced by a recurrent neural operator (RNO), embedded in an Abaqus UMAT without loss of numerical stability, and that uncertainty awareness can be carried from the training stage all the way to deployment via conformal prediction.

Unlike many plasticity surrogates which use learned gating with hidden-state dimensions in the tens to hundreds resulting in needing substantial training data, the RNO of Liu et al. [3] consists of two feed-forward sub-networks: a stress predictor f-net maps the current strain increment and K hidden-state variables h to the updated Cauchy stress, and a hidden-state evolution network g-net maps the same inputs to the rate of h. The RNO imposes the structural form $dh/dt = g(\varepsilon, h)$, $\sigma = f(\varepsilon, h)$, mirroring the differential-algebraic structure of internal-variable plasticity itself. This strong prior (i.e. physics informed RNO) permits a much smaller latent state.

Training strain trajectories combine two sources: (a) real-world trajectories extracted from full-field FE LC simulations of representative components (that is notched specimens, cantilevers under combined bending and tension) at every integration point and increment (b) augmented by random-walk trajectories that broaden coverage of the (strain, hidden-state) feature space, particularly in high-triaxiality and reverse-loading regions. An ensemble of $M = 5$ RNOs is trained on randomly partitioned subsets of this pool; at each acquisition round, the next training trajectories are selected from the pool by the highest ensemble variance, i.e. those on which the five members most disagree, targeting regions of feature space where the surrogate is least confident [3]. Figure 1 quantifies the resulting data efficiency on 25,000 random-walk trajectories spanning all six strain components, with 250 held out for testing. Accuracy is reported as CV-RMSE: the per-component RMSE normalised by the standard deviation of that component on the test set, in percent. Ensemble-variance acquisition consistently outperforms uniform random sampling, the standard baseline in the surrogate-plasticity literature: the relative improvement reaches 20 % on the combined CV-RMSE at ~2,400 trajectories, largest in the shear components

where random coverage of multi-axial states is sparsest. At the largest pool size, component-wise CV-RMSE is near 1.5 % for normal and ~4.5 % for shear components.

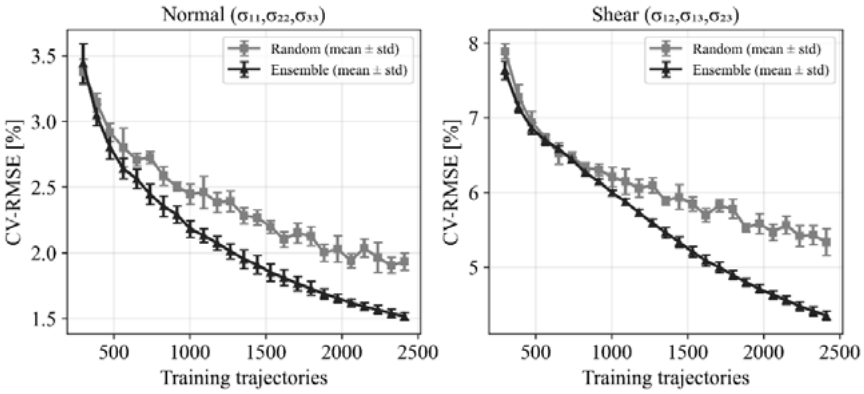

Figure 1. CV-RMSE on a held-out set of 250 random-walk strain trajectories, as a function of training-pool size, for ensemble-variance acquisition (purple) and uniform random sampling (grey); left: normal components (σ_{11}, σ_{22}, σ_{33}), right: shear (σ_{12}, σ_{13}, σ_{23}). Error bars denote mean ± std across the M = 5 ensemble members.

The trained RNO then is exported to a Fortran UMAT for Abaqus/Standard, which reads the weights once per analysis and, at every integration-point call, evaluates f-net for the stress, computes the consistent algorithmic tangent by central finite differences on f-net, and advances the hidden state with g-net. Deployment-time uncertainty is provided by conformal prediction [5]: per-component non-conformity scores from a held-out calibration set yield a (1-α) quantile q-hat that is stored in the UMAT as a Fortran PARAMETER, and the bounds σ ± q-hat are written into state variables queryable as ordinary field outputs. With α = 0.1 this gives 90 % marginal coverage of the true LC stress. On a 3D cantilever (50 × 10 × 5 mm, 450 C3D8 elements) under combined axial and transverse loading, the RNO UMAT reproduces the LC reference stress field to within 1.5 % RMS at moderate load levels, with Newton convergence in 3-6 iterations per increment, comparable to the analytical LC UMAT. At higher loads the per-IP iteration count rises with the fraction of integration points entering under-represented regions of feature space, and the conformal bounds widen accordingly, giving the analyst a clear deployment envelope rather than a silent failure mode. These results demonstrate that a properly trained RNO surrogate is a potential substitute for an analytical cyclic-plasticity UMAT in implicit FE analysis, delivers order-of-magnitude speed-up while numerically stable, uncertainty-aware and interpretable.

REFERENCES

1. Safari, S.; Wilcox, P.; Mostafavi, M.; Knowles, D. Data-driven multiscale modelling of history-dependent plasticity using recurrent neural operators. ASME Pressure Vessels and Piping Conference, PVP2025-151613, (2025).
2. Lemaitre, J.; Chaboche, J.-L. Mechanics of solid materials, Cambridge University Press, (1990).
3. Liu, B.; Ocegueda, E.; Trautner, M.; Stuart, A.M.; Bhattacharya, K. Learning macroscopic internal variables and history dependence from microscopic models. J. Mech. Phys. Solids, 178, 105329 (2023).
4. Beluch, W.H.; Genewein, T.; Nürnberger, A.; Köhler, J.M. The power of ensembles for active learning in image classification. Proceedings of the IEEE/CVF Conference on Computer Vision and Pattern Recognition (CVPR), 9368–9377 (2018).
5. Angelopoulos, A.N.; Bates, S. Conformal prediction: a gentle introduction. Found. Trends Mach. Learn., 16, 494–591 (2023).

Experimental observations on CTOD measurements obtained by DIC

Giancarlo Luis GÓMEZ GONZALES[1], José Manuel VASCO OLMO[1], Luis FELIPE SESÉ[1], Francisco Alberto DÍAZ GARRIDO[1]

[1] Department of Mechanical and Mining Engineering, University of Jaén, 23071 Jaén, Spain

glgomez@ujaen.es

This study presents an experimental analysis of the Crack-Tip Opening Displacement (CTOD) as a potential parameter for characterising fatigue crack propagation in ductile materials. It is known that alternative approaches based on Elastic-Plastic Fracture Mechanics (EPFM) are gaining relevance due to their greater capability to characterise local plasticity at the crack tip, which is directly related to fatigue damage. In this context, various researchers [1–4] have focused on nonlinear parameters, including the cyclic plastic strain range, the size of the cyclic plastic zone, the crack tip opening displacement (CTOD), and plastic energy dissipation. These parameters directly quantify plasticity at the crack tip and have shown a consistent correlation with crack growth rates under different loading scenarios, both constant and variable amplitude, thus constituting more reliable parameters for describing crack propagation.

In particular, CTOD is a relevant fracture mechanics parameter used to characterise crack opening and closure, providing a physical interpretation of progressive crack extension under cyclic loading in materials undergoing plastic deformation. The proportional relationship between the plastic component of the CTOD (CTODp) and the crack growth rate (da/dN) has been proposed and extensively investigated, both experimentally and numerically, in numerous studies [5–8].

This work presents the applicability of the plastic CTOD parameter for analysing fatigue crack propagation under two different scenarios: first, a constant load amplitude test including the application of a 50% overload (OL) cycle; and second, a constant K-amplitude test. The materials tested are titanium, and steel, respectively.

The DIC technique is employed, enabling CTOD measurements to be performed in the region behind the crack tip with sufficient spatial resolution. The experimental setup includes both 2D and 3D optical configurations using high-resolution cameras and a stereo microscope system.

Figure 1a shows the results for the titanium specimen under the constant load amplitude test with a 50% OL, where the plastic CTOD range versus crack growth rates (da/dN) are plotted on a linear scale. It can be observed that the da/dN -ΔCTODp relationship obtained from fatigue crack growth (FCG) test follows a linear trend, taking into account the load sequence effects due to the imposed overload. As shown in this figure, after the application of the overload at P1, the da/dN values begin to decrease following the linear trend observed prior to the overload, and after reaching a minimum at P2, the da/dN values increase again following the same trend.

Figure 1b shows the results for the steel specimen under the constant ΔK-amplitude test. It presents the plastic CTOD values obtained for crack lengths ranging from 22 to 28 mm. These experimental results indicate that the plastic CTOD remains approximately constant over all the crack lengths examined, reflecting the constant ΔK maintained during the fatigue test. The plastic CTOD was approximately 1.78 μm ± 0.10 μm. The small deviations, as mentioned previously,

are attributed to changes in material stiffness as the crack grows, which require continuous load adjustments to ensure a constant ΔK.

The behaviour of the plastic CTOD parameter under both experimental conditions highlights its potential as a key parameter for describing fatigue crack propagation, as it effectively quantifies plasticity at the crack tip and inherently incorporates critical plasticity-induced phenomena such as crack closure, crack tip blunting, and the influence of residual stresses.

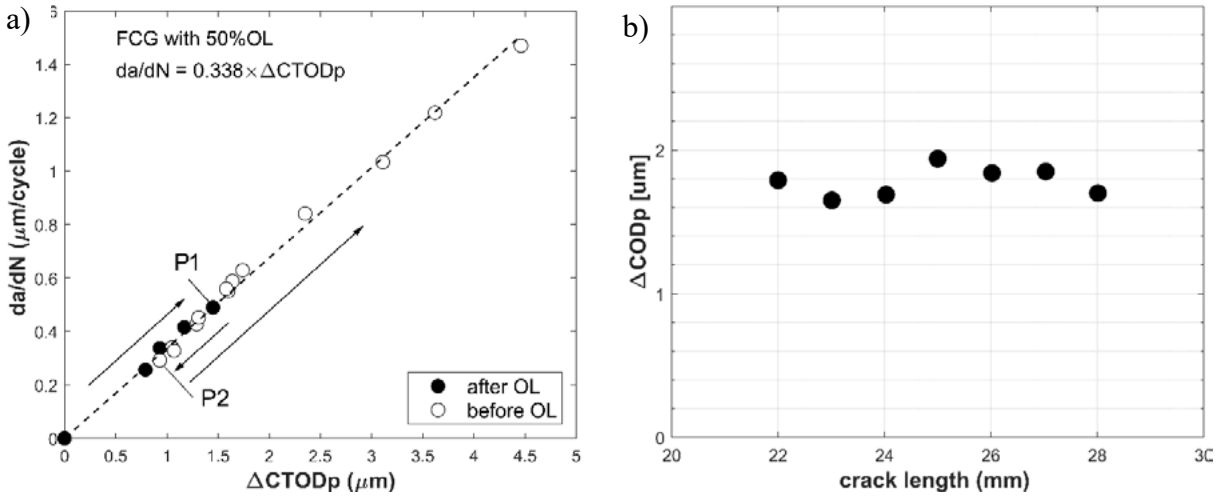

Figure 1. a) Plot of the da/dN-ΔCTODp relationship for the constant load amplitude test with OL application. b) Plot of ΔCTODp during crack propagation for the constant ΔK-amplitude test.

REFERENCES

1. Oplt, T.; Vojtek, T.; Kubíček, R.; Pokorný, P.; Hutař, P. Numerical modelling of fatigue crack closure and its implication on crack front curvature using ΔCTODp. Int. J. Fatigue, 171, 107570 (2023).
2. Gonzales, G.L.G.; Gonzalez, J.A.O.; Antunes, F.V.; Neto, D.M.; Diaz, F.A. Experimental determination of the reversed plastic zone size around fatigue crack using digital image correlation. Theor. Appl. Fract. Mech., 125, 103901 (2023).
3. Shahani, A.R.; Kashani, H.M.; Rastegar, M.; Dehkordi, M.B. A unified model for the fatigue crack growth rate in variable stress ratio. Fatigue Fract. Eng. Mater. Struct., 32, 105–118 (2009).
4. Donahue, R.J.; Clark, H.M.; Atanmo, P.; Kumble, R.; McEvily, A.J. Crack opening displacement and the rate of fatigue crack growth. Int. J. Fract. Mech., 8, 209–219 (1972).
5. Antunes, F.; Rodrigues, S.; Branco, R.; Camas, D. A numerical analysis of CTOD in constant amplitude fatigue crack growth. Theor. Appl. Fract. Mech., 85, 45–55 (2016).
6. Antunes, F.; Branco, R.; Prates, P.; Borrego, L. Fatigue crack growth modelling based on CTOD for the 7050-T6 alloy. Fatigue Fract. Eng. Mater. Struct., 40, 1309–1320 (2017).
7. Vasco-Olmo, J.; Díaz, F.; Antunes, F.; James, M. Characterisation of fatigue crack growth using digital image correlation measurements of plastic CTOD. Theor. Appl. Fract. Mech., 101, 332–341 (2019).
8. Vasco-Olmo, J.M.; Diaz Garrido, F.A.; Antunes, F.V.; James, M. Plastic CTOD as fatigue crack growth characterising parameter in 2024-T3 and 7050-T6 aluminium alloys using DIC. Fatigue Fract. Eng. Mater. Struct., 43, 1719–1730 (2020).

Synchrotron-based 3D characterization of torsional fatigue crack propagation in cast Al–Si alloys: influence of defects and microstructure

Viet-Duc LE[1], Franck MOREL[1], Nicolas SAINTIER[2], Pierre OSMOND[3], Daniel BELLETT[1], Wolfgang LUDWIG[4], Marta MAJKUT[5], Jean-Yves BUFFIERE[4]

[1]Arts et Metiers Institute of Technology, LAMPA, 49035 Angers, FRANCE
[2]Arts et Metiers Institute of Technology, I2M, 33405 Talence, FRANCE
[3] CETIM, 60300 Senlis, FRANCE
[4] INSA de Lyon, MATEIS, 69100 Villeurbanne, FRANCE
[5] ESRF, 38000 Grenoble, FRANCE

Viet-Duc.LE@ensam.eu

Fatigue behaviour of cast aluminium alloys is strongly influenced by both microstructural features and casting defects, particularly under multiaxial loading conditions [1]. While crack initiation mechanisms have been widely investigated, the propagation mechanisms under torsional loading remain less understood [2]. The objective of this work is therefore to characterise fatigue crack propagation mechanisms in a cast AlSi7Mg0.3-T7 alloy under high-cycle torsional fatigue loading, with a specific focus on the competing roles of defects and microstructure using advanced three-dimensional (3D) observations.

The adopted approach relies on synchrotron-based experimental techniques combining Diffraction Contrast Tomography (DCT) and in-situ X-ray phase contrast tomography [3]. These methods enable a full 3D characterisation of both the microstructure (grain morphology and crystallographic orientation) and the evolution of fatigue cracks during cyclic torsion loading around the fatigue limit. Approximately 80 cracks were analysed across three specimens, providing a statistically representative dataset. The investigated material exhibits relatively large grains (several hundred micrometres) and significant porosity, with pore sizes up to 200 µm.

The results reveal the coexistence of two distinct crack propagation mechanisms under torsional loading (figure 1). The first mechanism corresponds to shear-mode propagation, which is crystallographically controlled. In this case, cracks propagate along planes of maximum shear stress and align with slip systems exhibiting high Schmid factors. These cracks can grow relatively rapidly, with growth rates on the order of 10^{-8} m/cycle, but frequently experience arrests at grain boundaries. These arrests are primarily governed by unfavourable crystallographic conditions in adjacent grains, such as low Schmid factors and large misorientation angles (tilt and twist). Consequently, shear-mode cracks exhibit a typical microstructural short crack behaviour.

The second mechanism corresponds to opening-mode propagation. These cracks initiate exclusively from pores and propagate on planes of maximum normal stress, typically oriented at 45° relative to the specimen axis. In contrast to shear-mode cracks, opening-mode cracks are not significantly influenced by the surrounding microstructure and propagate steadily across grain boundaries. Their growth rates are lower, typically around 10^{-9} m/cycle, but show greater stability with limited crack arrest events.

A key outcome of this study is the direct comparison of the two propagation modes under identical loading conditions. While shear-mode cracks can initially grow faster, their propagation is highly intermittent due to microstructural barriers. Conversely, opening-mode cracks exhibit

slower but more continuous growth, ultimately dominating long crack propagation. The crack morphology also differs significantly: shear-mode cracks remain shallow and surface-dominated, whereas opening-mode cracks tend toward more equiaxed shapes.

Furthermore, the analysis of crack growth kinetics using stress intensity factors highlights distinct behaviours. Shear-mode cracks remain sensitive to microstructural effects up to stress intensity ranges of approximately $\Delta K_{II} \approx 6$ MPa√m, while opening-mode cracks exhibit a near-threshold stress intensity range of $\Delta K_I \approx 1$ MPa√m, consistent with values reported in the literature.

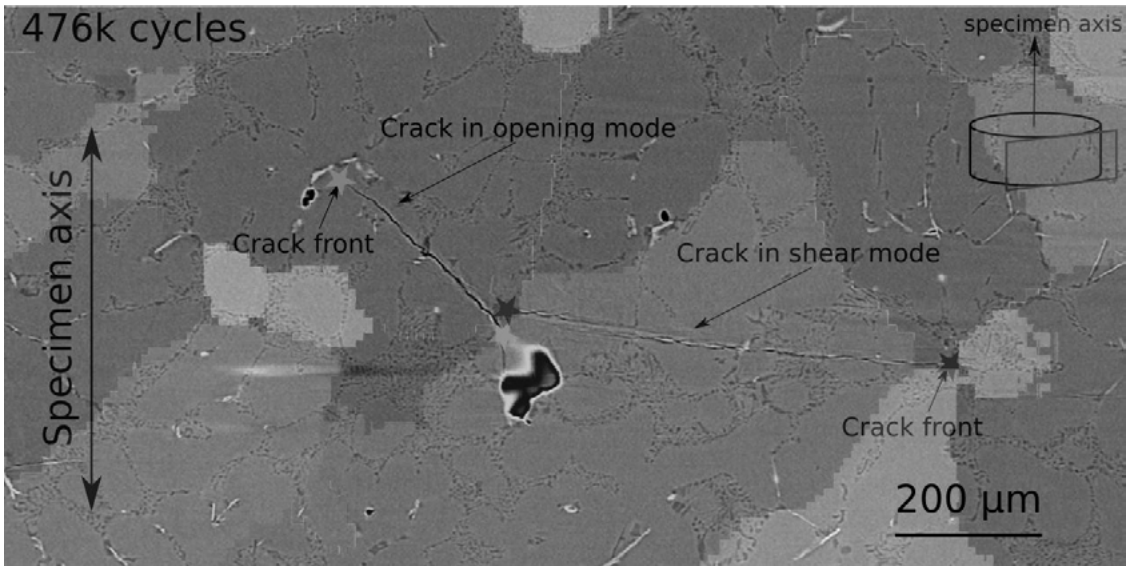

Figure 1. Shear-mode and opening-mode cracks propagating through grains surrounding a microshrinkage pore in a cast AlSi7Mg0.3-T7 alloy under high-cycle torsional loading.

REFERENCES

1. Le, V.-D.; Morel, F.; Bellett, D.; Saintier, N.; Osmond, P. Multiaxial high cycle fatigue damage mechanisms associated with the different microstructural heterogeneities of cast aluminium alloys. Mater. Sci. Eng. A, 649, 426–440 (2016).
2. Serrano-Munoz, I.; Shiozawa, D.; Dancette, S.; Verdu, C.; Buffiere, J.-Y. Torsional fatigue mechanisms of an A357 cast aluminium alloy. Acta Mater., 201, 435–447 (2020).
3. Le, V.-D.; Morel, F.; Saintier, N.; Osmond, P.; Bellett, D.; Ludwig, W.; Majkut, M.; Buffiere, J.-Y. Synchrotron X-ray 3D characterisation of fatigue crack initiation during in-situ torsion cyclic tests. Int. J. Fatigue, 193, 108762 (2025).

Fatigue crack paths through additively manufactured AlSi10Mg

Philip John WITHERS[1,2], Saad Syed AHMED[1], Sethu RANGARAJ[1], Ali GHOLINIA[1], Jianguang BAO[1]

[1] Henry Royce Institute, Dept. of Materials, Manchester University, Manchester, M13 9PL, UK
[2] Materials Sci. and Engineering Department, Monash University, Clayton, Vic 3800, Australia

p.j.withers@manchester.ac.uk

It is well known that manufacturing defects inherent to the additive manufacturing (AM) process can have a significant effect on the fatigue life and scatter in fatigue lifetimes of additively manufacturing materials [1]. Here we focus firstly on the initiation and growth of fatigue cracks from lack of fusion defects (LOF) before going on to consider where these cracks nucleate and how they propagate with the aim of better understanding microstructural aspects of the crack nucleation and growth process for laser powder bed (LPBF) manufactured AlSi10Mg.

A series of fatigue tests has been carried out on samples machined from an AM wall structure such that their tensile axis is either parallel (V-HCF) to, or perpendicular (H-HCF) to, the build direction. The maximum stress ranged from 170 to 120MPa and all the tests were undertaken using a load ratio of 0.1. Post mortem fracture surface investigations revealed that in all cases the critical defects are located on, or near, to the surface. The square root of the projected area of the critical defects ranged from ~40 to ~425μm and the lives from 55,000 to 650,000 cycles. While samples fatigued to lower fatigue amplitudes show longer lives, the fatigue data show considerable scatter largely due to the size of the associated critical defect. For the vertical samples the pancake shaped LOF defects tend to lie in plane and project a larger effective projected area, while for the horizontal samples the pancake shaped LOF defects tend to lie edge-on and project a smaller effective area giving rise to longer fatigue lives for H-HCF as observed previously [2], [3].

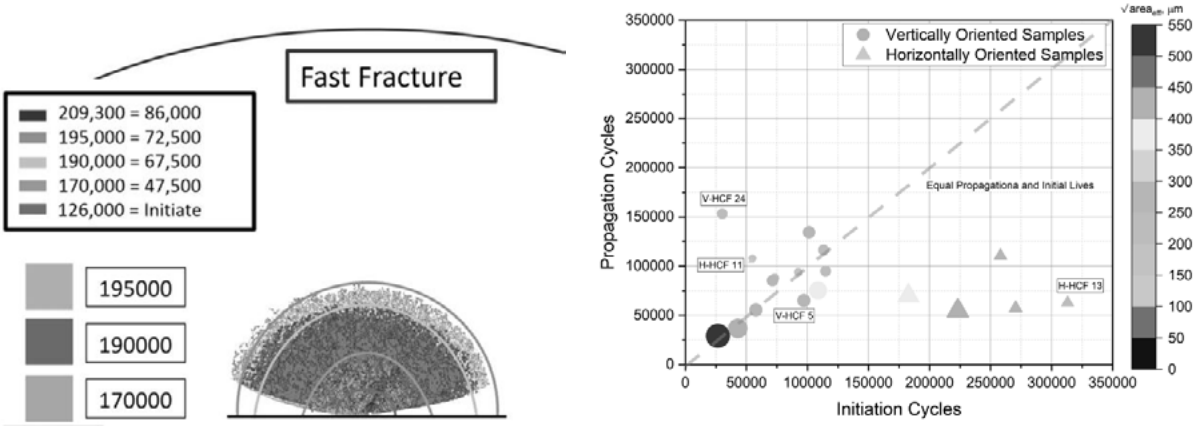

Figure 1. a) The crack front recorded by time-lapse μCT during fatigue testing of a V-HCF sample with the results from the single crack model [4] overlaid, b) Crack propagation vs initiation lives deduced from the single crack model with the symbol size and colour coding indicating the effective projected area of the critical defect.

Time-lapse X-ray computed micro-tomography (μCT) has been used to follow the initiation and the crack growth rate/ crack path for a fatigue crack initiating from a LOF defect in a V-HCF

sample. By comparing the crack growth rate and profile with the model developed by Qian et al. [4] developed for cracking in similar AlSi10Mg AM produced material we have been able to validate the appropriateness of the model for our AM builds (See Fig 1a). This model has then been used to infer the propagation life for all the H-HCF and V-HCF samples tested. Given we know the total fatigue life of each test we have been able to infer the initiation life of each sample. The results are plotted in fig. 1b. As one would expect the samples containing the largest critical defects show the shortest propagation lives for a given stress amplitude. It is also evident from Fig1b that the initiation lives of the H-VCF samples area to be significantly longer than for the V-HCF samples. For most of the V-HCF samples the initiation lives and the propagation lives appear to be similar (initiation life ≈ propagation life), whereas for the H-HCF samples the initiation life appears to be significantly longer than the propagation life, presumably because the LOF defects are edge on and less well configured to initiate crack growth.

In order to better understand the microstructural influences on the fatigue crack nucleation and propagation stages we have undertaken serial section scanning electron microscopy using a dual beam (plasma beam for serial sectioning; electron beam for imaging) microscope [5]. The EBSD maps indicate that the short cracks (see Fig 2b) are primarily located at, and propagate from, the melt pool boundaries (MPBs) which is consistent with most of the LOF defects being located in these regions. With regard to crack propagation paths (see Fig. 2c)., these short cracks exhibit primarily intergranular propagation with occasional transgranular features

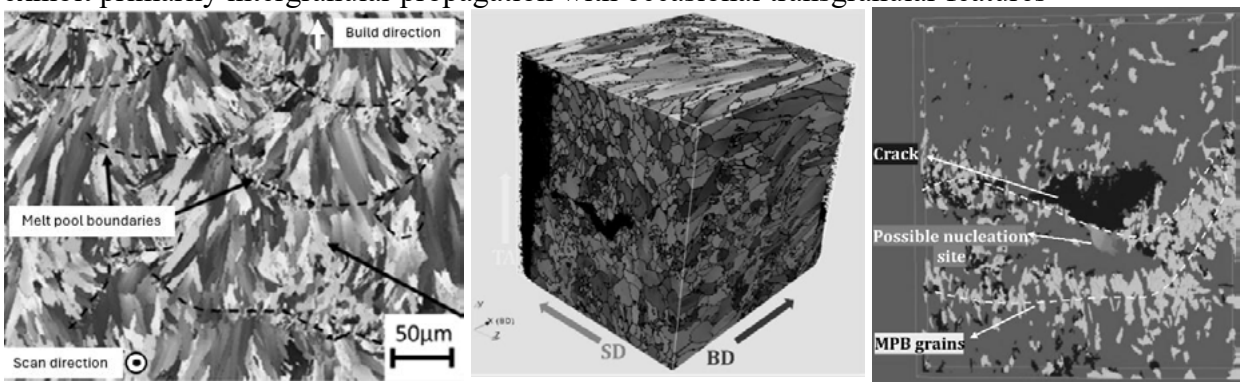

Figure 2. a) EBSD map showing the variation in grain size, b) 3D rendered EBSD map of the short-crack region obtained by serial sectioning (~170 × 170 × 160 μm³). The BD (build direction), TA (tensile axis) and SD (scanning direction) are indicated, c) 3D visualization of the crack - the dark region represents the primary crack, with smaller surrounding micropores, the white regions correspond to small grains lying at the MPBs.

REFERENCES

1. Tammas-Williams, S.; et al. The influence of porosity on fatigue crack initiation in additively manufactured titanium components. Sci. Rep., 7, 7308 (2017).
2. Larrosa, N.O.; et al. Linking microstructure and processing defects to mechanical properties of selectively laser melted AlSi10Mg alloy. Theor. Appl. Fract. Mech., 98, 123–133 (2018).
3. Wu, Z.; et al. The effect of defect population on the anisotropic fatigue resistance of AlSi10Mg alloy fabricated by laser powder bed fusion. Int. J. Fatigue, 151, 106317 (2021).
4. Qian, W.; et al. In situ X-ray imaging of fatigue crack growth from multiple defects in additively manufactured AlSi10Mg alloy. Int. J. Fatigue, 155, 106616 (2022).
5. Burnett, T.L.; et al. Large volume serial sectioning tomography by Xe plasma FIB dual beam microscopy. Ultramicroscopy, 161, 119–129 (2016).

3D characterisation of strain fields around propagating cracks in tailored fibre placement composites

Guowen SUN[1], Ria L MITCHELL[2], Fatma OMRANI[3], Matt SMITH[3], Clara FRIAS[3], J. Patrick A. FAIRCLOUGH[1], Christophe PINNA[1]

[1] The School of Mechanical, Aerospace and Civil Engineering, The University of Sheffield, Sheffield, S1 3JD, United Kingdom
[2] Sheffield Tomography Centre, The University of Sheffield, Sheffield, S1 3JD, United Kingdom, now at ZEISS Microscopy
[3] Advanced Manufacturing Research Centre, The University of Sheffield, Sheffield, S60 5TZ, United Kingdom

c.pinna@sheffield.ac.uk

Composites manufactured via Tailored fibre placement (TFP) exhibit complex fibre-bundle architectures that strongly affect local deformation and crack development under loading. 3D characterisation of deformation and damage is therefore necessary to understand the mechanisms controlling the strength of these composites. In this work X-ray computed tomography has been used in combination with in-situ tensile testing to capture progressive crack development through intermittent loading. The influence of deformation on crack initiation and propagation has been studied through the characterisation of 3D strain fields using Digital Volume Correlation (DVC).

A carbon fibre TFP composite with a $[0/60/-60]_s$ layup was manufactured and machined into dog-bone tensile specimens, with a design compatible with the 5kN Deben in-situ loading stage. A bespoke image segmentation procedure was developed to separate all phases of the TFP composite and to visualise crack morphologies in the fibre-bundle architecture. The acquired volumetric images were analysed using DVC to obtain 3D full-field strain measurements, with the detailed implementation including the mapping of the strain fields onto the reconstructed mesostructure of the composite reported in [1].

Although some cracks originated in resin-rich regions, the main damage mechanism in the TFP composite was clearly related to the development of cracks propagating along the fibre bundles of the composite, first in the +/- 60º plies (Figure 1(a)) and eventually along the 0º plies leading to final fracture. Initiation was observed at about 50%UTS with delamination only observed at 95%UTS. Stitching threads were seen to mainly affect crack propagation.

The first crack appearing in a fibre bundle is shown in Figure 1(b) with a maximum principal strain concentration around the crack shown in Figure 1(c). The crack then propagates in the resin located in between the carbon fibres in the fibre tow. Initiation was recorded for a local fibre-transverse strain value of 0.0082 in this particular ply with propagation following localised bands of strain concentration.

Results show the complexity of crack development in the 3D architecture of TFP composites with full-field strain measurements providing some insight into the mechanical conditions for crack development as well as validation means for the multi-scale modelling of these composites manufactured using one of the latest dry-fibre technology.

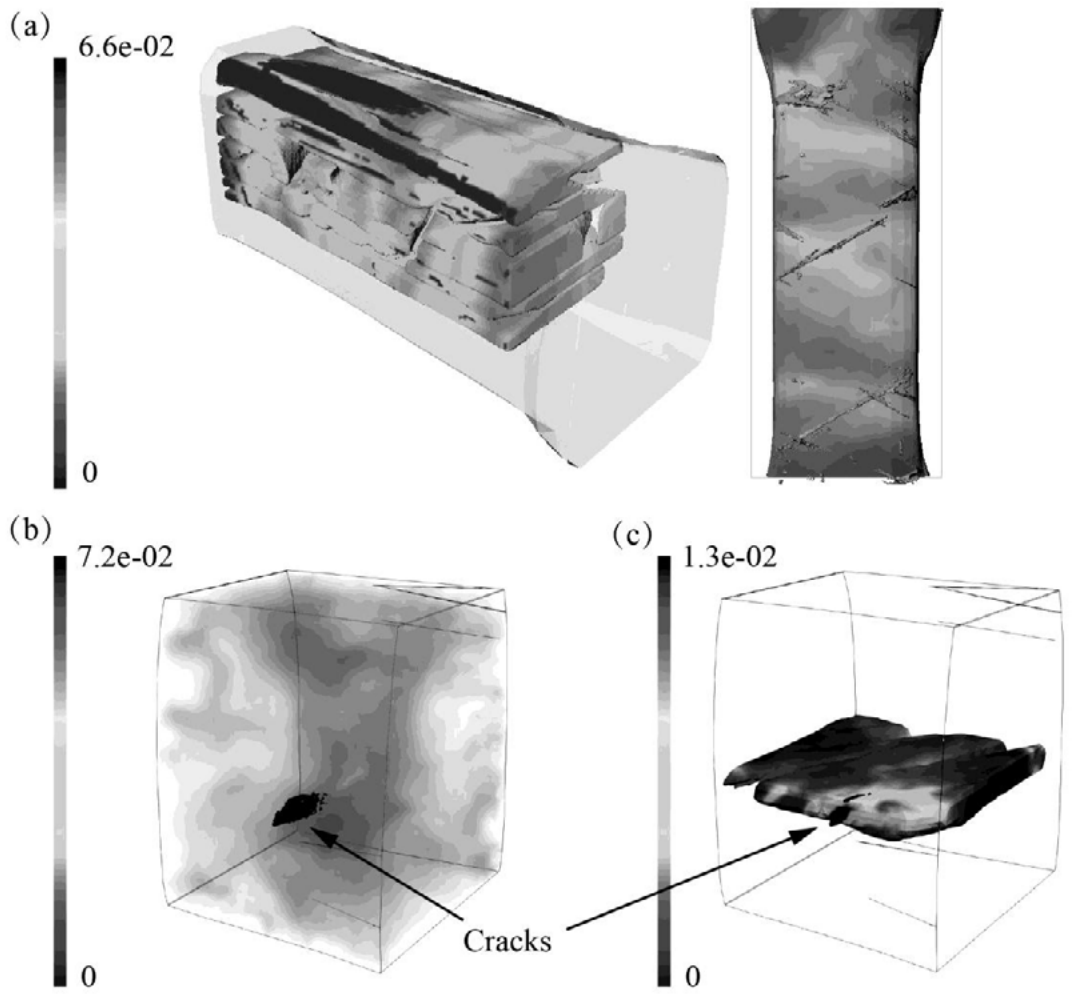

Figure 1. Maximum principal strain fields in the TFP composite under tensile loading and their relationship with crack development: (a) layer-wise strain distributions at 75% UTS, showing the overall correspondence between strain localisation and multi-crack patterns; (b) strain distribution in the volume of interest (VOI) at 50%UTS, highlighting the region where crack initiation was first identified; (c) strain map showing local strain concentration associated with crack initiation in the corresponding 60° layer.

REFERENCES

1. Sun, G.; Mitchell, R.L.; Chen, Z.; Omrani, F.; Smith, M.; Frias, C.; Fairclough, J.P.; Pinna, C. 3D tensile fracture analysis of tailored fibre placement composites using digital volume correlation. Theor. Appl. Fract. Mech., 105127 (2025).

Non-destructive evaluation of crack propagation by infrared thermography and acoustic emission: A brief review

Evangelos KORDATOS[1]

[1] School of Engineering and Built Environment, Sheffield Hallam University, Howard Street, Sheffield S1 1WB, UK

e.kordatos@shu.ac.uk

This study involves the determination of crack propagation rate through the combined use of thermography and acoustic emission. A lock-in thermography methodology was developed to quantify crack growth rate and predict the crack propagation path. Thermal waves generated by thermomechanical coupling and internal energy dissipation during cyclic loading were captured using an infrared camera. The resulting temperature fields were converted into stress fields through thermoelastic theory. Crack growth rates obtained from lock-in thermography were validated against measurements from the conventional compliance method, showing good agreement. Acoustic emission was additionally used to characterize different fracture mechanisms [1-2].

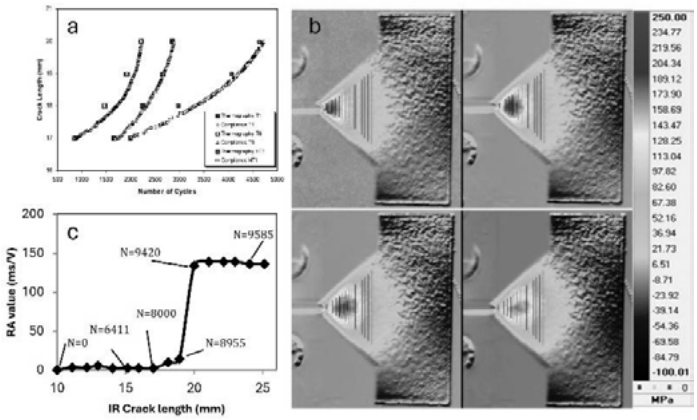

Figure 1. Crack growth rate by compliance vs. thermography (Reprinted with permission from John Wiley & Sons) [1], b. Progress of stress field due to crack propagation on a CT specimen [2], c. RA value vs. crack length as measured by thermography [2].

Infrared thermography (IRT) was employed also for real-time analysis of thermal phenomena in ceramic matrix composites subjected to cyclic loading. Cyclic mechanical stresses induce heat release associated with interfacial damage between matrix and reinforcement. Acoustic emission (AE) monitoring was performed in parallel to track acoustic activity associated with cumulative material damage. The mechanical behaviour of boron–magnesium–aluminium–silicon (BMAS) ceramic matrix composites reinforced with continuous silicon carbide (SiC) fibres was evaluated. Double Edge Notched (DEN) specimens were used to confine damage to a predefined region. Crack detection and propagation were monitored simultaneously using infrared thermography and acoustic emission [3].

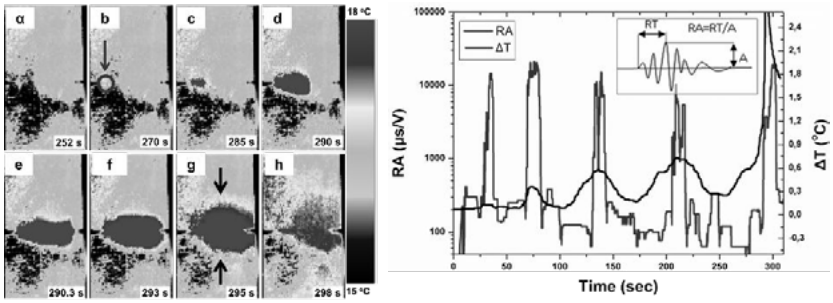

Figure 2. Crack propagation in DEN samples by IRT (left) and AE and IRT (right) [3].

Furthermore, an infrared thermography-based methodology for studying crack propagation behaviour and determining crack length in Compact Tension (CT) specimens was utilised. Crack propagation was monitored in SiC fibre-reinforced ceramic matrix composites where IRT and AE were applied as non-destructive techniques, and their results were validated against conventional crack length measurements obtained using a Crack Opening Displacement (COD) extensometer.

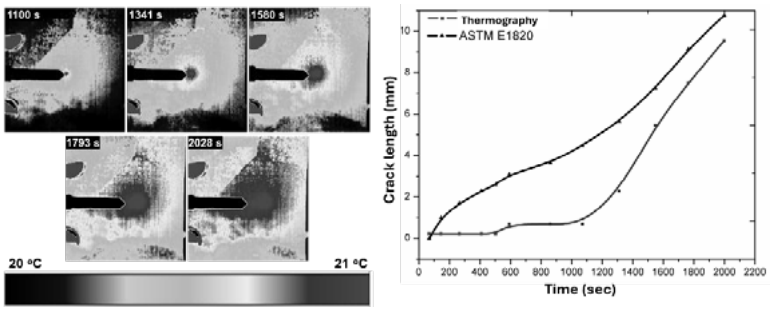

Figure 3. Crack propagation in CT samples by IRT (left) and COD vs IRT crack length (right) [4].

REFERENCES

1. Myriounis, D.; Kordatos, E.Z.; Hasan, S.; Matikas, T.E. Crack-tip stress field and fatigue crack growth monitoring using infrared lock-in thermography in A359/SiCp composites. Strain, 47, e619–e627 (2010).
2. Kordatos, E.Z.; Aggelis, D.G.; Matikas, T.E. Monitoring mechanical damage in structural materials using complementary NDE techniques based on thermography and acoustic emission. Compos. Part B Eng., 43, 2676–2686 (2012).
3. Kordatos, E.Z.; Aggelis, D.G.; Dassios, K.G.; Matikas, T.E. In-situ monitoring of damage evolution in glass matrix composites during cyclic loading using nondestructive techniques. Appl. Compos. Mater., 20, 961–973 (2013).
4. Dassios, K.G.; Kordatos, E.Z.; Aggelis, D.G.; Matikas, T.E. Crack growth monitoring in ceramic matrix composites by combined infrared thermography and acoustic emission. J. Am. Ceram. Soc., 97, 251–257 (2014).

The effect of notch on fatigue crack growth in a Charpy specimen

Aleksandar SEDMAK[1], Simon SEDMAK[2], Snezana KIRIN[2]

[1] Faculty of Mechanical Engineering, University of Belgrade, Serbia
[2] Innovation Center of the Faculty of Mechanical Engineering, Belgrade, Serbia

aleksandarsedmak@gmail.com

In this paper fatigue crack growth, experimentally observed on a standard Charpy specimen during testing by RUMUL Cracktronic device, was numerically simulated using XFEM and classical FEM with SMART option.

Regarding 3D XFEM, ABAQUS was used, with MORFEO/ABAQUS as a post-processing option to calculate stress intensity factors and number of cycles needed for crack grow from initial to any other size. Free crack growth option, automatically controlled by the software was used here to calculate stresses and stress intensity factors, as well as the deflection angle in relation to the initial crack growth direction, to "open" the crack in steps.

The finite element mesh with 67254 hexahedral elements and 72699 nodes, Fig. 1a, was used to model Charpy specimen with 2 mm deep notch, which was treated as the initial crack length. Figure 1b shows the initial crack (notch) on a standard Charpy specimen and the mesh around it, [12]. Crack growth was modelled by 28 steps, each 0.3 mm. Paris law coefficients ($C=2.11\cdot10^{-15}$, $m=6.166$), Young modulus $E=2.1\cdot10^5$ MPa, and Poisson ratio $\nu=0.3$, were used, while the loading was defined as the bending amplitude stress ($\sigma_{amp}=7$ MPa), [2]. Results are shown in Fig. 3, together with the experimental and analytical ones, obtained by direct integration of Paris law, [2].

a) 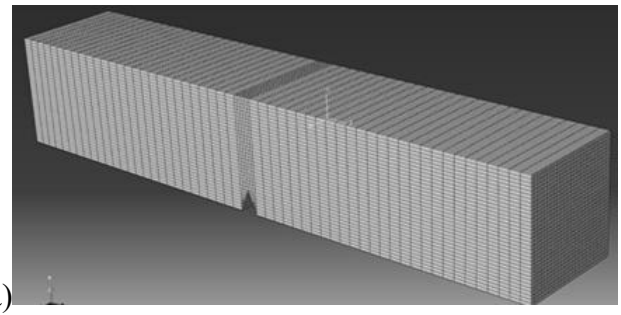 b) 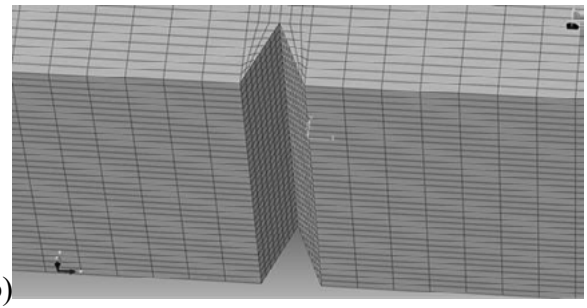

Figure 1. a) Finite element network of the Charpy specimen model (b) Initial crack (notch) in a standard Charpy specimen, [1].

a) 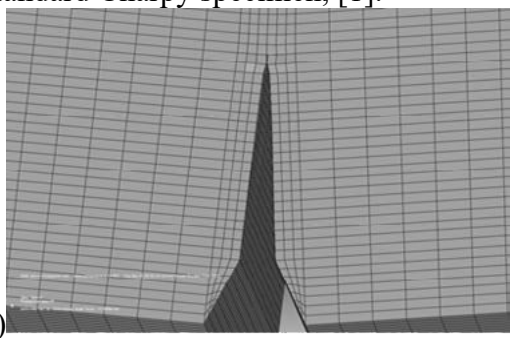 b) 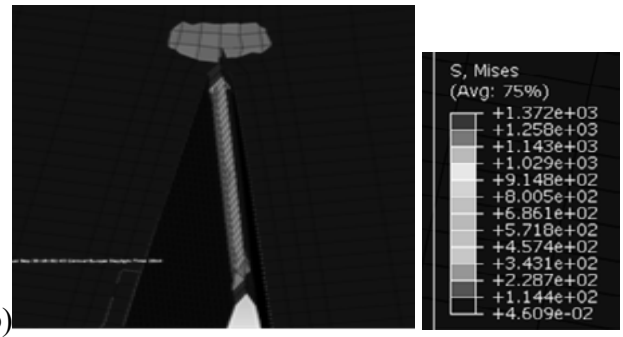

Figure 2. a) Crack growth, (b) Von Mises stresses after 27th step of crack growth, [2].

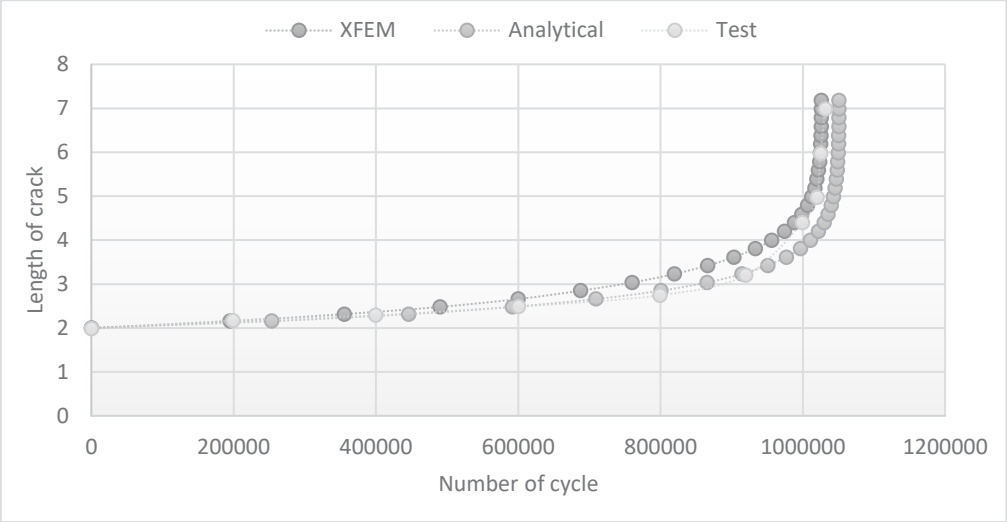

Figure 3. Comparative display of experimental, analytical and 3D XFEM results

Comparison between experimental, analytical and numerical result indicates good agreement with small differences between numerical and experimental results at the mid-range and between numerical and analytical results for large number of cycles. One can conclude that differences between XFEM and experimental results are due to inaccurate simulation of crack initiation. Namely, one should notice that in the experiment, crack initiates from the notch, whereas in XFEM simulation it is already positioned there, so that its growth starts without initiation period. Naturally, after significant amount of crack growth this difference tends to zero.

To further investigate this issue, one should use a new option provided in ANSYS Mechanical APDL 19.2 version - Separating Morphing and Adaptive Remeshing Technology (SMART) – to enable automatic re-meshing process in the scope of classical FEM. Anyhow, even better agreement might be expected if crack initiation is modelled by newest option also provided by ANSYS – no need for introduction of the initial crack – which is obtained by the software itself at the point of the highest stress concentration, as shown in [3]. Namely, when the crack is not presented in the simulation, a local criterion might be defined for crack initialization. When the criterion is satisfied, an elliptical crack is automatically inserted at the critical location. The maximum principal stress is usually used as the criterion for crack initiation. At the same time, local mesh is automatically redesigned to generate crack fronts and crack surfaces. Results obtained in this way for fatigue crack growth simulation in Charpy specimen are now under consideration and will be available in the full version of this paper.

REFERENCES

1. Grbović, A.; Sedmak, A.; Lazić-Vulićević, Lj.; Zaidi, R.; Kirin, S. Extended finite element method simulation of fatigue crack growth in Charpy specimen. Structural Integrity and Life, 23, 235–238 (2023).
2. Sedmak, A. Fatigue crack growth simulation by extended finite element method: a review of case studies. Fatigue Fract. Eng. Mater. Struct., e14277 (2024).
3. Raicevic, N.; Grbovic, A.; Kastratovic, G.; Vidanovic, N.; Sedmak, A. Fatigue life prediction of topologically optimized torque link adjusted for additive manufacturing. Int. J. Fatigue, 176, 107907 (2023).

Notch and fracture mechanics-based assessment of multiaxial fatigue thresholds of defects and sharp notches in metallic materials

Francesco COLLINI[1], Daniele RIGON[1], Giovanni MENEGHETTI[1]

[1] Department of Industrial Engineering, University of Padova, via Venezia 1, Padova (Italy)

giovanni.meneghetti@unipd.it

The fatigue assessment of metallic components containing defects, cracks, and sharp notches under multiaxial loading is still a major issue in the fatigue design of mechanical components. While current fatigue threshold models often refer to specific stress raisers, the present work proposes a unified framework recently developed for estimating constant-amplitude multiaxial fatigue thresholds in metallic materials weakened by defects, cracks, and sharp U- and V-notches [1] (Fig. 1a).

The approach extends the diagram originally proposed by Atzori, Lazzarin, and Meneghetti (the ALM diagram) for Mode I conditions [2,3] to general multiaxial local stress states by adopting the averaged strain energy density (SED) criterion as the governing fatigue parameter. This assumption is particularly effective as the SED is a scalar quantity that enables a direct comparison among defects and notches characterized by different geometries and combinations of Mode I, II, and III local stresses. On this basis, the model introduces three equivalent quantities for multiaxial loading: an equivalent plain fatigue limit $\Delta\sigma_{\mathrm{eq},\Delta\bar{w},0}$, an equivalent threshold parameter for long cracks or sharp V-notches $\Delta K^{V}_{\mathrm{eq},\Delta\bar{w},th}$, and an equivalent defect/notch size a^{V}_{eq}. As a result, the ALM model can be represented in unified diagram shown in Fig. 1b.

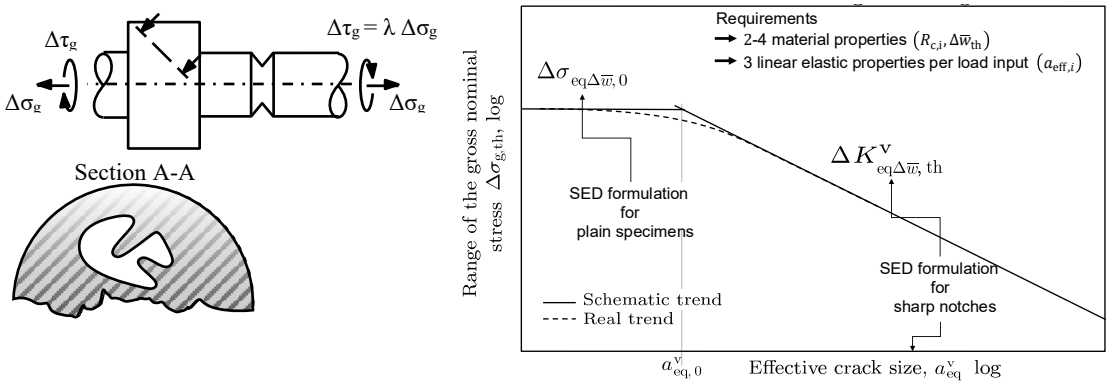

Figure 1. (a) The general case of local multiaxial stresses caused by multiple remote loads and (b) ALM diagram for multiaxial loading condition.

For crack-like defects, the framework combines local nominal stress decomposition with fracture-mechanics-based estimations of mixed-mode stress intensity factors and evaluating the appropriate a^{V}_{eq}. Thus, it allows to assess the fatigue threshold of defective materials as a short-crack problem and to describe the transition between defect-free behaviour and long-crack/sharp-notch behaviour within a unified diagram through an equivalent El-Haddad type equation (Fig. 1b).

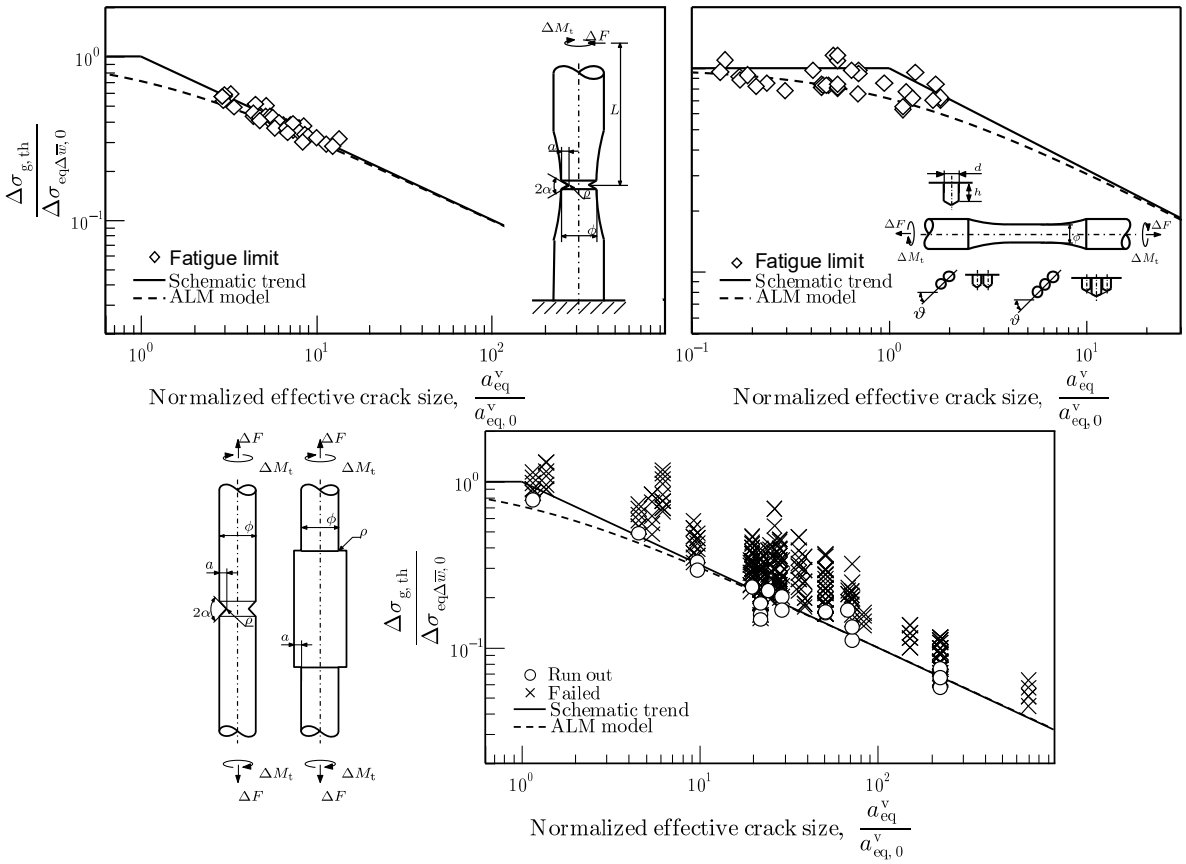

Figure 2. Comparisons between theoretical estimation of multiaxial fatigue thresholds with (a) fatigue limit of severely notched components (b) defective materials (c) and failed/run-out fatigue tests on notched components.

The model was validated against 128 experimental multiaxial fatigue limits collected from the literature for steel, cast iron, and Ti-6Al-4V specimens containing sharp V-notches and artificial or crack-like defects as reported in Fig. 2 [1]. The comparison showed a satisfactory overall agreement: approximately 80% of the experimental data were estimated with an error lower than 15%, while the remaining results were estimated within 30%.

In conclusion, the proposed SED-based multiaxial ALM approach provides an engineering tool for the fatigue threshold assessment of metallic materials containing defects or sharp notches subjected to local Modes I, II, and III stresses, bridging notch mechanics, fracture mechanics and defect sensitivity within a single design theoretical framework.

REFERENCES

1. Collini, F.; Rigon, D.; Meneghetti, G. Notch and fracture mechanics-based assessment of multiaxial fatigue thresholds of defects and sharp notches in metallic materials. Fatigue Fract. Eng. Mater. Struct., 48, 1929–1970 (2025).
2. Atzori, B.; Lazzarin, P.; Meneghetti, G. Fracture mechanics and notch sensitivity. Fatigue Fract. Eng. Mater. Struct., 26, 257–267 (2003).
3. Atzori, B.; Lazzarin, P.; Meneghetti, G. A unified treatment of the mode I fatigue limit of components containing notches or defects. Int. J. Fract., 133, 61–87 (2005).

Theoretical and practical implications derived from the formulation of the Theory of Critical Distances

Sergio CICERO[1], David TAYLOR[2], Luca SUSMEL[3]

[1] LADICIM, Universidad de Cantabria, ETS Ingenieros de Caminos, Avenida Los Castros 44, Santander, 39005, Spain
[2] Department of Mechanical, Manufacturing and Biomedical Engineering, School of Engineering, Trinity College Dublin, Dublin 2, Ireland
[3] School of Engineering and Built Environment, Sheffield Hallam University, Harmer Building, Sheffield, S1 1WB, United Kingdom

ciceros@unican.es

The Theory of Critical Distances [1] comprises several methodologies that allow fracture, fatigue and stress corrosion cracking phenomena to be analysed. Such methodologies are usually referred to as the Point Method (PM), the Line Method (LM), the Area Method (AM) and the Volume Method (VM). All of them provide analyses where the corresponding material resistance (e.g., fracture toughness, fatigue threshold, stress corrosion cracking threshold) is used together with an additional material parameter with length units (the critical distance, L). The accuracy of these four approaches is very similar, but the PM and the LM have a much simpler application.

When dealing with fracture processes, the TCD allows fracture conditions for structural materials in the presence of notch-type defects to be established, and simple formulas for estimating the apparent fracture toughness (i.e., the fracture resistance in the presence of notches) to be obtained. This work provides a number basic reasonings related to both the PM and/or the LM formulations that allow different straightforward conclusions to be derived, with significant theoretical and practical implications. Real cases with experimental results are also included, exemplifying what is discussed in the theoretical analysis.

Two basic formulas are used: the Point Method failure criterion (equation (1)), and the apparent fracture toughness prediction derived from the Line Method and the Creager-Paris stress distribution ahead of the notch tip (equation (2)). These two equations allow different practical implications to be derived, which may be useful when dealing with critical (i.e., fracture) or subcritical cracking processes (e.g., fatigue, stress corrosion cracking). These implications may have usefulness at different stages of the component lifecycle, from the initial design to the final failure analysis, if applicable, as well as its service life.

$$\sigma\left(\frac{L}{2}\right) = \sigma_0 \tag{1}$$

$$K_{mat}^{N} = K_{mat}\sqrt{1+\frac{\rho}{4L}} \tag{2}$$

Essentially, by knowing the ultimate tensile strength (σ_u) (or, more generally, the inherent strength, σ_0), the fracture toughness (K_{mat}), and the corresponding critical distance (L), it is possible to compare the performance of different materials in engineering applications in the presence of any kind of geometrical feature (notch). As an example, if two materials have the same L, the one with the higher σ_0 will withstand a greater critical load, P_{crit} (Figure 1).

Finally, beyond this sort of comparisons, two scientific issues with important engineering implications are simply addressed: first, it is shown and justified that, given two materials, one may be superior in cracked conditions or in the presence of sharp notches (the one with higher K_{mat}) whilst the other can be superior for blunter notches (see Figure 2). This is a kind of mistake which a designer might easily make, assuming that one material will always be superior to the other; second, the application of the apparent fracture toughness prediction mentioned above to structural integrity assessments using Failure Assessment Diagrams is able to explain how introducing larger notch radii can generate significant changes in the failure micromechanisms.

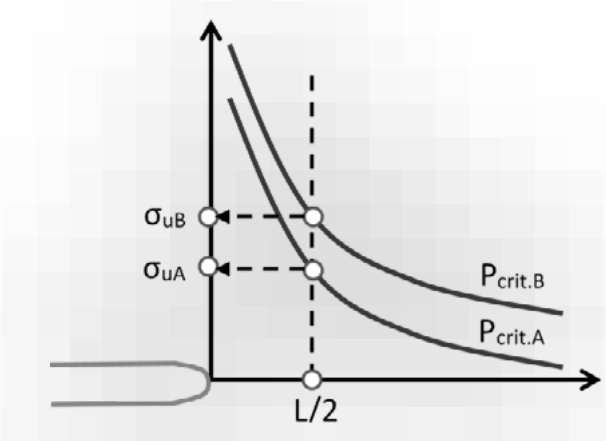

Figure 1. Schematic of the critical condition in two materials, A and B, with the same critical distance (L) and following the Point Method. Here, σ_0 is assumed to be equal to σ_u.

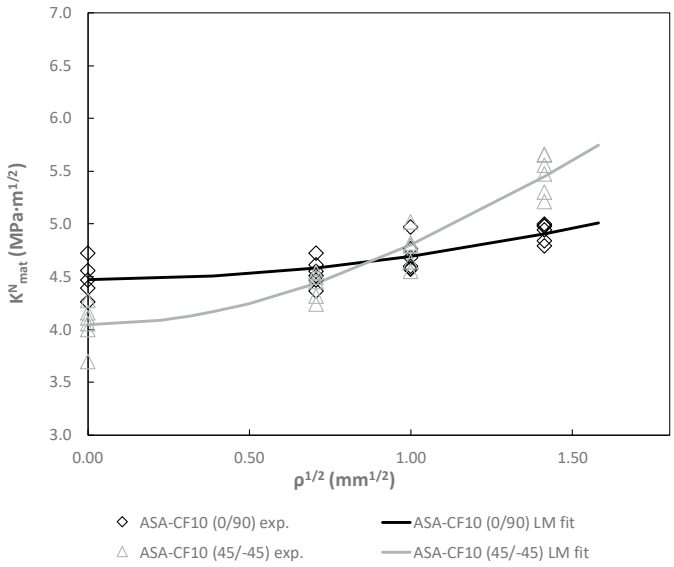

Figure 2. Evolution of apparent fracture toughness (K^N_{mat}) in ASA-CF10 with two different printing raster orientations (0/90, 45-45) [2].

REFERENCES

1. Taylor, D. The theory of critical distances: a new perspective in fracture mechanics, Elsevier, (2007).
2. Cicero, S.; Arrieta, S.; Devito, F.; Arroyo, B.; Lavecchia, F. Fracture behaviour of additively manufactured carbon fibre reinforced acrylonitrile–styrene–acrylate containing cracks and notches. J. Compos. Sci., 9, 185 (2025).

Notch sensitivity of fatigue behaviour up to very-high-cycle fatigue regime for a structural steel

Youshi HONG[1], Qingqing JIANG[1], Chengqi SUN[1]

[1] Institute of Mechanics, Chinese Academy of Sciences, Beijing 100190, China

hongys@imech.ac.cn

Surface notches significantly affect the fatigue behavior of structural steels, which can act as fatigue crack initiation sites at relatively low stress levels. Crack initiation behavior induced by surface notches, especially in high-cycle fatigue (HCF) and very-high-cycle fatigue (VHCF) regimes, still remains insufficiently investigated.

The material employed in this study was a structural steel with the chemical composition (wt.%): 0.42 C, 0.31 Si, 0.82 Mn, 0.0072 P, 0.0084 S, 0.02 Al, 0.0037 N, 0.0006 O and Fe balance. Five groups of specimens were prepared for fatigue tests, with their details shown as follows: Group A: Induction-heated at high frequency for 3 s, quenched in BW water-based quenchant, tempered at 220 °C for 2 h, and with a smooth gauge section. Group B: Heated at 860 °C for 10 min in a salt-bath furnace, quenched in a nitrate solution at 170 °C, and tempered at 230 °C for 2 h. (Groups A and B with identical microstructures and tensile properties: average yield strength 1552 MPa and tensile strength 1883 MPa.) Group C: Same heat treatment as Group B, with indent notches on the gauge section surface. Group D: Same heat treatment as Group B, with drill-hole notches on the gauge section surface. Group E: Same heat treatment as Group B, with a circumferential notch on the gauge section surface.

Fatigue tests were conducted on a rotary bending machine at room temperature in air, with a loading frequency of 52.5 Hz and a stress ratio of $R = -1$. Fig. 1 shows the obtained S–N data for Groups A and D. For group A, the fatigue strength decreases with the increase of fatigue life, and crack origin tends to be from the interior of specimen when the fatigue life beyond 5×10^6. For Group D, the fatigue strength is substantially lower than that of Group A, and there is a plateau region between 10^5 and 10^8 cycles. Fig. 2 shows the obtained S–N data for Groups B, C and D, illustrating the fatigue strength at 10^8 cycles is 710 MPa for Group B, 610 MPa for Group C, and 480 MPa for Group D. Evidently, the existence of surface notches greatly degrades the fatigue resistance of the structural steel. For Group C with indent notch, the fatigue strength decreases by 14% comparing with the value of Group B with smooth gauge section, and for Group D with drill-hole notches, such a decrease is 32%. The fractography observations showed that for Group B, crack initiation is from specimen surface, for Group C, crack initiation is also from specimen surface, and the indent notch is not sensitive to crack initiation, and for Group D, all failures are due to crack initiation from surface notches. This indicates that the surface notch size of 200 μm in diameter and 200 μm in depth is an overwhelming source responsible for crack initiation. The notch effect on the degradation of fatigue strength was analyzed by Murakami's model [1] and Shyam's model [2]. Fracture surfaces, particularly the micro-morphologies of crack initiation regions, were characterized by using scanning electron microscopy (SEM) and transmission electron microscopy (TEM), and thus the crack initiation mechanism for the specimens with and without surface notches of structural steel was comprehensively addressed. In addition, the fatigue data of Group E was also obtained, showing the fatigue strength of circumferential notched specimens is close to that of smooth specimens.

However, after grinding the notch root, the fatigue strength of circumferential notched specimens substantially reduced. This needs further investigation.

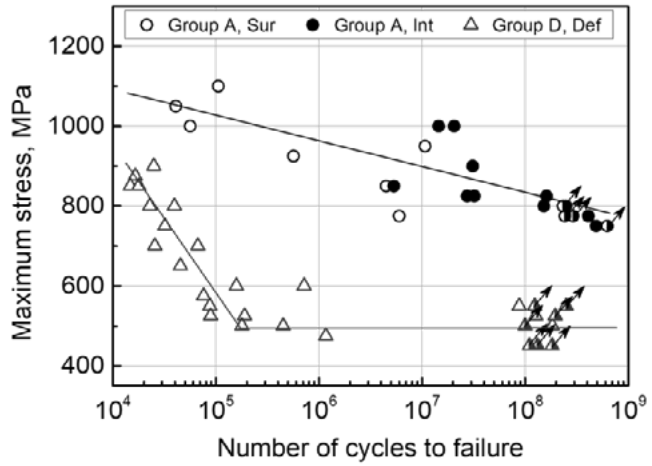

Figure 1. *S–N* data for Groups A and D. Sur: crack initiation from surface, Int: crack initiation from interior, Def: crack initiation from defect, point with arrow: runout specimen [3].

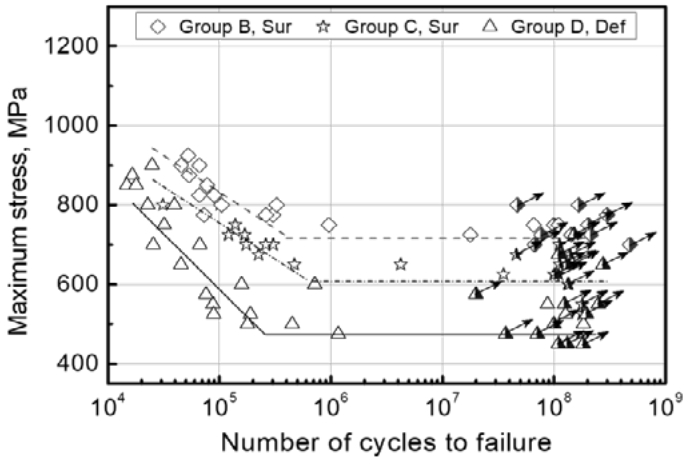

Figure 2. *S–N* data for Groups B, C and D. Sur: crack initiation from surface, Def: crack initiation from defect, point with arrow: runout specimen [4].

REFERENCES

1. Murakami, Y. Metal fatigue: effects of small defects and nonmetallic inclusions, Elsevier, London, (2002).
2. Shyam, A.; Blau, P.; Jordan, T.; Yang, N. Effect of submillimeter size holes on the fatigue limit of a high strength tool steel. Fatigue Fract. Eng. Mater. Struct., 37, 368–379 (2014).
3. Jiang, Q.; Sun, C.; Liu, X.; Hong, Y. Very-high-cycle fatigue behavior of a structural steel with and without induced surface defects. Int. J. Fatigue, 93, 352–362 (2016).
4. Hong, Y.; Jiang, Q.; Sun, C. Effects of induced surface notches on fatigue behavior of a structural steel. Proceedings of the 14th International Conference on Fracture (ICF14), Rhodes, Greece, 18–23 June, (2017).

Experimental fatigue behaviour and TCD-based life estimation of micro-defected X60 pipeline steel under unsoaked and hydrogen-soaked conditions in the medium-cycle regime

Hongsong WANG[1], Robert BEST[2], Dirk ENGELBERG[3], Iman HAJIRASOULIHA[1], Nicolas Oscar LARROSA[4,5], Fabio SCENINI[3,6], Luca SUSMEL[7]

[1] School of Mechanical, Aerospace and Civil Engineering, The University of Sheffield, Mappin Street, Sheffield S1 3JD, UK
[2] National Gas Transmission, Warwick Technology Park, Gallows Hill, CV34 6DA, UK
[3] Corrosion@Manchester, Department of Materials, The University of Manchester, Manchester, M13 9PL, UK
[4] School of Electrical, Electronic and Mechanical Engineering, University of Bristol, UK
[5] TECNALIA R&I, Basque Research and Technology Alliance (BRTA), Mikeletegi Pasealekua 2, 20009 Donostia-San Sebastián, Gipuzkoa, Spain
[6] Royce Institute, The University of Manchester, Manchester, M13 9PL, UK
[7] Materials and Engineering Research Institute (MERI), Sheffield Hallam University, Harmer Building, Sheffield, S1 1WB, UK

L.Susmel@shu.ac.uk

The main aim of this work was to investigate the effects of defect size and hydrogen exposure in pipeline steel containing small artificial defects, and to evaluate the applicability of the Theory of Critical Distances (TCD) for predicting fatigue life in the medium-cycle regime, under unsoaked and hydrogen-soaked condition.

The Theory of Critical Distances is a local stress-based method used to assess the fatigue and fracture behaviour of notched or defect-containing materials by introducing a material characteristic length to account for stress gradients near stress raisers [1]. Instead of relying solely on the maximum stress at the defect boundary, the method evaluates the stress over a critical distance from the stress concentration site, thereby relating local geometry to fatigue behaviour in a physically meaningful manner. In the present study, fatigue life was estimated using the method proposed by Susmel and Taylor [2] for the medium-cycle fatigue regime, in which the critical distance is treated as a function of the number of cycles to failure rather than as a constant associated only with the fatigue limit. This formulation extends the applicability of TCD to life prediction over the approximate range of 10^4 to $2x10^6$ cycles.

The experimental tests were carried out using material extracted from a 1970s vintage API 5L X60 pipeline steel representative of UK gas transmission infrastructure. Flat plate specimens with dimensions of 100 × 10 × 2 mm were prepared with a centred artificial micro-hole of diameter between 50 and 500 μm. Tension–tension constant-amplitude axial fatigue tests were performed at a load ratio of R = 0.1 in accordance with ASTM E466 [3] under both unsoaked and hydrogen-soaked conditions.

The fatigue results and corresponding S–N curves were analysed and post-processed to characterise the influence of defect size on the fatigue endurance limit. The results showed a clear reduction in fatigue endurance limit with increasing defect size. The difference between the endurance limit of hydrogen soaked and unsoaked specimens are negligible, while the inverse slope of hydrogen-soaked samples is larger than the unsoaked samples, showing that the

hydrogen-soaked S-N curve is flatter than unsoaked ones. This indicated that the hydrogen-soaked samples will have a shorter fatigue life in medium cycle fatigue regime, given the same stress applied [4]. Using this trend, we can use the stress-based fatigue life estimation method to estimate the medium cycle regime fatigue life of the samples to help validate our experimental results. TCD-based fatigue life estimates of hydrogen-soaked specimens and unsoaked specimens were obtained and compared with the experimental S–N data. The scatter bands and accuracy of the estimation were calculated, which showed great agreement in the medium-cycle regime (Figure 1).

Combining experimental fatigue testing with TCD-based local stress analysis, a useful framework for estimating the fatigue performance of pipeline steels containing micro-defects under both air and hydrogen-affected conditions can be provided. The method is particularly promising for assessing the fatigue behaviour associated with defect-sensitive early-stage crack propagation in the medium-cycle regime, and therefore offers useful insight for the structural integrity assessment of existing assets and the development of hydrogen-ready pipeline infrastructure.

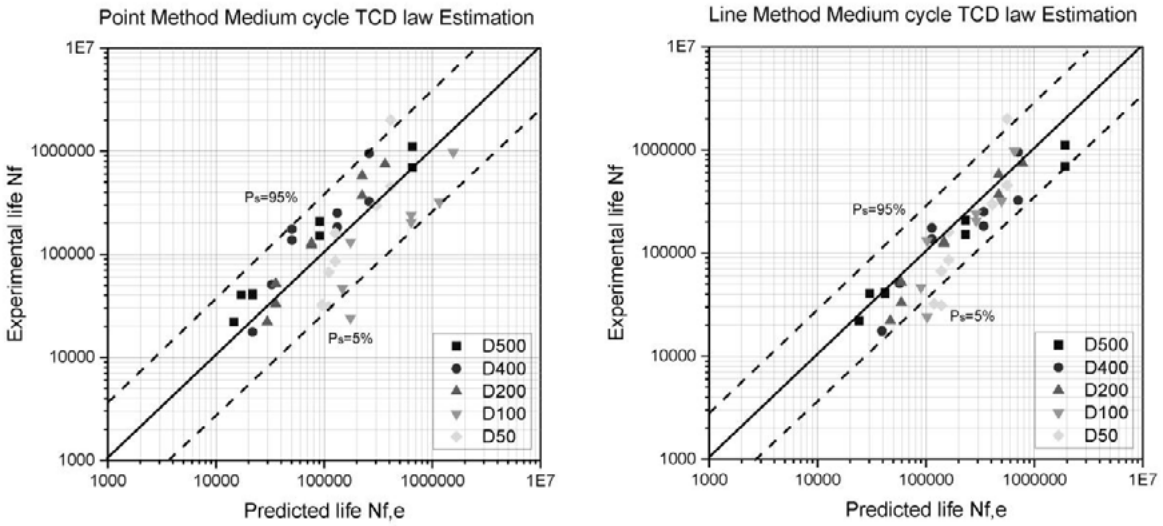

Figure 1. (a) Hydrogen-soaked samples fatigue life estimation in medium cycle regime using TCD Point Method; (b) Hydrogen-soaked samples fatigue life estimation in medium cycle regime using TCD Line Method.

REFERENCES

1. Taylor, D. The theory of critical distances. Eng. Fract. Mech., 75, 1696–1705 (2008).
2. Susmel, L.; Taylor, D. A novel formulation of the theory of critical distances to estimate lifetime of notched components in the medium-cycle fatigue regime. Fatigue Fract. Eng. Mater. Struct., 30, 567–581 (2007).
3. ASTM E466-21. Standard practice for conducting force controlled constant amplitude axial fatigue tests of metallic materials, ASTM International, West Conshohocken, PA, (2021).
4. Wang, H.; Larrosa, N.O.; Engelberg, D.; Best, R.; Susmel, L. A statistical review of hydrogen effects on the fatigue and fracture behavior of steel. Fatigue Fract. Eng. Mater. Struct., 48, 3109–3139 (2025).

Damage tolerance assessment of hot-section components: fracture toughness testing and fatigue life prediction

Xing SONG[1], Shun-Peng ZHU[1], Qingyuan WANG[2]

[1] School of Mechanical and Electrical Engineering, University of Electronic Science and Technology of China, Chengdu, 611731, China
[2] MOE Key Laboratory of Deep Earth Science and Engineering, College of Architecture and Environment, Sichuan University, Chengdu 610065, China

zspeng2007@uestc.edu.cn

Hot-section components, such as turbine discs and combustion chambers, are typically designed as damage-tolerant materials and are required to withstand extreme thermomechanical loads. Elevated temperatures, cyclic loading and inherent structural defects inevitably lead to fatigue crack initiation and propagation. Therefore, accurate assessment of fracture toughness and residual life is essential to ensure the structural integrity and safety of hot-section components.

The objective of this study is to establish a unified damage tolerance assessment framework that integrates fracture toughness evaluation, crack propagation monitoring and fatigue life prediction for hot-section structures.

To this end, a comprehensive damage tolerance assessment of hot-section structures was conducted, including elevated-temperature fracture toughness testing, real-time crack propagation monitoring, fracture toughness model and residual fatigue life prediction. Representative specimens were designed to capture geometric features and stress distribution. Two experimental platforms for real-time crack propagation monitoring were established. One used the direct current potential drop technique and the other employed acoustic emission. Based on these platforms, a linear-elastic fracture toughness evaluation model incorporating the equivalent energy density method was developed and applied to high- and low-temperature bolt structures. Moreover, an elastic-plastic fracture toughness (J_{IC}) model and a critical fatigue crack size evaluation framework were established using a failure assessment diagram that considers crack-size evolution, with application to turbine disk structures. The proposed fracture toughness models achieve a prediction accuracy within a ±1.5 scatter band, as shown in Fig. 1(a).

Fractographic analysis indicates that crack propagation prior to final failure sequentially experiences a linear-elastic dominated stage followed by an elastic-plastic dominated stage. Based on this mechanism, the predicted fracture toughness was adopted as the crack propagation failure criterion, and a segmented crack growth model was established, in which elastic and elastic-plastic crack driving forces were employed in different propagation stages. The fatigue life prediction accuracy is within a ±3 scatter band. Furthermore, an acoustic emission-based real-time crack propagation monitoring framework was proposed for fan disk structures.

Overall, this work establishes an integrated damage tolerance assessment framework spanning crack propagation characterization, fracture toughness evaluation and fatigue life prediction, providing methodological support for structural integrity assessment of hot-section components under extreme service conditions.

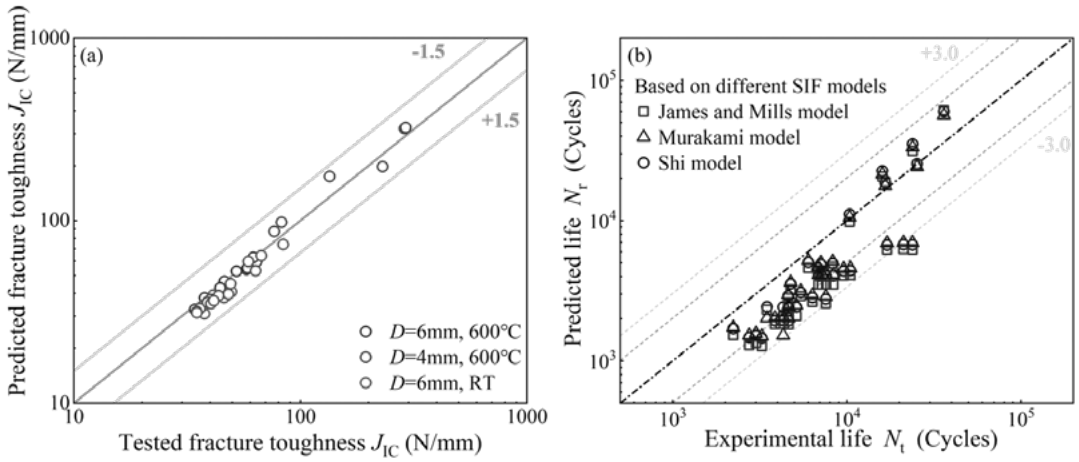

Figure 1. (a) Predicted fracture toughness under different geometric dimensions and temperatures; (b) Fatigue life prediction results obtained by combining the proposed model with three different crack driving force models.

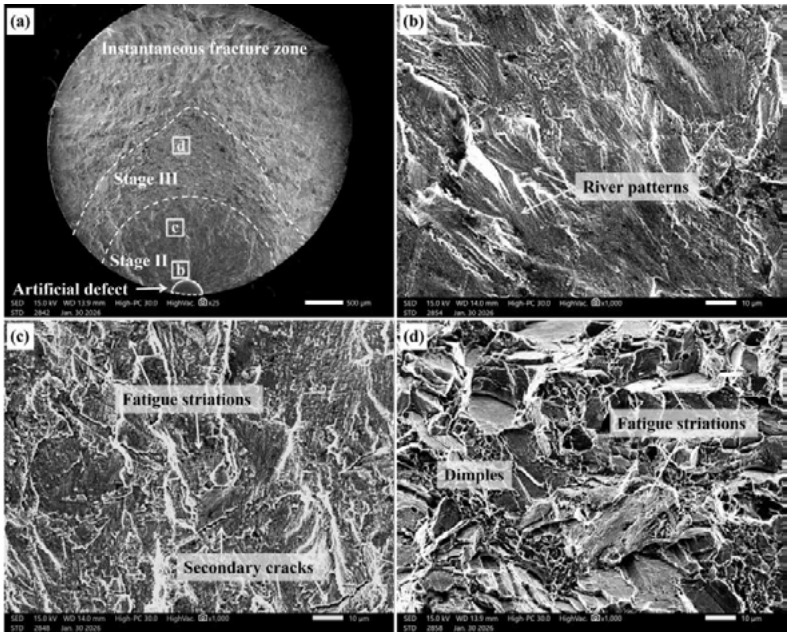

Figure 2. Typical fatigue fracture morphologies of the FGH96 round bar specimen containing a surface defect tested at 600°C under a maximum stress of 900 MPa.

A novel double indentation method to evaluate mixed-mode stress intensity factors and cleavage toughness

Zikang ZHANG[1], James MARROW[1]

[1] Department of Materials, University of Oxford, Parks Road, Oxford, OX1 3PH, UK

zikang.zhang@materials.ox.ac.uk

Accurate characterisation of crack-tip fields at the micron scale is essential for understanding the fracture behaviour of brittle materials, yet conventional indentation-based methods infer toughness from post-mortem crack length measurements with the assumption of idealised crack geometries. In this work, we present a double-indentation strategy for characterisation of mixed-mode cleavage cracks, in which a spherical indent is first used to generate a broad residual stress field, then a sharp Berkovich indent is introduced within this field to initiate and extend a crack until arrest (Figure 1). High-resolution electron backscatter diffraction (HR-EBSD) is then used to map the local elastic deformation-gradient field around the arrested crack tip. From these measurements, a full three-dimensional J-integral is evaluated and decomposed into the stress intensity factors (SIFs) K_I, K_{II} and K_{III}.

Experiments with nano-indentations on (001) 8 mol% Y_2O_3-stabilised zirconia (8YSZ) single crystals with differently oriented Berkovich indents to select preferential cleavage planes show fracture toughness values, estimated from the extracted mixed-mode SIFs using a maximum potential energy release rate (MPERR) criterion, that are consistent with literature data (Table 1). By avoiding reliance on crack-length measurements and assumed crack morphologies, this method provides a robust route for critical crack-tip field characterisation and microstructure-scale fracture analysis in brittle materials.

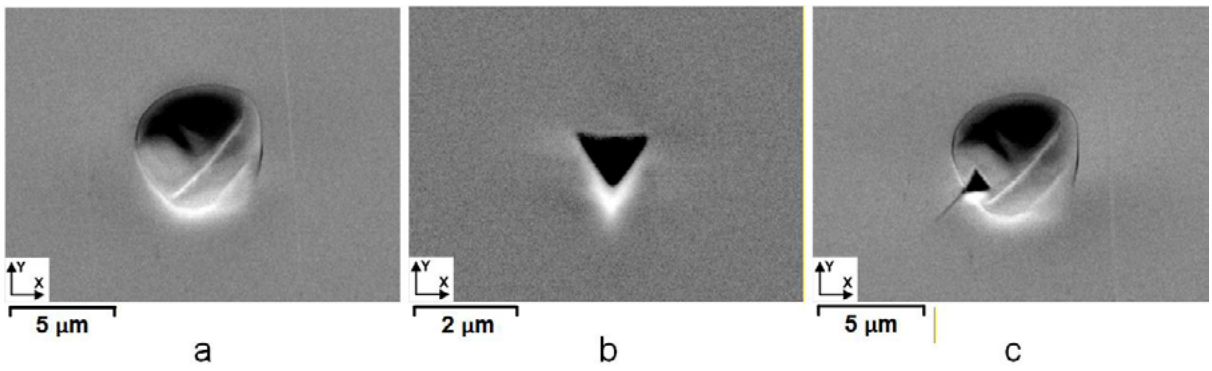

Figure 1. Scanning electron microscope (SEM) observations of nano-indentations on the (001) surface of 8 mol% Y_2O_3-stabilised zirconia single crystal: a. Single spherical indentation; b. Single Berkovich indentation; c. Double indentation to introduce cleavage on (100).

Table 1. Mixed-mode stress intensity factors, J, and MPERR-based equivalent fracture toughness K_{IC} for different cleavage planes. The representative values reported for K_I, K_{II} and K_{III} are the mean ± standard error for a single indentation crack in each case, calculated over the analysed J-integral contours for that crack. The J and K_{IC} data are the mean obtained from 4 independent experiments with the reported uncertainties as the standard error of the mean.

Plane	K_I (MPa·m$^{1/2}$)	K_{II} (MPa·m$^{1/2}$)	K_{III} (MPa·m$^{1/2}$)	MPERR-based equivalent K_{IC} (MPa·m$^{1/2}$)	J (J/m^2)	Literature K_{IC} (MPa·m$^{1/2}$)
{100}	1.82±0.08	0.05±0.02	0.09±0.03	1.85±0.09	14.41±1.41	1.90±0.10 [4]
{110}	1.12±0.09	0.86±0.07	0.11±0.04	1.49±0.11	8.36±1.28	1.48±0.04 [4]
{111}	0.92±0.07	0.84±0.06	0.51±0.04	1.44±0.13	7.94±1.38	1.48±0.07 [5]

REFERENCES

1. Su, X.; Zhang, Z.; Williamson, M.; Vuksic, M.; Koko, A.; Marrow, T.J. Measurement of cleavage toughness of brittle materials by local elastic field analysis. Acta Mater., 304, 121797 (2026).
2. Koko, A.; Becker, T.H.; Elmukashfi, E.; Pugno, N.M.; Wilkinson, A.J.; Marrow, T.J. HR-EBSD analysis of in situ stable crack growth at the micron scale. J. Mech. Phys. Solids, 172, 105173 (2023).
3. Koko, A.; Elmukashfi, E.; Becker, T.H.; Karamched, P.S.; Wilkinson, A.J.; Marrow, T.J. In situ characterisation of the strain fields of intragranular slip bands in ferrite by high-resolution electron backscatter diffraction. Acta Mater., 239, 118284 (2022).
4. Pajares, A.; Guiberteau, F.; Dominguez-Rodriguez, A.; Heuer, A.H. Microhardness and fracture toughness anisotropy in cubic zirconium oxide single crystals. J. Am. Ceram. Soc., 71, C332–C333 (1988).
5. Stanescu, J.D.; Chan, H.M. Indentation study of fracture toughness anisotropy in cubic zirconium oxide single crystals. J. Mater. Sci. Lett., 11, 1364–1366 (1992).

Size-dependent fracture in anisotropic beam lattice materials

İrem YAGMUROGLU[1], Harm ASKES[2]

[1] Department of Civil Engineering, Istanbul University-Cerrahpaşa, Turkey
[2] Faculty of Science and Engineering, Maastricht University, Netherlands

irem.yagmuroglu@iuc.edu.tr, harm.askes@maastrichtuniversity.nl

With recent progress in advanced manufacturing processes such as 3D printing, new lightweight materials consisting of beam lattices can be developed. Since the main mechanical action is via normal force (rather than shear force or bending moment), lattice structures offer competitive strength-to-weight ratios. In the development of materials with a lattice microstructure, both continuum models and discrete models offer distinct advantages – thus, it is important to ensure that the two sets of models share a common basis. This can be achieved via continualisation procedures: starting from a discrete description and modelling the individual struts with beam finite elements, equivalent continuum models can be formulated by applying Taylor series [5, 6, 7, 8] and, for reasons of thermodynamic stability, Padé Approximations [5] or other regularisation techniques [6].

The resulting models can be of the simplest form of classical continuum mechanics, but also nonlocal models equipped with higher-order terms are possible, leading e.g. to gradient elasticity models that include higher-order spatial derivatives of the kinematic variables [1, 4] whereby the accompanying constitutive parameters are written in terms of the strut length of the lattice [5, 10]. Particular care may be required to ensure that the continuum models retain the intrinsic anisotropy that characterises periodic beam lattices, but it has been shown that such models are able to describe the stresses and strains around sharp cracks and re-entrant corners without the singularities that plague classical elasticity models [3, 4, 9].

In this contribution, we will investigate the size-dependent mechanical behaviour of periodic beam lattices using both discrete models and nonlocal continuum models. With the ability of gradient elasticity models to describe localised yet non-singular crack tip stresses, it becomes possible to predict the strength of a component using elastic analysis. However, the structural strength typically depends on the actual size of the component due to the interaction between macrostructural dimensions and microstructural strut length. This phenomenon is commonly known as "size effect" and it can be described by nonlocal continuum models [2, 4].

Here, we focus on size effects of structural strength as it manifests itself in components consisting of anisotropic material. The level of anisotropy can be controlled by the intrinsic cross-sectional area of the lattice struts, whilst a further parameter may be taken to be the ratio of strut lengths in the various directions. Furthermore, we will study size effects of components with pre-existing cracks whereby the crack dimension scales with the macrostructural dimensions and cracks whereby the crack dimensions are independent of the macrostructural dimensions. Finally, we will verify to what extent the phenomenological size effect laws suggested in the literature for isotropic media are applicable, or can be extended, to anisotropic media. Throughout, we will compare the results of the underlying discrete model with those of the derived anisotropic gradient elasticity continuum model.

REFERENCES

1. Aifantis, E.C. On the role of gradients in the localization of deformation and fracture. Int. J. Eng. Sci., 30, 1279–1299 (1992).
2. Aifantis, E.C. Strain gradient interpretation of size effects. Int. J. Fract., 95, 299–314 (1999).
3. Altan, S.B.; Aifantis, E.C. On the structure of the mode III crack-tip in gradient elasticity. Scr. Metall. Mater., 26, 319–324 (1992).
4. Askes, H.; Aifantis, E.C. Gradient elasticity in statics and dynamics: an overview of formulations, length scale identification procedures, finite element implementations and new results. Int. J. Solids Struct., 48, 1962–1990 (2011).
5. Askes, H.; Lombardo, M.; Nguyen, D.C.D. Homogenisation of periodic lattices with lumped and distributed mass: beam models, continualisation and stabilisation. Int. J. Solids Struct., 302, 112988 (2024).
6. Bacigalupo, A.; Gambarotta, L. A dynamic high-frequency consistent continualization of beam lattice materials. Compos. Struct., 272, 114146 (2021).
7. Bažant, Z.P.; Christensen, M. Analogy between micropolar continuum and grid frameworks under initial stress. Int. J. Solids Struct., 8, 327–346 (1972).
8. Kumar, R.S.; McDowell, D.L. Generalized continuum modeling of 2-D periodic cellular solids. Int. J. Solids Struct., 41, 7399–7422 (2004).
9. Ru, C.Q.; Aifantis, E.C. A simple approach to solve boundary-value problems in gradient elasticity. Acta Mech., 101, 59–68 (1993).
10. Yağmuroğlu, İ.; Askes, H. Anisotropic nonlocality for crack tip fields in microstructured periodic beam lattices. Theor. Appl. Fract. Mech., 141, 105177 (2026).

A review of the influence of manufacturing parameters on fracture toughness of additively manufactured polymers

Liviu MARSAVINA[1], Sergiu GALATANU[1], Emanoil LINUL[1]

[1] Department Mechanics and Strength of Materials, University Politehnica Timisoara, Romania

liviu.marsavina@upt.ro

Fused Deposition Modeling (FDM) represents an additive manufacturing technique based on melting of thermoplastic filament through a heater and deposits layer by layer on a bed. FDM relays on a series of manufacturing parameters, influencing the mechanical properties of the obtained component, Gao et al. [1]. The most important manufacturing parameters, considered for fracture toughness are shown in Fig. 1.

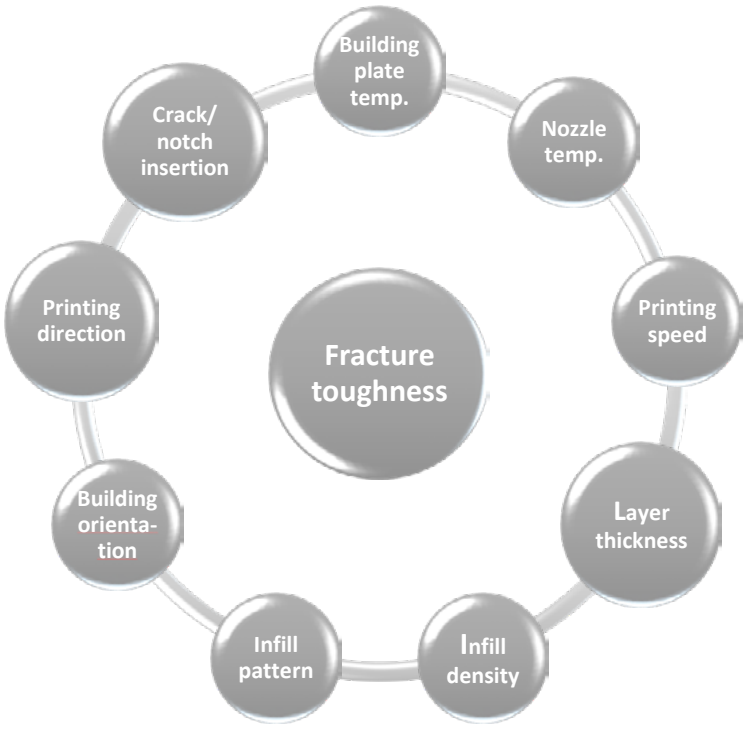

Figure 1. Manufacturing parameters influencing the fracture toughness of FDM components

The values of fracture toughness values ranges from 0.5 MPa $m^{0.5}$ to 7.5 MPa $m^{0.5}$, with the lower values for low densities infill [2], respectively higher values for 100 % infill density [3].

Another influential parameters affecting fracture toughness is the layer thickness. Studies consistently report that reducing layer thickness improves interlayer adhesion by increasing the contact area and promoting polymer chain diffusion across adjacent layers. As a result, thinner layers generally lead to higher fracture toughness and more ductile failure behavior. Conversely, thicker layers tend to introduce voids and weak interfaces, facilitating crack initiation and propagation along layer boundaries.

Increasing the nozzle temperature facilitates better diffusion, lower size of the interlayer voids and as consequence an increase in fracture toughness [4].

Raster angle and build orientation are also dominant factors governing fracture performance. When filaments are aligned parallel to the loading direction (0° raster angle), the load is primarily carried by the continuous polymer strands, resulting in higher fracture toughness. In contrast, specimens printed with a 90° raster angle or in the vertical orientation exhibit significantly reduced fracture toughness due to the perpendicular to loading direction of interlayers and weak interlayer bonding. In such cases, crack propagation typically occurs along interfacial regions, leading to brittle fracture modes. Intermediate raster configurations, such as ±45°, provide more isotropic behavior but generally yield moderate fracture toughness compared to fully aligned structures [3].

A better understanding of the effect of manufacturing parameters helps to optimize the FDM manufacturing parameters, and is essential for enhancing the fracture toughness of PLA components.

ACKNOWLEDGEMENTS

This work was supported by a grant of the Ministry of Research, Innovation and Digitization, CNCS-UEFISCDI, project number PN-IV-P1-PCE-2023-1446, within PNCDI IV.

REFERENCES

1. Gao, G.; Xu, F.; Xu, J.; Liu, Z. A survey of the influence of process parameters on mechanical properties of fused deposition modeling parts. Micromachines, 13, 553 (2022).
2. Milovanovici, A.; Golubovic, Z.; Trajkovic, I.; Sedmak, A.; Milosevici, M.; Valean, E.; Marsavina, L. Influence of printing parameters on the eligibility of plane-strain fracture toughness results for PLA polymer. Procedia Struct. Integr., 41, 290–297 (2021).
3. Marșavina, L.; Vălean, C.; Mărghitaș, M.; Linul, E.; Razavi, N. Effect of the manufacturing parameters on the tensile and fracture properties of FDM 3D-printed PLA specimens. Eng. Fract. Mech., 274, 108766 (2022).
4. Aliheidari, N.; Tripuraneni, R.; Ameli, A.; Nadimpalli, S. Fracture resistance measurement of fused deposition modeling 3D printed polymers. Polym. Test., 60, 94–101 (2017).

Microstructure-resolved hydrogen transport and its effect on crack-tip fields in polycrystalline materials

Andrey JIVKOV[1], Ava KHAJEIAN[1], Kiprian BERBATOV[1]

[1] School of Engineering, The University of Manchester, Oxford Road, Manchester M13 9PL

andrey.jivkov@manchester.ac.uk

Crack-tip fields in structural alloys are commonly characterised in terms of stress and strain distributions obtained from continuum plasticity. In hydrogen-sensitive materials, however, these fields, together with temperature, also act as drivers for mass transport processes, leading to the redistribution and trapping of hydrogen within the microstructure. This introduces an additional layer of evolution in which local material resistance is modified by hydrogen concentration and temperature. Conventional approaches typically represent these effects through homogenised descriptions, without resolving the role of grains and grain boundaries in mediating transport and degradation. As a result, the connection between crack-tip driving forces and the underlying microstructural pathways of hydrogen accumulation remains unclear.

In this work, a staged framework is developed to link crack-tip mechanics with microstructure-resolved hydrogen transport and degradation. A grain-resolved domain containing a pre-existing crack is first analysed using conventional elastic-plastic mechanics to determine the hydrostatic stress field in the vicinity of the crack tip. This field is then transferred to a combinatorial model defined on the same microstructural geometry, where hydrogen diffusion, stress-assisted transport and trapping in grains and at grain boundaries are described on a cell-complex representation of the material. The formulation follows established concepts of hydrogen transport driven by gradients of chemical potential and hydrostatic stress, together with local trapping at interfaces and defects [1-3], while the combinatorial representation provides a consistent discrete framework for transport and interaction on complex microstructures [4, 5].

The resulting hydrogen concentration and temperature fields are spatially heterogeneous and reflect both the crack-tip stress distribution and the underlying grain structure. Preferential hydrogen accumulation is predicted at grain boundaries and in regions of elevated hydrostatic stress ahead of the crack tip, consistent with the expected coupling between stress and diffusion. These fields are then used to define local constitutive and cohesive properties, specifically the yield stress within grains and the strength and energy of grain boundaries, through hydrogen- and temperature-dependent degradation relations, consistent with established mechanisms of hydrogen-assisted deformation and decohesion [6].

A second mechanical analysis incorporating these degraded properties demonstrates a clear modification of the crack-tip fields. The plastic zone ahead of the crack is redistributed and locally enlarged in regions of hydrogen accumulation, while the reduction in grain-boundary strength introduces preferential zones for decohesion. These effects lead to a measurable change in the crack driving force, quantified through the variation of a global fracture parameter, indicating that transport-induced degradation modifies both the local and global response of the crack-tip region.

The results show that a nominally smooth crack-tip stress field gives rise to a strongly heterogeneous degradation field once hydrogen transport and trapping are resolved on the

microstructure. This highlights that crack-tip behaviour in hydrogen-affected materials cannot be understood solely in mechanical terms but emerges from a coupled interaction between stress-driven transport and microstructure-dependent degradation. The proposed framework provides a consistent pathway for incorporating such effects into models of fracture and fatigue, while retaining a clear separation between transport, degradation, and mechanical response.

REFERENCES

1. Sofronis, P.; McMeeking, RM. Numerical analysis of hydrogen transport near a blunting crack tip. J. Mech. Phys. Solids, 37, 317-350 (1989).
2. Oriani, R.A. The diffusion and trapping of hydrogen in steel. Acta Metal., 18, 147-157 (1970).
3. Barrera, O.; Bombac, D.; Chen, Y.; et al. Understanding and mitigating hydrogen embrittlement of steels: a review of experimental, modelling and design progress from atomistic to continuum. J. Mater. Sci., 53, 6251–6290 (2018).
4. Berbatov, K.; Boom, P.D.; Hazel, A.L.; Jivkov, A.P. Diffusion in multi-dimensional solids using Forman's combinatorial differential forms. Appl. Math. Model., 110, 172-192 (2022).
5. Berbatov, K.; Jivkov, A.P. Variational formulations of transport phenomena on combinatorial meshes. J. Comp. Appl. Math., in press (2026) https://doi.org/10.48550/arXiv.2505.09443.
6. Robertson, I.M.; Sofronis, P.; Nagao, A.; et al. Hydrogen Embrittlement Understood. Metall. Mater. Trans, B 46, 1085–1103 (2015).

Influence of overloads on the propagation of 3D short fatigue cracks

Lucas SANCIET-MUNIER[1], Nathalie LIMODIN[1], Jean-Yves BUFFIERE[2], Jean-François WITZ[1], Julien RÉTHORÉ[3], Michel CORET[3], Ghita Bahaj FILALI[3], Andrew KING[4], Joel LACHAMBRE[2], Arnaud WECK[5]

[1] LaMcube Villeneuve d'Ascq, France.
[2] MATEIS, INSA Lyon Villeurbanne, France.
[3] GeM Centrale Nantes, Nantes France.
[4] Synchrotron SOLEIL Saint Aubin, France.
[5] Dept Mech. Eng. Univ. of Ottawa, Ottawa, Canada.

jean-yves.buffiere@insa-lyon.fr

In Structural components, *e.g.* aircraft, railways, or automotive applications, are inevitably submitted to Variable Amplitude fatigue [1]. Even when components are designed for constant amplitude loading, occurrence of overloads or underloads in service is frequent and affect the fatigue crack growth rate. In most metallic alloys a few cycles of crack acceleration followed by FCG retardation are usually observed after a tensile overload. Since the early seventies, the study and modelling of overload has been focused on long through cracks. However fatigue cracks are inherently 3D objects that remain part-through short cracks during a large fraction of the fatigue life [1]. Due to a lack of experimental data, the fundamental mechanisms of the propagation of 3D cracks under non-constant amplitude loading have not received enough attention yet. The goal of this study is thus to understand overload effects on physically small 3D fatigue cracks in order to build predictive models.

The material of the study, an AlSi7Mg0.6 cast aluminium alloy, specifically designed by the to provide a fine speckle pattern of eutectic Silicon particles for Digital Volume Correlation (DVC). Besides it has a grain size (≅150µm) small enough to ensure a relatively smooth crack plane. The experimental procedure consisted in subjecting corner-notched dog-bone type samples to cyclic tensile loading (frequency=20Hz, R=0.27) in-situ at PSICHÉ X-ray tomography beamline of SOLEIL synchrotron. When the crack has propagated away from the previous overload, another overload was applied until the unbroken ligament became too small. Up to 4 overloads, at decreasing load ratio (F_{OL}/F_{max} from 1.8 to 1.3), could be applied on one specimen. During the loading sequence, 3D tomography scans of the sample were regularly acquired before, during and after a single overload. On some key cycles, several acquisitions were obtained at intermediate load steps between the extrema to study crack opening and closure.

Analysis of the raw tomographic volumes allows the crack fronts, hence crack growth rates, to be obtained while analysis of the displacement fields from DVC allows extracting Stress Intensity Factors (SIF) and crack opening displacement along the crack front. DVC was performed with UFreckles software [2] using a size of element of 8 pixels (20.8µm) and SIF were computed by projecting the 3D displacement field onto Williams series solutions [3]. Characteristic periods of crack retardation after overloads are observed, with crack growth recovery occurring first in the bulk of the sample, then later close to the free surfaces.

Interestingly, no correlation between the measured Stress Intensity Factors (SIF) and crack growth rates after the overload is evidenced. The SIF range of post-overload cycles are unaffected by the overload. Although the crack is effectively blocked after the overload, the value of ΔK_I

remains the same. Finite Element calculation using DVC as boundary conditions corroborates the SIF values obtained with DVC and allows to characterize the evolution of the plastic zone along the crack front to confirm the larger plastic zone close to the free surfaces in relation with a larger closure effect.

If the SIF parameter is no more an appropriate driving force after the overload, the analysis of the crack opening displacement from measured displacement fields allows to understand what happens at the crack tip during the overload cycle with plastic deformation, crack tip blunting and residual effect of the overload. Finally, the evolution of crack tip opening after the overload seems a more promising parameter to correlate with fatigue crack growth delay and crack recovery than the SIF.

This study allows to characterize the effect of tensile overloads on a 3D short fatigue crack evidencing strong differences between the free surfaces and the bulk that could not have been observed and quantified without x-ray tomography and digital volume correlation.

REFERENCES

1. Schijve, J. Fatigue of structures and materials, Springer, (2001).
2. Réthoré, J. UFreckles. Zenodo, (2018). https://doi.org/10.5281/zenodo.1433776 (2018)
3. Lachambre, J.; Réthoré, J.; Weck, A.; Buffiere, J.-Y. Extraction of stress intensity factors for 3D small fatigue cracks using digital volume correlation and X-ray tomography. Int. J. Fatigue, 71, 3–10 (2015).

Influence of Periodic Overloads and Underloads on Fatigue Crack Growth in ER70S-6 WAAM Carbon Steel

Mariela MENDEZ-MORALES[1], Ricardo BRANCO[2], Joel JESUS[2], Trayana TANKOVA[3], Carlos REBELO[1]

[1] University of Coimbra, ISISE, ARISE, Department of Civil Engineering, Rua Luis Reis Santos, 3030-790 Coimbra, Portugal
[2] University of Coimbra, CEMMPRE, ARISE, Department of Mechanical Engineering, Rua Luis Reis Santos, 3030-788 Coimbra, Portugal
[3] Delft University Technology, Department of Engineering Structures, Stevinweg 1, 2628 CN Delft, the Netherlands

mendezmorales@dec.uc.pt

Despite recent advances in metal additive manufacturing, and in particular in direct energy deposition processes such as Wire Arc Additive Manufacturing (WAAM), the fatigue behaviour of WAAM carbon steels remains insufficiently understood, especially in terms of fatigue crack growth [1,2]. In addition, only a limited number of studies have addressed the combined influence of build orientation and load sequence effects, including overloads and underloads. These effects are of particular relevance for modern structural applications, such as wind turbine towers, which may experience transient high-load events. In the construction sector, WAAM carbon steel has gained increasing attention owing to its capability to produce large-scale structural components at high deposition rates and relatively low cost compared to other additive manufacturing processes or conventional fabrication strategies for complex geometries [3].

To contextualise the loading conditions in wind turbine support structures, typical load spectra derived from aeroelastic simulations are considered based on IEC 61400 [4] fatigue design load cases. These include constant amplitude fatigue-relevant conditions such as normal power production and idling (DLC 1.2 and DLC 6.4) as well as transient events such as sudden faults in the system (e.g., grid loss), start-up, and shutdown scenarios (DLC 2.4, DLC 3.1, and DLC 4.1), which motivate the investigation of overload and underload effects.

In the present study, compact tension (CT) specimens of WAAM ER70S-6 carbon steel were extracted in two orthogonal orientations, with the crack plane oriented both parallel (denominated H) and perpendicular (denominated V) to the deposition layers. Fatigue crack growth tests were performed under constant amplitude loading at different stress ratios. The experimental campaign is currently being extended to include variable-amplitude loading sequenced incorporating periodic single overload and underload cycles with varying load ratios. Full-field displacement and strain measurements were obtained by means of Digital Image Correlation (DIC) to characterise the evolution of crack closure effects during the different loading conditions. The crack growth rates obtained under constant amplitude loading are presented in

Figure **1**, in terms of both the stress-intensity factor range (ΔK) and the effective stress-intensity factor range (ΔK_{eff}) [5].

Preliminary results indicate that build orientation has a measurable influence on the fatigue crack growth behaviour of WAAM ER70S-6 carbon steel. However, the results shown in

Figure **1**(b) suggest that a unified fatigue crack growth curve can be established when considering the effective stress-intensity factor range, indicating that the observed differences in

crack propagation are likely associated with crack closure phenomena. Ongoing work focuses on quantifying the influence of overload and underload sequences on crack growth behaviour, including potential retardation and acceleration effects. The outcomes of this study provide a basis for improved fatigue crack growth modelling of WAAM carbon steels and support their application in damage-tolerant structural design under variable-amplitude loading.

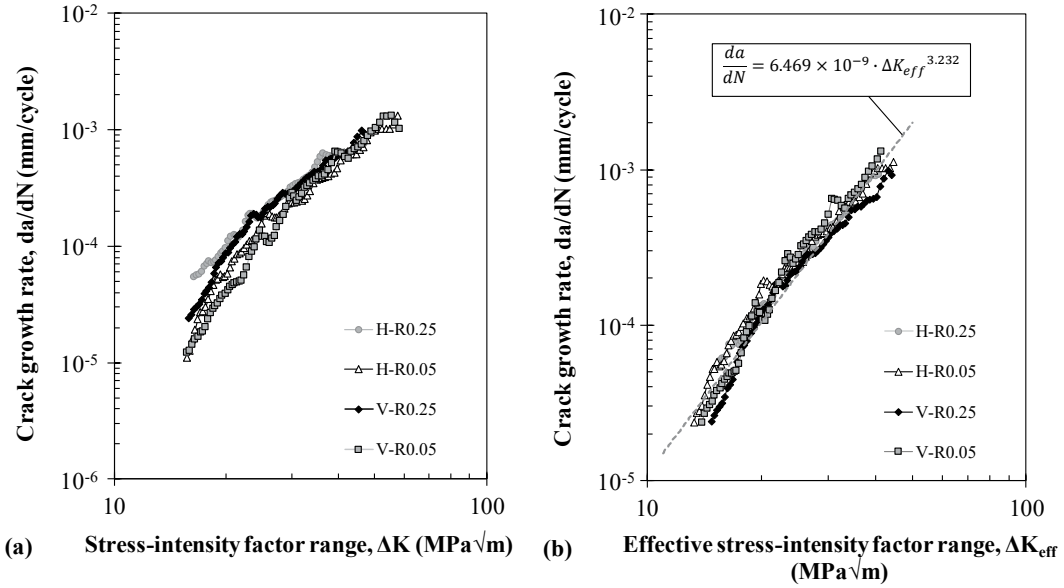

Figure 1. Fatigue crack growth rate against (a) stress-intensity factor range and (b) effective stress-intensity factor range for crack planes parallel (H) and perpendicular (V) to the deposition layers at 0.25 and 0.05 stress ranges [5].

REFERENCES

1. Ermakova, A.; Mehmanparast, A.; Ganguly, S.; Razavi, N.; Berto, F. Fatigue crack growth behaviour of wire and arc additively manufactured ER70S-6 low carbon steel components. Int. J. Fract., 235, 47–59 (2022).
2. Huang, C.; Zheng, Y.; Chen, T.; Ghafoori, E.; Gardner, L. Fatigue crack growth behaviour of wire arc additively manufactured steels. Int. J. Fatigue, 173, 107705 (2023).
3. Gardner, L. Metal additive manufacturing in structural engineering – review, advances, opportunities and outlook. Structures, 47, 2178–2193 (2023).
4. IEC. IEC 61400-1: Wind turbines – Part 1: Design requirements, (2005).
5. Mendez-Morales, M.; Jesus, J.S.; Branco, R.; Tankova, T.; Rebelo, C. Fatigue crack growth of untreated and heat-treated WAAM ER70S-6 carbon steel. Int. J. Fatigue, 198, 109008 (2025).

Fast identification of the Paris law parameter during ultrasonic fatigue crack propagation test

Nicolas RANC[1], Ronan DELALANDE[1], Lionel ANDENAS[1], Eric MONTEIRO[1], Mathieu DUCOUSSO[1,2]

[1] PIMM, Arts et Métiers Insitute of Technlogy, 151 bd de l'Hopital, 75013 Paris, France
[2] SAFRAN Tech, rue des jeunes bois, Magny les Hameaux, 78772, France

nicolas.ranc@ensam.eu

Determining the propagation threshold and crack growth rate of fatigue cracks is a key issue in the mechanical design of structural components. It requires the performance of standardised tests (ASTM E647), which can be time expensive due to the very long propagation times, especially for low amplitude fatigue loads (i.e. low value of the intensity factor of small stresses). The objective of this study is to develop a new experimental methodology to monitor a fatigue crack propagation during an ultrasonic fatigue test in order to identify the *C* and *n* parameters of the Paris law in just a few minutes.

The experimental setup used in this study, shown in Figure 1, consists of a parallelepiped-shaped aluminum alloy specimen with a notch at the center, mounted on an ultrasonic fatigue machine operating at a frequency of 20 kHz.

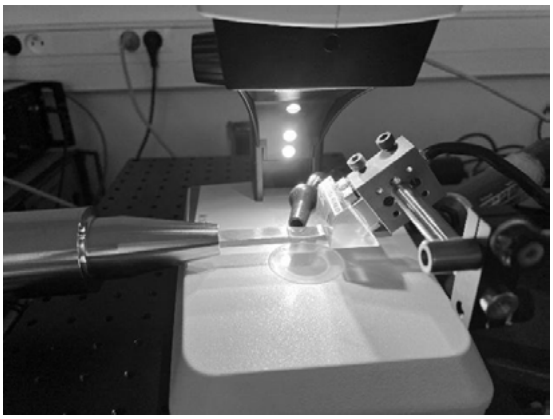

Figure 1. General view of the experimental.

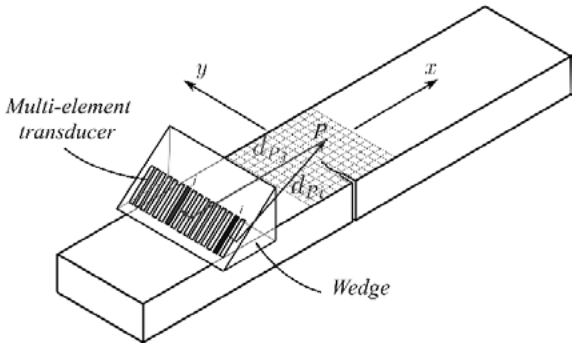

Figure 2. Illustration of TFM.

A phased-array consisting of 128 piezo electric transducers is used to generate Rayleigh waves and recorded the signal reflected by the crack. The central frequency of the tranducers is 15 MHz, corresponding to a wavelength of the generated Rayleigh waves 200 µm. The crack morphology is imaged using a Total Focusing Method (TFM), obtained from Plane Wave Imaging configuration. Such method allows to generate high resolved images, in which the square pixel size is 25 µm and the imaging frequency is 50 Hz. An illustration of the imaging setup is proposed on figure 2. On that image one can observed the crack, in front of the phased-array and placed on the middle of the grid defined for the TFM imaging.

The figure 3 illustrates the crack image obtained after reconstruction. A projection along the crack propagation axis allows the crack's position to be identified for each image. This process is repeated at a frequency of 50 Hz to track the crack's propagation. Concurrently, a binocular microscope allows the crack initiation to be visualized.

To identify the parameters of a Paris fatigue crack law, the notched specimen is subjected to increasing vibration amplitude. As soon as crack initiation is observed through the binocular microscope, the amplitude is kept constant. Crack propagation is then recorded using the ultrasonic imaging system. When the crack length becomes too long, the vibration frequency of the ultrasonic fatigue system exceeds its frequency range and the machine stops.

To determine the stress intensity factor as a function of the vibration amplitude applied to the end of a specimen, a 2D frequency analysis of the cracked specimen is performed. This allows for the identification of the following equation:

$$\Delta K = \frac{\alpha E U_0 \sqrt{a}}{w} \tag{1}$$

where E is the Young modulus, U_0 the amplitude of the displacement of the specimen edge, a the crack length, w the width of the specimen and α a coefficient. Integrating the Paris law using the above equation for the stress intensity factor yields the following equation:

$$a(t) = \left(a_0^{1-\frac{n}{2}} + \left(1 - \frac{n}{2}\right) \frac{f C \alpha E U_0}{w} (t - t_0) \right)^{\frac{1}{1-\frac{n}{2}}} \tag{2}$$

with a_0 the crack length at time t_0, f the loading frequency and C and n the Paris law parameters. The parameters n and C are then optimized to reduce the discrepancy between the theoretical and experimental results. The experimental values obtained are n = 3.07 et C = 6.83x10^{-6} mm/cycle/(MPa$\sqrt{m}$)^n.

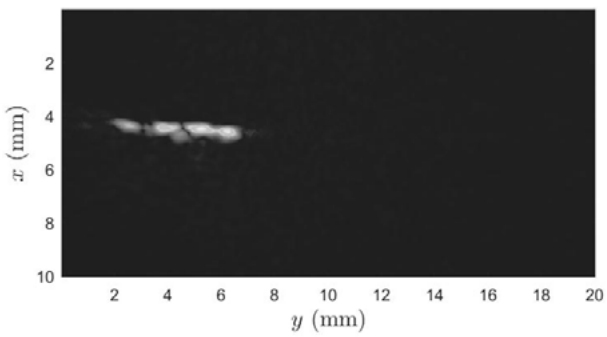

Figure 3. Crack imaging.

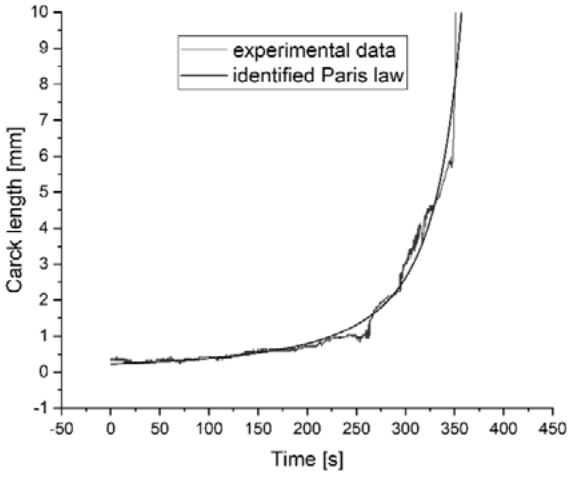

Figure 4. Crack length evolution.

REFERENCES

1. Ducousso, M.; Ghibaudo, O.; Amiel, S. Surface imaging using total focusing method on surface waves for non-destructive testing. NDT & E Int., 146, 103176 (2024).
2. Ranc, N.; Ducousso, M.; Tannous, N.; Blanche, A. Real-time monitoring of crack propagation during ultrasonic fatigue tests for fast identification of Paris' law parameters. Proceedings of the VHCF9 Conference, 26–28 June, (2024).

Multiscale analysis and prediction of crack-tip field for fatigue crack growth in anisotropic titanium alloys

Haoruo CHEN[1], Zheng LIU[1], Xu CHEN[1]

[1] School of Chemical Engineering & Technology, Tianjin University, Tianjin, China

xchen@tju.edu.cn

TA15 titanium alloy, a near-α high Al-equivalent titanium alloy, is extensively employed in aerospace components due to its excellent strength, thermal stability and weldability. Owning to its strong basal texture induced by rolling process, the fatigue crack growth (FCG) behavior of TA15 shows clear orientation dependence [1]. In addition, the stress ratio (R) significantly influences the crack-tip driving force and crack-closure behavior [2]. This study systematically investigates the coupled effects of spatial orientation and stress ratio on FCG rate and crack-tip plasticity in rolled TA15 titanium alloy.

To address this challenge, FCG tests were conducted using compact tension (CT) specimens at room temperature with three spatial orientations (0°, 30°, and 52.5°) and three stress ratios (R =0.1, 0.3 and 0.5). Digital Image Correlation (DIC) was employed to measure crack opening displacement (COD) and strain fields, enabling determination of crack closure effect (F_{open}/F_{max}) and evolution of crack-tip plastic zones.

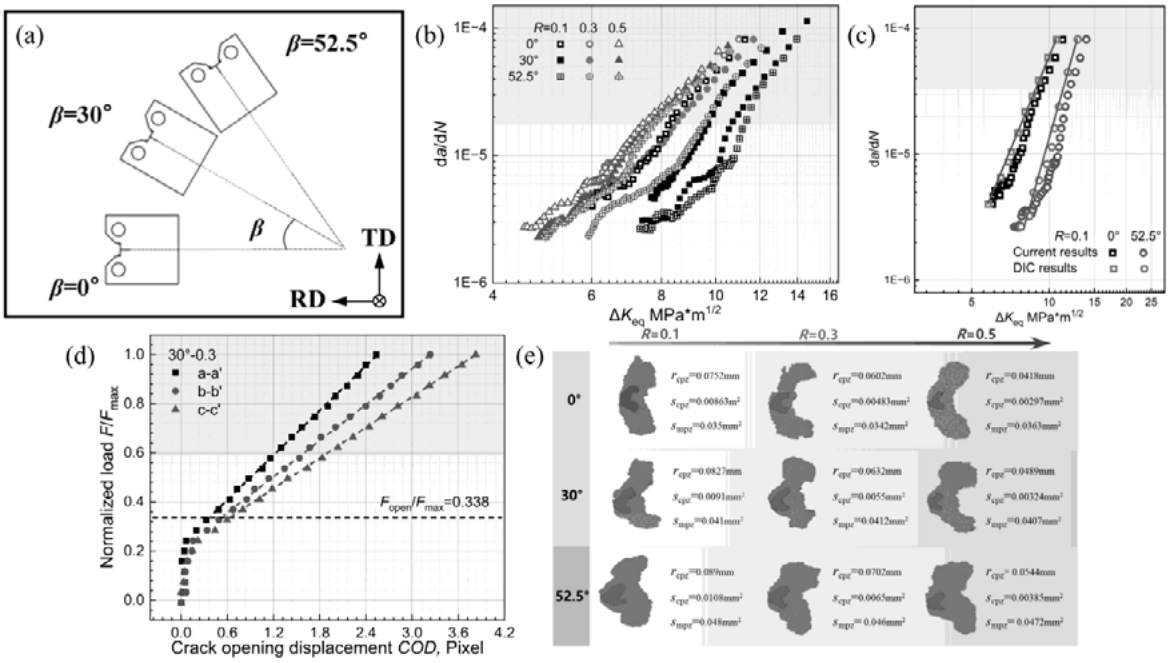

Figure 1. FCG test for TA15 titanium alloy considering spatial orientation and stress ratio: (a) Experimental scheme; (b) FCG results; (c) FCG results based on DIC; (d) Measurement of crack closure effect; (e) Measurement of plastic zone around crack tip.

The results reveal that crack deflection become more remarkable with increasing spatial orientation, leading to enhanced roughness-induced crack closure and reduced crack growth rate

(0° > 30° > 52.5°). Increasing stress ratio significantly accelerates crack growth and weakens orientation dependence. Crack deflection angles decrease significantly at higher stress ratio, and the difference of FCG rate at different spatial orientations recedes as well. Besides, this study realizes the actual FCG curve based on the displacement field obtained from DIC. Compared with traditional finite element methods, it more accurately reflects crack growth under the constraints of the real microstructure.

Accurate acquisition of crack-tip plastic zones based on strain field form DIC revealed that increasing stress ratio significantly reduces the cyclic plastic zone (CPZ), lowering cyclic energy dissipation and accelerating crack growth, while the monotonic plastic zone (MPZ) remains nearly unchanged. Increasing orientation angle enlarges both CPZ and MPZ, enhancing plastic deformation and crack growth resistance. From SEM observation, lower spatial orientation and higher stress ratio results in a larger cleavge plane reflects its coupled effect on FCG rate.

Crack closure analysis shows that Fopen/Fmax increases as spatial orientation increases, indicating stronger mechanical interlocking for more tortuous crack paths. Although Fopen/Fmax increases with stress ratio, its relative contribution to FCG resistance diminishes as R increases [3]. After introducing ΔKeff to correct the driving force, the da/dN–ΔKeff curves under different orientations and stress ratios converge into a unified trend, particularly in the Paris regime. Finally, fracture surfaces' roughness was measured and a prediction model based on roughness factor γ and stress ratio R was proposed.

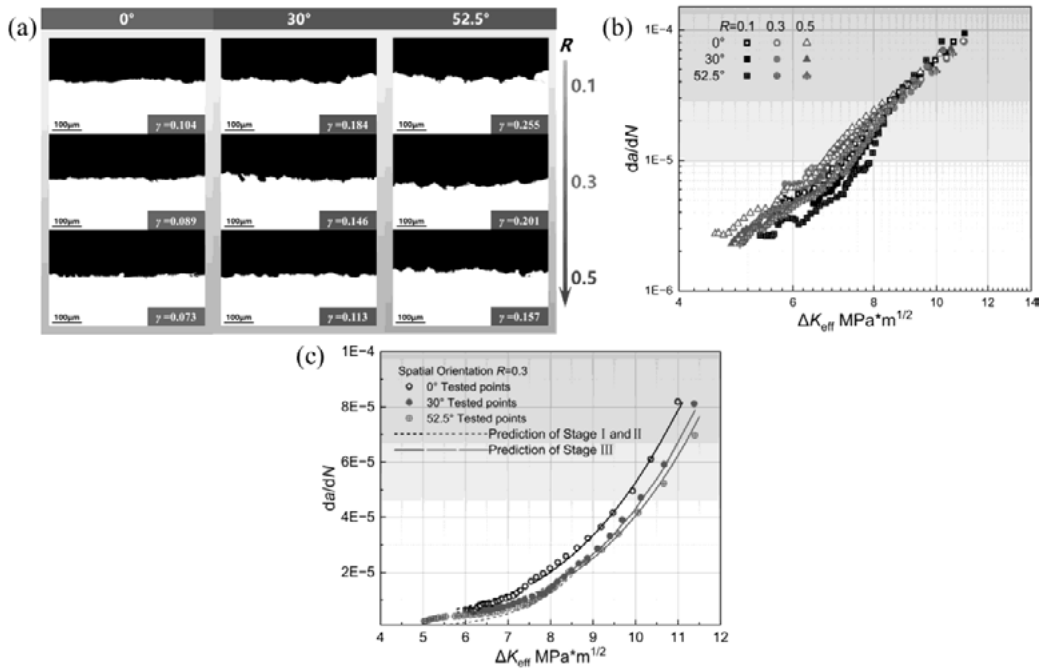

Figure 2. Unification and prediction of FCG law: (a) Measurement of fracture surface roughness; (b) Corrected ΔK_{eff}- da/dN curve; (c) Model prediction result at R=0.3.

REFERENCES

1. Chen, W.; Zeng, W.; Zhao, Y.; et al. Fracture toughness anisotropy of Ti17 billet processed by β forging. Mater. Sci. Eng. A, 807, 140825 (2021).
2. Shi, L.; Zhang, Z.; Chen, X. Fatigue crack growth behavior in CoCrFeMnNi high entropy alloy with harmonic structure topology. Int. J. Fatigue, 172, 107656 (2023).
3. Cui, P.; Zhang, J.; Guo, W. A theoretical model for three-dimensional fatigue crack closure and growth under variable amplitude loadings. Int. J. Fatigue, 199, 109042 (2025).

Bias reduction in Paris curve fitting to aggregate fatigue crack growth data

Moray STIVEN[1], Carol JOHNSTON[2], Ali MEHMANPARAST[1]

[1] Department of Naval Architecture, Ocean and Marine Engineering, University of Strathclyde, Glasgow G1 1XQ, United Kingdom
[2] TWI Ltd, Granta Park, Great Abington, Cambridge, United Kingdom

ali.mehmanparast@strath.ac.uk

Fitting Paris curves to aggregate datasets is essential when a single curve is required from multiple tests to represent the overall fatigue crack growth rate behaviour of the material. While aggregating data from different sources, the data can vary in the number of data points per test, the ΔK range covered, and the level of scatter. The aggregate dataset is usually filtered, then collated to fit a master Paris curve to all the data. This method inherently involves bias, as any heterogeneity between data series will induce a biasing effect on the mean and mean+2SD upper bound curves.

In an attempt to reduce bias in aggregate Paris curves, a method was developed recently by Stiven et al [1], which applied a weight value to each datapoint, allowing the aggregate fit to be more fairly influenced by the population of data points across different tests. Two methods for calculating the weighting values were used. The first accounted for the number of data points in each test, ensuring that specimens with a larger number of reported data points did not disproportionately influence the regression analysis. As each data series represents one test, this aimed to apply an equal weight to each test. This weighting method ensures that the sum of the weights for all points in each data series (i.e., specimen) is equal to 1. The second method aimed to additionally account for the variance in ΔK ranges, which different series cover. Data series covering a wide ΔK range provide more comprehensive information about crack growth behaviour and are therefore considered more informative than those covering a narrow range. Once a weight has been assigned to each data point, a weighted regression can be performed, ensuring the weighted standard deviation is employed.

These methods proved useful for the extreme case shown in Figure 1, where the analysed data included two tests exhibiting a distinct separation in FCGR and a significant variance in the number of data points per series. The difference between the unweighted and weighted mean+2SD curves for this specific case is between 37–46% in fatigue crack growth in the ΔK range. As the material database becomes larger and includes more data series, the biasing influences tend to become more balanced, generally resulting in a reduced effect of weighting. This is, however, unique to each specific database and depends on which data series are and are not included.

An important limitation affecting both unweighted and weighted linear regression on aggregate datasets is that of Simpson's paradox. Although fatigue crack growth data may not suffer from the extreme case of trend reversal, classically used to explain the paradox, the slope of the aggregate Paris curve can nonetheless be influenced. An investigation by Anderson [2] has been conducted, where the slope of each series was fixed, fitting only the intercept value, and taking the mean of these intercept values to define the aggregate fit. This method combats the bias effect due to variance in data density, ΔK ranges, and slope changes due to Simpson's paradox. However, the slopes are artificially fixed and therefore not data-driven, which becomes more problematic

for bilinear fits. Additionally, the upper bound curves are based on scatter in the intercept alone and therefore do not account for scatter within individual series.

The case shown in Figure 1 is an extreme one, while repeating tests the Paris region often does not display such large variance. The weighted regression methods are therefore best used to indicate the significance of any bias effects, which depend on the specific dataset under consideration. These methods have not been extended to the fatigue crack growth data in the near threshold region, which represents a key area for future work. The nature of threshold data, characterised by the asymptotic drop in the fatigue crack growth rate and typically exhibiting large variance, makes it particularly well-suited to bias-reducing approaches.

A broader consideration is that collating data series across multiple test variables, such as material subgrades or test centres, is often unavoidable in practice due to limited data availability. Developing separate Paris curve recommendations for every unique combination of variables is unfeasible, as the individual datasets would be too small to be statistically reliable. This necessity of combining heterogeneous data further motivates the use of bias-reducing regression methods, yet the true extent of bias in such multi-variable scenarios remains unclear given the limitations discussed. Future work should therefore aim to develop improved approaches that can more reliably quantify and remove these effects.

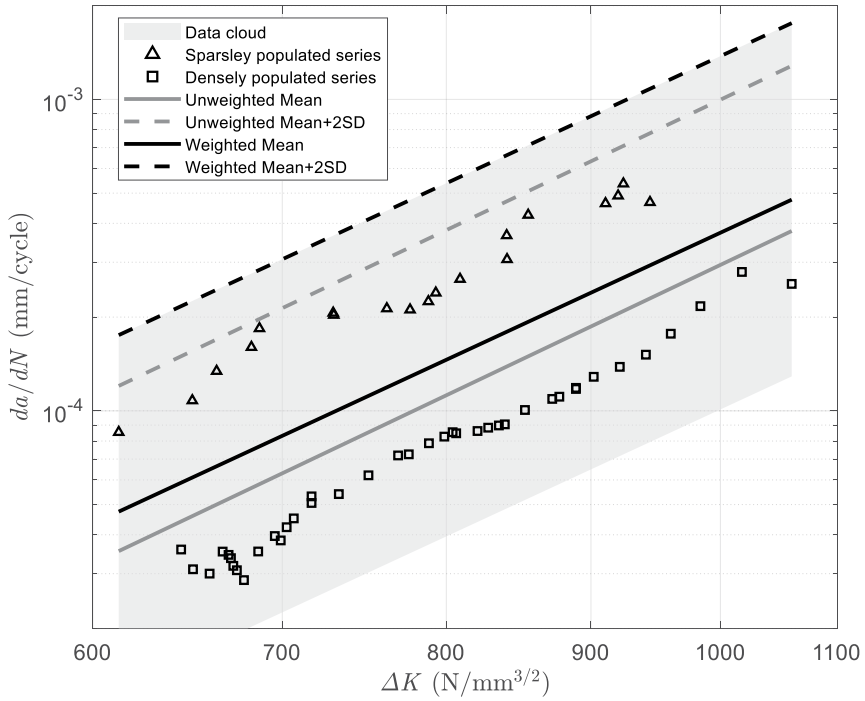

Figure 1. Weighting method 1, effect on aggregate fatigue crack growth data fit using two data series of varying density [1].

REFERENCES

1. Stiven, M.; et al. A comprehensive review and analysis of S355 fatigue crack growth rate data for offshore wind applications: seawater free-corrosion environment. Int. J. Fatigue, 209, 109613 (2026).
2. Anderson, T.L. Refitting Paris fatigue constants for API 5L steels and seam welds. Pipeline Research Council International, PR723-243802-R01, (2024).

Energy release rate of a mixed-mode crack exposed to large deformation

Andrea SPAGNOLI[1], Ruggero MACALUSO[1], Michele TERZANO[2]

[1] Department of Engineering and Architecture, University of Parma, Italy
[2] Institute of Biomechanics, Graz University of Technology, Graz, Austria

spagnoli@unipr.it

Fracture mechanics of compliant solids is of primary relevance in several applications, including soft robotics, stretchable electronics and the biomechanics of soft tissues such as skin, arterial walls, ligaments and tendons [1–3]. Soft materials exhibit distinctive fracture behaviour, characterized by large pre-failure deformations and enhanced tear resistance [4,5]. Since the pioneering work of Rivlin and Thomas [6], the fracture resistance of elastomers has been commonly described through the concept of critical tearing energy [6–8].

Standardized experimental procedures have enabled its measurement, often allowing the use of linear elastic fracture mechanics (LEFM) assumptions, thereby neglecting the influence of large deformations on crack-tip fields. More recent studies have highlighted the limitations of this approach. In particular, mode-I fracture tests under pure shear conditions have revealed the influence of specimen geometry, initial crack length and the adopted hyperelastic constitutive model on the evaluation of tearing energy [9,10]. Additional experimental configurations, such as the poker-chip test, have emphasized the interplay between fracture and cavitation phenomena [11,12]. From a theoretical standpoint, finite-strain analyses of crack-tip fields date back several decades [13–15], but only recently have they gained broader attention through comprehensive reviews and renewed interest in the mechanics of soft materials [16,17]. Furthermore, key aspects such as flaw sensitivity, crack blunting and the emergence of intrinsic length scales have been extensively investigated in recent contributions [18–21].

As already pointed out by Kendall and Fuller [22], the crack resistance of soft materials is strongly influenced by the nonlinear characteristics of their stress–strain response. In this context, the present work investigates the dependence of the energy release rate on the constitutive description of nonlinear elasticity. A representative problem consisting of a thin plate subjected to uniaxial stretch and containing a central crack is analysed through finite element simulations. The material behaviour is described using an incompressible generalized neo-Hookean model, and the effect of strain hardening is systematically explored. The energy release rate is evaluated via the J-integral (e.g. using the configurational force method [23]) and compared with LEFM predictions. In addition, mixed-mode (I+II) conditions are examined by considering a skewed crack configuration, providing further insight into the role of large deformations on fracture driving forces.

REFERENCES

1. Taylor, D.; O'Mara, N.; Ryan, E.; Takaza, M.; Simms, C. The fracture toughness of soft tissues. J. Mech. Behav. Biomed. Mater., 6, 139–147 (2012).

2. Yang, W.; Sherman, V.R.; Gludovatz, B.; Schaible, E.; Stewart, P.; Ritchie, R.O.; Meyers, M.A. On the tear resistance of skin. Nat. Commun., 6, 6649 (2015).
3. Bircher, K.; Zündel, M.; Pensalfini, M.; Ehret, A.E.; Mazza, E. Tear resistance of soft collagenous tissues. Nat. Commun., 10, 792 (2019).
4. Creton, C.; Ciccotti, M. Fracture and adhesion of soft materials: a review. Rep. Prog. Phys., 79, 046601 (2016).
5. Spagnoli, A.; Brighenti, R.; Cosma, M.P.; Terzano, M. Fracture in soft elastic materials: continuum description, molecular aspects and applications. Adv. Appl. Mech., 55, 255–307 (2022).
6. Rivlin, R.S.; Thomas, A.G. Rupture of rubber. I. Characteristic energy for tearing. J. Polym. Sci., 10, 291–318 (1953).
7. Greensmith, H.W. Rupture of rubber. X. The change in stored energy on making a small cut in a test piece held in simple extension. J. Appl. Polym. Sci., 7, 993–1002 (1963).
8. Gent, A.N. Adhesion and strength of viscoelastic solids. Langmuir, 12, 4492–4496 (1996).
9. Kahle, E.; Ehret, A.E.; Mazza, E. The influence of aspect ratio on the determination of tearing energy in mode I fracture tests. Eng. Fract. Mech., 287, 109315 (2023).
10. Zhu, B.; Wang, J.; Zehnder, A.T.; Hui, C.Y. Energy release rate of a mode-I crack in pure shear specimens subjected to large deformation. Int. J. Fract., 245, 171–182 (2024).
11. Lefèvre, V.; Ravi-Chandar, K.; Lopez-Pamies, O. Cavitation in rubber: An elastic instability or a fracture phenomenon? Int. J. Fract., 192, 1–23 (2015).
12. Hao, S.; Suo, Z.; Huang, R. Why does an elastomer layer confined between two rigid blocks grow numerous cavities? J. Mech. Phys. Solids, 173, 105223 (2023).
13. Knowles, J.K.; Sternberg, E. An asymptotic finite-deformation analysis of the elastostatic field near the tip of a crack. J. Elast., 3, 67–107 (1973).
14. Stephenson, R.A. The equilibrium field near the tip of a crack for finite plane strain of incompressible elastic materials. J. Elast., 12, 65–99 (1982).
15. Geubelle, P.H.; Knauss, W.G. Finite strains at the tip of a crack in a sheet of hyperelastic material. J. Elast., 35, 61–98 (1994).
16. Long, R.; Krishnan, V.R.; Hui, C.Y. Finite strain analysis of crack tip fields in incompressible hyperelastic solids loaded in plane stress. J. Mech. Phys. Solids, 59, 672–695 (2011).
17. Long, R.; Hui, C.Y. Crack tip fields in soft elastic solids subjected to large quasi-static deformation — A review. Extrem. Mech. Lett., 4, 131–155 (2015).
18. Hui, C.Y.; Jagota, A.; Bennison, S.J.; Londono, J.D. Crack blunting and the strength of soft elastic solids. Proc. R. Soc. A, 459, 1489–1516 (2003).
19. Chen, C.; Wang, Z.; Suo, Z. Flaw sensitivity of highly stretchable materials. Extrem. Mech. Lett., 10, 50–57 (2017).
20. Long, R.; Hui, C.Y.; Gong, J.P.; Bouchbinder, E. The fracture of highly deformable soft materials: a tale of two length scales. Annu. Rev. Condens. Matter Phys., 12, 71–94 (2021).
21. Kahle, E.; Alberini, R.; Ehret, A.E.; Mazza, E.; Spagnoli, A. Length scales in the tear resistance of soft tissues and elastomers. Int. J. Fract., 249, 27 (2025).
22. Kendall, K.; Fuller, K.N.G. J-shaped stress/strain curves and crack resistance of biological materials. J. Phys. D Appl. Phys., 20, 1596–1600 (1987).
23. Moreno-Mateos, M. A.; Steinmann, P. Configurational force method enables fracture assessment in soft materials. Journal of the Mechanics and Physics of Solids, 186, 105602 (2024).

A fatigue damage parameter incorporating the micro-porosity distribution field effect in SLM materials

Piao LI[1], Haibiao YIN[2]

[1] Zhejiang-Italy Joint Lab for Smart Materials and Advanced Structures, School of Mechanical Engineering and Mechanics, Ningbo University, Ningbo 315211, China
[2] State Key Laboratory of Mechanics and Control for Aerospace Structures, Nanjing University of Aeronautics and Astronautics, Nanjing 210016

lipiao@nuaa.edu.cn

Selective Laser Melting (SLM) alloys have been increasingly employed in advanced engineering applications such as aerospace; however, the inherent dispersed micro-porosity within these materials exerts a pronounced influence on their fatigue performance. In this study, a fatigue damage parameter considering the effect of the microporosity distribution field is proposed, which captures the coupled influence of micropores on both the far-field stress distribution and local damage evolution, as illustrated in Fig. 1.

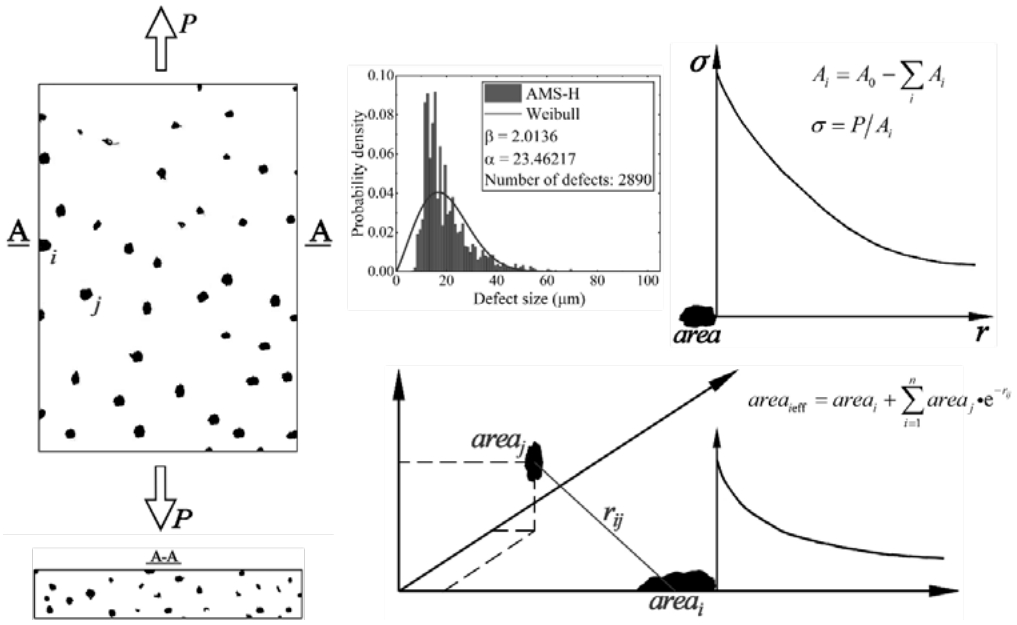

Figure 1. The illustration of micro-porosity distribution field-based modelling.

First, the size and spatial distribution of micropores is characterized using optical microscopy and CT scanning, yielding corresponding datasets for pore size and spatial location. Statistical analysis indicates that the pore size follows a Weibull distribution, while the spatial distribution is uniform, as expressed in the following equations, where $f(area)$ denotes the projected area of a micropore, $g(r)$ represents the average distance between defects, and α and β are the Weibull distribution parameters.

$$f(area)=\frac{\alpha}{\beta}(area)^{\alpha-1}\exp\left[-\frac{(area)^{\alpha}}{\beta}\right] \qquad (area\geq 0)$$
$$g(r)=\frac{1}{\bar{r}} \tag{1}$$

Next, under stationary random vibration fatigue loading, the micropore area gradually increases with damage accumulation. This process manifests macroscopically as a continuous reduction in the first natural frequency of the specimen. The evolution of micropore area alters the effective load-bearing area, thereby influencing the actual stress field distribution. In this study, the degradation of the natural frequency is employed to quantify the evolution of micropore area and fatigue damage, as expressed by:

$$A(n)=A(0)\left(1-c\frac{f_{\mathrm{I}}(n)}{f_{\mathrm{I}}(0)}\right)$$
$$\sigma(n)=\left[A(0)/A(n)\right]\sigma(0) \tag{2}$$

where $f_{\mathrm{I}}(0)$ and $f_{\mathrm{I}}(n)$ denote the initial and instantaneous first natural frequencies, respectively; $A(0)$ and $A(n)$ represent the initial and effective load-bearing areas; and $\sigma(0)$ and $\sigma(n)$ correspond to the nominal and instantaneous stresses.

Furthermore, the interaction effect among micropores is taken into account. The projected pore area on the plane perpendicular to the principal stress is defined as the damage characteristic area, and the influence of surrounding pores on a critical pore is established, as illustrated in Fig. 1. Let the critical pore be denoted as *i*, and the distance to any surrounding pore *j* be r_{ij}; a smaller r_{ij} implies a stronger interaction effect. An influence function is defined, and the contributions of *m* neighboring pores are incorporated into the defect size to obtain an equivalent defect area, expressed as:

$$\varphi(r_{ij})=\mathrm{e}^{-\kappa(r_{ij}/\bar{r})}$$
$$area_{i\mathrm{eff}}=area_i+\sum_{j=1}^{m}area_j\bullet\varphi(r_{ij}) \tag{3}$$

Finally, based on Murakami's theory [1], the parameter is treated as an equivalent crack, and combined with an equivalent crack growth model [2], the fatigue life under the actual stress field is predicted.

To validate the proposed model, fatigue tests were conducted on two SLM alloys. The predicted fatigue lives show sound agreement with the experimental results, and fracture surface analysis further confirms the micropore-dominated crack propagation mechanism.

REFERENCES

1. Murakami, Y. Metal fatigue: effects of small defects and nonmetallic inclusions, Elsevier, Oxford, (2002).
2. Yin, H.; Yang, Y.; Li, P.; Yao, W. The defect-propagation-based model for random vibration fatigue life analysis of SLM aluminum alloys. Int. J. Fatigue, 203, 109345 (2026).

Effect of stochastic scatter Paris-Erdogan constants on in-plane mixed mode fatigue life predictions

Oguzhan DEMIR[1], Mehmet Faruk YAREN[2]

[1] Dept. of Mechanical Engineering, Bilecik Seyh Edebali University, 11230, Bilecik, TURKEY
[2] Dept. of Mechanical Engineering, Sakarya University, 54050, Sakarya, TURKEY

myaren@sakarya.edu.tr

Mixed-mode fracture commonly arise in structural components due to various factors; misaligned cracks, multiaxial stress states, and complex boundary conditions. Predicting mixed mode fatigue crack growth (FCG) life and paths remains challenging due to many significant factors, such as due to the absence of a universally accepted driving force for determining the equivalent stress intensity factor (SIF) and the crack deflection angle.

A further critical issue is the reliance on Paris-Erdogan constants (C and n) calibrated from pure mode-I data. While convenient, this approach is questionable for anisotropic materials such as rolled structures, where microstructural properties vary with direction due to grain elongation and the repositioning of boundaries during the rolling process. As crack orientations continuously shift relative to the rolling direction during mixed-mode growth, mode-I constants may fail to capture the direction-dependent fracture response, leading to inaccurate life predictions.

Furthermore, FCG data exhibits inherent statistical scatter, and stochastic variations in C and n significantly propagate, causing substantial fluctuations in fatigue life predictions [1–4].

This study quantifies the propagation of scatter in mode-I calibrated Paris-Erdogan constants into mixed-mode life predictions across varying crack depths and loading angles, and assesses the limits of their applicability under evolving mode mixity and crack orientation.

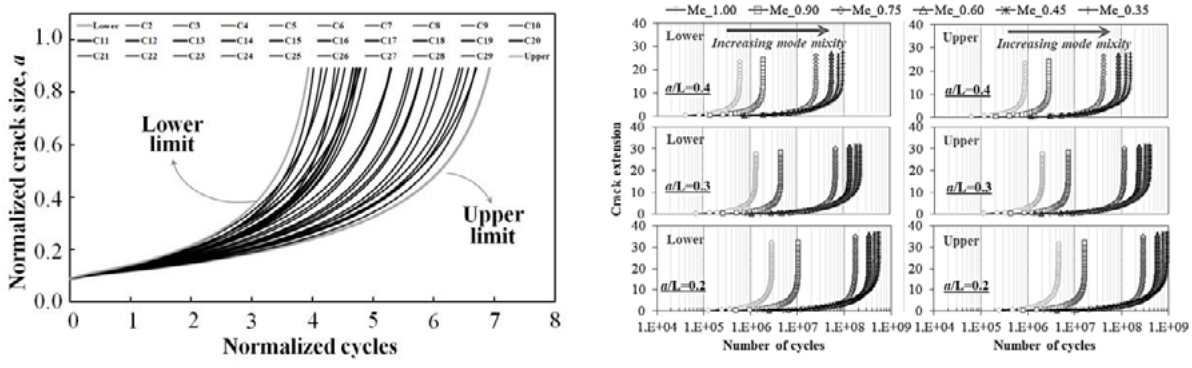

(a) (b)

Figure 1. (a) FCG curves obtained from the mode-I experiments [5], (b) Crack extensions as a function of predicted number of cycles under different mode mixity for SECC specimen.

The current study utilizes experimental mode-I FCG data from Wu and Ni [5], involving 30 tests of 2024-T351 aluminum alloy, to define the probabilistic bounds of material behavior. Two sets of FCG constants (C and n) representing the "lower" and "upper" limits of the fatigue life spectrum (Figure 1-a) were selected to define the probabilistic bounds for the simulations. Mixed-mode FCG simulations were then carried out for three specimen geometries at various initial crack depth ratios and loading angles.

The predicted FCG life curves (Figure 1-b) reveal that the stochastic scatter in *C* and *n* leads to substantial life discrepancies, which are inversely proportional to the initial crack ratio due to the cumulative error propagation during extended stable growth phases.

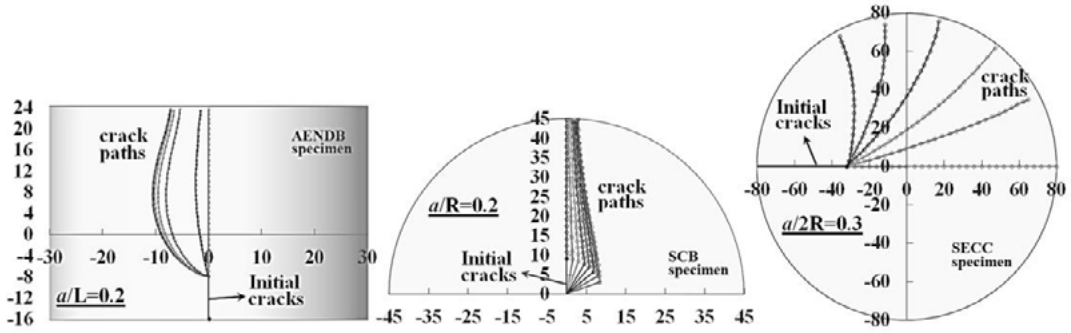

Figure 2. Fatigue crack paths for different crack aspect ratios under different mode mixity.

Simulation results (Figure 2) indicate that stochastic variation in *C* and *n* have a negligible effect on crack trajectories, but significantly affect their temporal propagation along these paths.

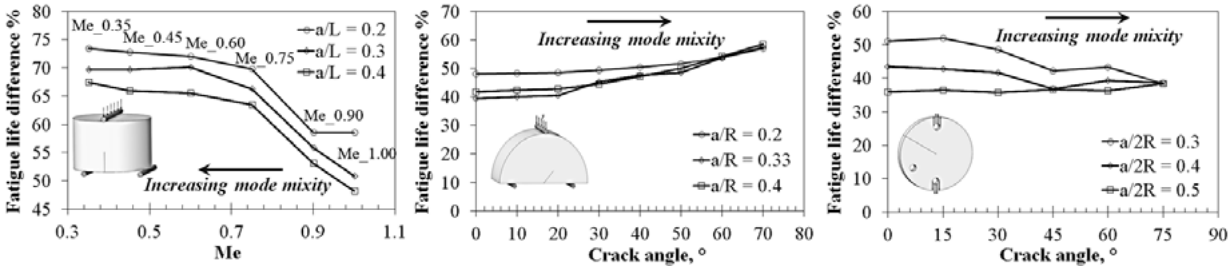

Figure 3. Variation of fatigue life percentage difference as a function of mode mixity.

The fatigue life differences (Figure 3) reveal that prediction uncertainty arising from Paris-Erdogan constants persists under all loading conditions and amplifies with increasing mode mixity. Discrepancies reach ~75% in AENDB and SCB specimens, while SECC specimen remains within the 35–50%. Furthermore, a consistent inverse relationship exists between the initial crack depth ratio and uncertainty magnitude; lower initial ratios yield higher percentage differences, as prolonged stable growth phases multiply material stochasticity. This suggests that relying on deterministic mode-I data is particularly non-conservative for components with small initial cracks under multiaxial stress.

REFERENCES

1. Virkler, D.A.; Hillberry, B.M.; Goel, P.K. The statistical nature of fatigue crack propagation. J. Eng. Mater. Technol., 101, 148–153 (1979).
2. Bigerelle, M. Bootstrap analysis of FCGR, application to the Paris relationship and to lifetime prediction. Int. J. Fatigue, 21, 299–307 (1999).
3. Sankararaman, S.; Ling, Y.; Mahadevan, S. Uncertainty quantification and model validation of fatigue crack growth prediction. Eng. Fract. Mech., 78, 1487–1504 (2011).
4. Chowdhury, S.; Deeb, M.; Zabel, V. Effects of parameter estimation techniques and uncertainty on the selection of fatigue crack growth model. Structures, 19, 128–142 (2019).
5. Wu, W.F.; Ni, C.C. A study of stochastic fatigue crack growth modeling through experimental data. Probabilist. Eng. Mech., 18, 107–118 (2003).

Local scale parameters in continuum damage mechanics and phase field fracture models for crack growth characterization

Valery SHLYANNIKOV[1], Ruslan KHAMIDULLIN[1], Dmitry KOSOV[1]

[1] Institute of Power Engineering and Advanced Technologies, FRC Kazan Scientific Center of Russian Academy of Sciences, Kazan

shlyannikov@mail.ru, v.shlyannikov@gmail.com

A coupled strain gradient–based plasticity and phase-field fracture formulation is presented for the characterization of crack growth in elastic–plastic solids. Damage evolution is driven by the plastic work stored in the local dislocation structure. Motivated by crystal plasticity theory, a local storage energy density is introduced, accounting for both the evolution of dislocation densities and the associated stress fields as driving forces for fracture. Material deformation is described using a conventional mechanism-based strain gradient plasticity model.

The proposed coupled plasticity–damage framework is implemented numerically and employed to simulate crack growth under various boundary value problems. Parametric studies are conducted on cracked bodies to assess the influence of intrinsic length scales associated with plastic strain gradients and the phase-field fracture formulation. Numerical results demonstrate the evolution of the damage variable, geometrically necessary and statistically stored dislocation densities, stored energy density, and stress–strain fields as functions of the plastic and fracture length-scale parameters.

The predictive capability of the model for elastic–plastic fracture is further demonstrated through the analysis of fracture resistance properties for Ti6Al4V titanium and XH73M nickel-based alloys. Crack propagation is simulated for a compact tension specimen with thickness 4 and 10 mm, and crack growth resistance is quantified by predicting the crack extension Δa as a function of the applied stress intensity factor K_1, yielding crack growth resistance R-curves. These R-curves are subsequently reformulated in terms of the energy release rate G_c. By comparing experimentally measured critical energy release rates with numerically obtained values of the stored energy density, pairs of plastic and fracture length scales are identified that provide a strong correlation with the observed fracture resistance behavior. These length-scale pairs are then employed to model the dominant fracture mechanisms in crystalline materials.

Crack nucleation and subsequent failure are investigated in compact specimens with a polycrystalline microstructure. The material microstructure is inherently heterogeneous, comprising irregularly shaped grains separated by distinct grain boundaries. Experimental observations indicate the presence of either transgranular or intergranular dominant failure modes. To capture these mechanisms, the finite element mesh is generated using a Voronoi tessellation–based approach, enabling the construction of statistically representative polycrystalline microstructures with randomly oriented grains. The tessellation is calibrated to reproduce the average grain size and morphology of the XH73M nickel-based alloy. Distinct fracture resistance properties are assigned to grain interiors and grain boundaries to model competing failure mechanisms. The results demonstrate that the stored energy density serves as an effective crack-driving force, enabling accurate prediction of microstructural crack nucleation and growth through its explicit dependence on the plastic and fracture length scales.

Fatigue damage in additively manufactured Ti-6Al-4V lattices: a new parameter based on stiffness and ratcheting

Pablo M. CEREZO[1], Yawen HUANG[2], Alejandro S. CRUCES[1], Teresa GURAYA[3], Philipp NIEKE[4], Zhan WEN CHEN[2], Pablo LOPEZ-CRESPO[1]

[1] Department of Civil and Materials Engineering, University of Malaga, C/Dr Ortiz Ramos s/n, 29071, Malaga, Spain
[2] Department of Mechanical Engineering, Auckland University of Technology, Auckland, New Zealand
[3] Department of Mining & Metallurgical Engineering & Materials Science, University of the Basque Country UPV/EHU, Bilbao, Spain
[4] Zenith Tecnica, Auckland, New Zealand

pm@uma.es

The increasing demand for advanced orthopaedic implants with long-term stability has driven the development of Ti-6Al-4V architected cellular materials fabricated via Electron Beam Powder Bed Fusion (EBPBF). While these structures effectively mitigate stress shielding by replicating bone compliance, predicting their fatigue behaviour remains a formidable analytical challenge. Traditionally, fatigue damage initiation in additive manufacturing (AM) lattices is evaluated using arbitrary empirical thresholds, such as a 1% increase in macroscopic strain amplitude [1]. However, this kinematic metric conflates early, stable plastic accommodation with the onset of physical cracking. To resolve this ambiguity, this study investigates the fundamental micro-mechanical precursors to fatigue failure, aiming to establish a novel, physics-based constitutive criterion for predicting damage initiation.

To achieve this, simple cubic (SC) Ti-6Al-4V lattices oriented in the loading direction were subjected to cyclic compression (R=10) at maximum stress levels of 35 MPa and 50 MPa. An interrupted testing methodology was employed, systematically pausing the fatigue tests at predefined life fractions controlled by an accumulated ratcheting strain parameter, m-parameter. This approach allowed for the extraction of macroscopic mechanical indicators, namely the cycle-by-cycle evolution of dynamic stiffness E^*, ratcheting strain, ϵ_r, and a geometric shape factor, dH/dV. Concurrently, the underlying microstructural and morphological evolution of the critical nodal junctions was tracked using high-resolution Field Emission Scanning Electron Microscopy (FE-SEM) and Electron Backscatter Diffraction (EBSD).

Experimental observations reveal that the macroscopic signature of crack initiation is accurately captured by a biphasic constitutive coupling between dynamic stiffness and ratcheting strain, as illustrated in Figure 1. During Stage I (the induction period), the stiffness exhibits a quadratic decay exclusively driven by geometric softening. Microstructurally, this phase is dominated by a substantial accumulation of geometrically necessary dislocations (GNDs) at the internal nodal radii, which forces the structural cells to undergo geometric flattening without the formation of physical cracks. Subsequently, the mechanical response transitions into Stage II, characterised by a linear degradation of stiffness governed by the nucleation of vertical Mode I micro-cracks. This mathematical transition precisely marks the physical threshold of damage initiation, demonstrating that the conventional 1% strain rule significantly overestimates early damage.

Furthermore, the established analytical framework highlights a critical bifurcation in the failure mechanics dependent on the defect population. At elevated stress levels (50 MPa), lack-of-fusion (LOF) defects function as immediate stochastic drivers that completely bypass the Stage I plastic accommodation phase, leading to rapid fracture. Conversely, under deterministic, plasticity-driven conditions (35 MPa), the structure progresses through the initial stages and eventually transitions to Stage III, where cracks deflect to 45° under a shear-dominated Mode II. Ultimately, this progression culminates in Stage IV, resulting in a sudden cascade effect and catastrophic structural collapse.

In conclusion, the proposed stiffness-ratcheting parameter successfully decouples plastic flattening from true physical cracking, offering a robust, stress-independent tool to pinpoint fatigue initiation in AM lattices. The research confirms that local geometric distortion dictates failure localisation, providing a comprehensive four-stage damage chronology that is vital for the design and safety assessment of future multiaxial biomedical implants.

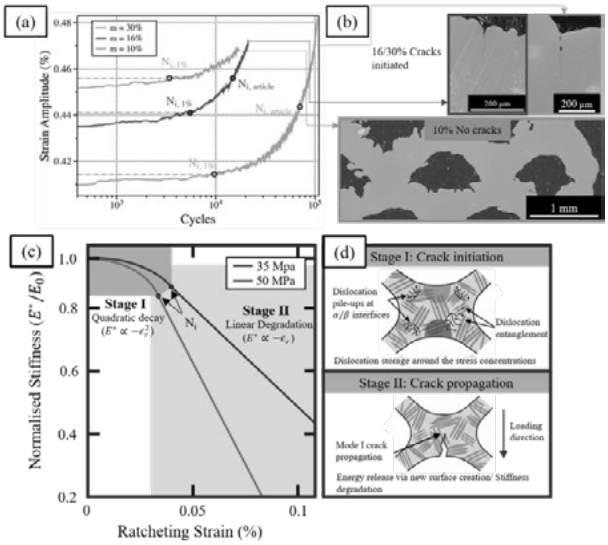

Figure 1. Macroscopic signature of fatigue damage initiation, N_i. (a) Comparison of the proposed criteria against the traditional 1% strain limit, 50 MPa. (b) SEM validation, plastic accommodation at m=10% transitioning to incipient Mode I cracking at m=30%. (c-d) Biphasic model and micro-mechanical interpretation: the shift from Stage I quadratic stiffness decay (geometric flattening) to Stage II linear degradation marks the precise onset of physical micro-cracks.

REFERENCES

1. Benedetti, M.; du Plessis, A.; Ritchie, R.O.; Dallago, M.; Razavi, N.; Berto, F. Architected cellular materials: a review on their mechanical properties towards fatigue-tolerant design and fabrication. Mater. Sci. Eng. R Rep., 144, 100606 (2021).
2. Boniotti, L.; Beretta, S.; Patriarca, L.; Rigoni, L.; Foletti, S. Experimental and numerical investigation on compressive fatigue strength of lattice structures of AlSi7Mg manufactured by SLM. Int. J. Fatigue, 128, 105181 (2019).
3. Huang, Y.; Chen, Z.W. Electron beam powder bed fusion additive manufacturing of Ti6Al4V alloy lattice structures: orientation-dependent fatigue strength and crack growth behaviour under compressive cyclic loading. J. Mech. Behav. Biomed. Mater., 173, 107201 (2026).
4. Huang, Y.; Chen, Z.W.; Wan, A.R.O.; Schmidt, K.; Sefont, P.; Singamneni, S. Electron beam powder bed fusion additive manufacturing of Ti6Al4V alloy lattice structures: orientation-dependent compressive strength and fracture behavior. Int. J. Adv. Manuf. Technol., 132, 3299–3311 (2024).

Numerical modelling of roughness-induced crack closure

Edmundo SÉRGIO[1], Fernando ANTUNES[1], Diogo NETO[1]

[1] Centre for Mechanical Engineering, Materials and Processes, University of Coimbra

edmundo.sergio@uc.pt

Fatigue crack growth (FCG) in metallic materials is primarily caused by cyclic plastic deformation. However, in the near-threshold regime, wedging phenomena such as roughness induced crack closure (RICC) become pertinent crack-tip shielding processes. The interaction between RICC and plasticity induced crack closure (PICC) is complex and has received limited attention, despite being important for FCG predictions.

The RICC mechanism is often linked to the fatigue crack growth threshold [1]. This stage emerges when the plastic zone remains smaller than key microstructural features such as grain size, resulting in faceted fracture surfaces, crack deflection mechanisms and nonlinear crack profiles. The occurrence of irreversible (inelastic) deformation, at the crack tip, origins mixed-mode crack propagation and surface mismatches during unloading, causing non-uniform crack tip opening and closure [2]. The interaction of fracture surface asperities behind the crack tip causes relative shear displacements (Mode II) between the crack faces. This results in asperity interlocking and mismatches that enhance RICC, reducing the FCG rate and determining the near threshold behaviour [3].

To predict the RICC effects, Greenwood and Tripp (GT) rough contact model was incorporated into an FCG model [4] to account for the effects of RICC. This framework considers the accumulated plastic strain at the crack tip as the main damage mechanism. The crack extension is performed using a node release strategy, where PICC is naturally described due to the residual plastic deformation in the crack flanks. The GT model accounts for the effects of the faceted crack surfaces, causing premature contact between the crack flanks. In the case of two rough surfaces in contact, Greenwood and Tripp proposed that the gap between two rough surfaces, λ, depends on the augmented normal contact pressure:

$$\hat{p}_{\mathrm{n}} = \frac{16\sqrt{2}}{15}\pi(\eta\kappa\gamma)^2\sqrt{\frac{\gamma}{k}}\,E'F_{\mathrm{n}}(\lambda), \tag{1}$$

where the rough surface is statistically parametrized by the number of asperity peaks per unit area, η, the average asperity tip radius, κ, and the standard deviation of asperity heights γ. $F_{\mathrm{n}}(\lambda)$ are statistical functions derived from the Gaussian distribution of asperity heights. Finally, E' represents the composite (equivalent) Young's modulus of elasticity of the two surfaces.

The FCG predictions were obtained with the FCG model, for the entire range of experimental ΔK values obtained at R=0.1 considering a AA2024-T351 alloy. The results are presented in Figure 1, comparing the numerical FCG rate for the distinct contact parameters (*Flat*; $\eta\kappa\gamma$=0.06, 0.6 and 6) with the experimental results.

The *Flat* model presents a perfectly linear trend in *log-log* scales, while for $\eta\kappa\gamma$=0.06 the trend slightly deviates from the linearity at lower ΔK levels, approaching the curvature verified in the experimental data. Nevertheless, in both cases, the experimental FCGR is overpredicted. On the other hand, the $\eta\kappa\gamma$=0.6 and $\eta\kappa\gamma$=6 parameters underestimate the experimental FCG rate and overestimate the deviation from linearity. Nevertheless, the overall trend is correct. In fact, for SIFs above $\Delta K \sim 11\ \mathrm{MPa.m^{0.5}}$ the numerical results provide a linear trend, close to the

experimental data. Below this value, crack closure plays a key role and a curvilinear trend is obtained, due to the lower registered *da/dN* values, caused by a higher shielding of the crack tip. Therefore, RICC must be the cause of this type of experimental behaviour and was successfully numerically evaluated.

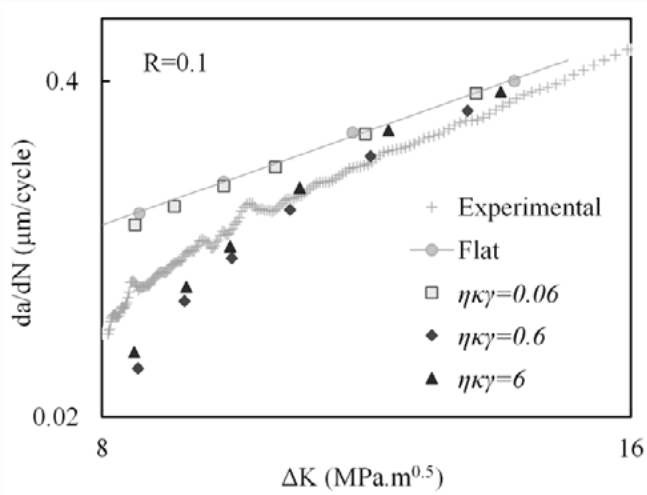

Figure 1. Comparison between the experimental and numerical FCGR considering the distinct sets of contact parameters. Both near threshold and Paris regimes were considered.

The results demonstrate that the present framework is able to represent the physical mechanisms governing crack closure and FCG across different propagation regimes, where conventional Paris-law approaches often become unreliable.

REFERENCES

1. Chen, D.L.; Chaturvedi, M.C. Near-threshold fatigue crack growth behavior of 2195 aluminum-lithium-alloy—prediction of crack propagation direction and influence of stress ratio. Metall. Mater. Trans. A, 31, 1531–1541 (2000).
2. Pokorný, P.; Vojtek, T.; Náhlík, L.; Hutař, P. Crack closure in near-threshold fatigue crack propagation in railway axle steel EA4T. Eng. Fract. Mech., 185, 2–19 (2017).
3. Parry, M.R.; Syngellakis, S.; Sinclair, I. Numerical modelling of combined roughness and plasticity induced crack closure effects in fatigue. Mater. Sci. Eng. A, 291, 224–234 (2000).
4. Borges, M.; Neto, D.M.; Antunes, F.V. Numerical simulation of fatigue crack growth based on accumulated plastic strain. Theor. Appl. Fract. Mech., 108, 102676 (2020).

ISBN 978-88-6938-530-8